ELUCIDATING TUMOR SUPPRESSIVE FUNCTION OF FRATAXIN IN COLORECTAL CANCER WITH A QUANTITATIVE PROTEOMICS APPROACH

TAN XING FEI

B. Sc (Hons), NUS

A THESIS SUBMITTED

FOR THE DEGREE OF DOCTOR OF PHILOSOPHY

DEPARTMENT OF BIOLOGICAL SCIENCES

NATIONAL UNIVERSITY OF SINGAPORE

2014

DECLARATION

I hereby declare that this thesis is my original work and it has been written by me in its entirety. I have duly acknowledged all the sources of information which have been used in the thesis.

This thesis has also not been submitted for any degree in any university previously.

Tan Xing Fei

23rd January 2014

Acknowledgement

It is my utmost pleasure to express deepest appreciation to my guide and advisor, Dr Lin Qingsong. Without his guidance and supervision, this thesis would not have been possible. Dr Lin's ever timely encouragement and mentorship enabled me to stay focused and motivated me throughout my candidature.

I am grateful to Dr Bi Xuezhi for being a wonderful mentor, imparting most useful skills and knowledge to me when I first started. I would like to express my gratitude to Oncoproteomics Research group and Protein and Proteomics Center for guidance and support in all academic and technical aspects.

I extend my thanks to fellow lab members for providing a warm and engaging research environment during these years. Special thanks to Mr. Lim Teck Kwang for his technical expertise, and advice. Finally, I am grateful for the understanding and constant support from my family, friends and loved ones.

Table of Contents

Summary

Metabolic and energetic requirements of cancer cells are very different from normal cells. Tumor cells use predominantly glycolysis for ATP production, unlike in normal cells, where the main source of ATP is oxidative phosphorylation in the mitochondria. This is termed Warburg effect and such a metabolic reprogramming is a hallmark of cancer that is essential for cancer cells to maintain aggressive growth. Frataxin (FXN) is a mitochondrial protein that reportedly influences both glucose and iron metabolism in the cell. FXN interacts functionally with the electron transport chain proteins in the mitochondria to influence oxidative phosphorylation, and FXN deficiency resulted in defective mitochondrial ATP production. Studies have shown that FXN knockout increases tumorigenicity in cancer cell lines and induces tumor formation in animal model. Over-expression of FXN has been demonstrated to possess anti-cancer effects. However, the molecular mechanisms of FXN as a potential tumor suppressor are largely unknown. This thesis aims to elucidate the role of FXN over-expression in tumor cells. Proteome and metabolic changes induced by stable over-expression of FXN in colorectal cancer cell line HCT116 (OF) were investigated in this study. Using iTRAQ analysis, abundance of 276 proteins was found to be significantly different. Pathway analysis of these dysregulated targets recapitulated perturbed (i) mitochondrial ATP production, (ii) cellular reactive oxygen species (ROS) status and (iii) cell cycle and proliferation. Functional assays were performed to validate the effect of FXN over-expression. OF cells were demonstrated to possess characteristics of increased oxidative phosphorylation, better resistance towards endogenous ROS insult and a decreased intracellular ROS. Our cell

cycle analysis suggested that reduced cell proliferation in OF cells might be due to a delayed transition of G1 to S phase. Further examination of perturbed targets points to alteration of hypoxia state of the cells. Destabilization of HIF-1α in OF cells was demonstrated to be associated with metabolic changes and anti-cancer effect observed. Among them, a downstream target of HIF-1α, EMMPRIN, which is associated with tumor progression and malignancy, has a lower abundance in OF cells.

List of Figures

List of tables

List of Abbreviations

CAN	Acetonitrile
ATP	Adenosine-5-Triphosphate
CAT	Chloramphenicol Acetyltransferase
DCFH-DA	2',7'-Dichlorfluorescein-Diacetate
DIGE	Difference Gel Electrophoresis
EMMPRIN	Extracellular Matrix Metalloproteinase Inducer
ESI	Electrospray Ionization
ETC	Electron Transport Chain
FADH	Flavin Adenine Dinucleotide
FBS	Fetal Bovine Serum
FDG	2-[18F]-Fluoro-2-Deoxyglucose
FRDA	Friedreich's Ataxia
FT-ICR	Fourier Transform-Ion Cyclotron Resonance
FXN	Frataxin
GC	Gas Chromatography
GSSG	Oxidized Glutathione
GSH	Reduced Glutathione
HIF-1	Hypoxia-Inducible Factor 1
HILIC	Hydrophilic Interaction Chromatography
ICAT	Isotope-Coded Affinity Tags
ISC	Iron Sulphur Cluster
iTRAQ	Isobaric Tags for Relative and Absolute Quantitation
LC	Liquid Chromatography

LMW	Low Molecular Weight
LTQ	Linear Ion Trap
m/z	Mass-To-Charge
MALDI	Matrix-Assisted Laser Desorption Ionization
MDS	Multidimensional Scaling
MMTS	Methyl Methane-Thiosulfonate
MS	Mass Spectrometry
MudPIT	Multidimensional Protein Identification Technology
NADH	Nicotinamide Adenine Dinucleotide
NMR	Nuclear Magnetic Resonance
OE	Over-expression
OF	Over-expressing Frataxin
OXPHOS	Oxidative Phosphorylation
PAGE	Polyacrylamide Gel Electrophoresis
PCA	Principle Component Analysis
PET	Positron Emission Tomography
PHDs	HIF Prolyl Hydroxylases
PI	Propidium Iodide
pRB	Retinoblastoma
Q	Quadrupoles
ROS	Reactive Oxidative Species
SCX	Strong Cation Exchange
SILAC	Stable Isotope Labeling by Amino acids in Cell culture
SRM/MRM	Selected/Multiple Reaction Monitoring

SWATH-MS	Sequential Windowed data independent Acquisition of the Total High-resolution Mass Spectra
TBHP	Tert-Butyl Hydroperoxide
TCA	Tricarboxylic Acid
TCEP	Tris-(2-Carboxyethyl) Phosphine
TEAB	Triethylammonium Bicarbonate
TGFβ	Transforming Growth Factor Beta
TIC	Total Ion Chromatography
TMT	Tandem Mass Tag
TOF	Time-Of-Flight

Chapter 1: Introduction

1.1 Cancer

Cancer is the most common cause of death in developed countries and the second biggest reason for mortality in developing countries [1]. Presenting as a complex syndrome that could affect any part of the body, cancer is best characterized by rapid and uncontrolled growth of abnormal cells with the capacity to spread to distant sites as metastases. Cancer pathogenesis generally begins with '*in situ*' growth, followed by invasion, extravasation and eventually metastasis. In Singapore, around 10,000 cases of cancer is reported yearly with an increasing trend. In Singapore, colorectal cancer is the most common cancer in Singaporean males and second most common cancer amongst Singaporean females (Source: National Cancer Centre, Singapore).

1.1.1 Hallmarks of cancer

Characteristics of cancer may be summarized into six hallmarks (Fig 1-1). These include sustaining proliferative signaling, evading growth suppressors, activating invasion and metastasis, enabling replicative immortality, inducing angiogenesis and resisting cell death [2]. These capabilities are often progressively acquired during cancer pathogenesis and provide driving forces in disease progression.

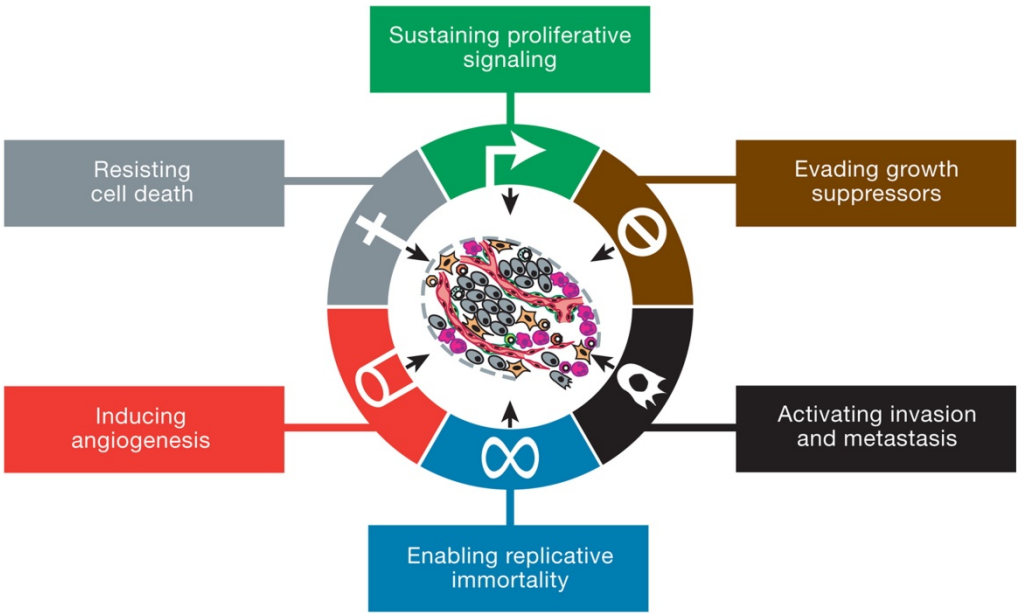

Figure 1-1: Hallmarks of cancer. Six original hallmarks of cancer, describing the biological capabilities attained during tumorigenesis. These hallmarks are presumably the result of underlying genome instability of cancer cells. (Adopted from Hanahan D. and Weinberg R.A. [3] with permission).

Sustaining proliferative signaling refers to the ability to sustain proliferation without the need for external growth-promoting signals. Through mutations, cancer cells may acquire the capability to sustain growth signaling in a few ways. For example, cancer cells may be capable of autocrine secretion or may acquire an activating mutation downstream of signaling molecules such as the Rat sarcoma (Ras) oncogene or even transcription factors such as Myc that drive cellular proliferation [4]. At the same time, anti-proliferative mechanisms must be suppressed during tumorigenesis. For example, transforming growth factor beta (TGFβ) that activates tumor suppressor retinoblastoma (pRB), to inhibit cell cycle progression may be triggered [5]. The loss of functional pRB is common in many tumors and a driving factor in tumor progression [6].

The ability of tumors to grow and increase in mass is not only the result of uncontrolled proliferation but also with evasion of programmed cell death, apoptosis. Apoptosis is an innate cellular suicide mechanism often triggered to remove undesired cells from the body. For aberrant cancer cells to survive, apoptosis has to be circumvented. Cancer cells resist cell death through regulating both anti-apoptotic and pro-apoptotic signals [7].

Even after successfully escaping from apoptosis, cancer cells still may not divide forever as there exists a built-in replicative limit. Telomeres are DNA regions that cap the end of chromosomes to prevent lethal chromosomal end-to-end joining. Telomeres erode with each cell division, placing a limit on the number of times a cell can divide. In cancerous states, enabling replicative immortality is most commonly achieved by continuous addition of telomeres by the enzyme telomerase [8].

After overcoming restraints to growth signaling, apoptosis and replicative mortality, tumor cells expand in numbers and accumulate in mass. At this stage, nutrients would become inevitably scarce and the proliferating tumor mass requires new sources of materials for further growth. Tumor cells thus promote the formation of nascent blood vessels and capillaries by turning on the angiogenic switch and hijacking the normal angiogenic machinery [9]. With vasculation at the primary tumor site, the tumor mass gains nourishment for further expansion and more importantly gains access to the circulation for dissemination.

Metastatic spread takes two major phases: intravasation of tumor cells into blood vessel, and extravasation and adaption to microenvironment at distant site. The activation of invasive and metastatic phenotype is triggered by many classes of

proteins collectively involved in epithelial-to-mesenchymal transition, cell motility, adhesion, and extracellular protease activity [10].

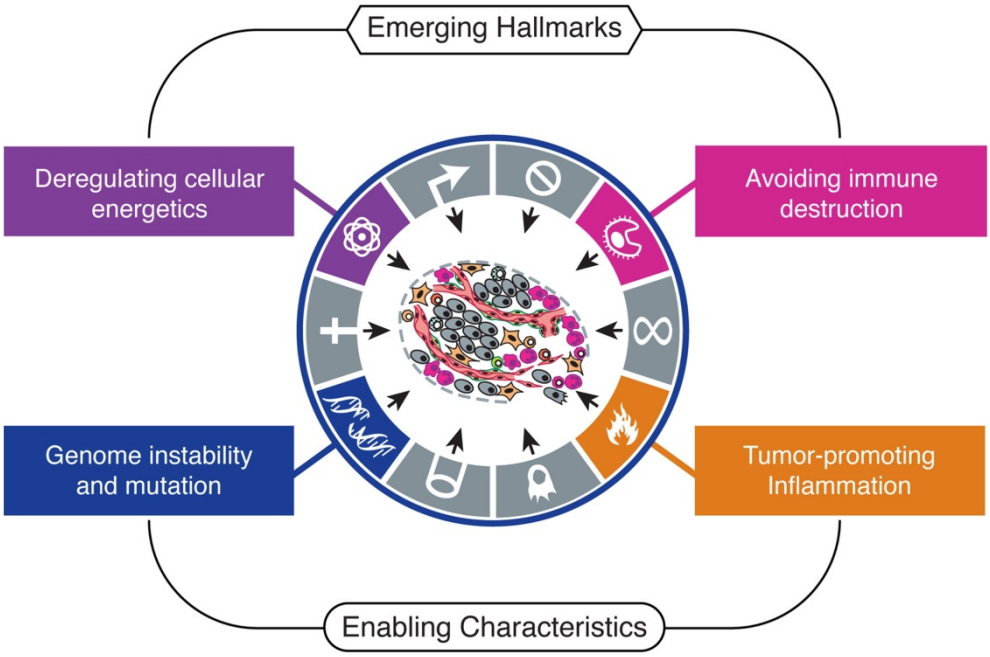

Figure 1-2: Emerging Hallmarks and enabling characteristics of cancer. New findings suggest that deregulation of cellular energetics and avoiding immune destruction are additional hallmarks of cancer. In addition, genome instability and mutation, and tumor-promoting inflammation characteristics further support cancer progression. (Adopted from Hanahan D. and Weinberg R.A. [3] with permission).

In recent years, new hallmarks of cancer have emerged with more extensive study. Two enabling characteristics (Fig 1-2) further aid cancer cells in the acquisition of the six original cancer hallmarks described previously. Genomic instability is the basis for genetic changes that endow cancer cells with these hallmarks. Cancer progression is a multistep acquisition of aberrant advantages over normal cells, which may be understood as the activation of proto-oncogene with the loss of functional tumor suppressors. In this respect, accumulation of mutation due to genomic instability is the main driving force.

The second enabling characteristic involves inflammatory response during early malignancy that promotes tumorigenesis. It is now a consensus that immune cells can infiltrate almost all types of neoplastic lesions and at various stages of cancer progression [11]. Initially these immune responses were thought to be the body's effort in eliminating tumors. Increasing evidence recently however show that cancer cells may instead coax immune cells into supplying bioactive molecules to the tumor microenvironment, to contribute to both tumor initiation and progression [12].

Considering the dual roles of inflammation, immune responses constitute a key defence mechanism in tumor eradication. Since avoiding immune destruction is one of the emerging hallmarks of cancer pathogenesis, cancer cells evolve strategies to evade detection, attack and elimination by immune cells. Some of these mechanisms involve secretion of immunosuppressive factors [13] or the recruitment of regulatory T-cells [14] to further suppress host immune responses.

The last hallmark of cancer is deregulating cellular energetics. These involve reprogramming of the general energy metabolism to support rapid proliferation. This emerging hallmark would be further discussed detail in subsequent sections with incorporation of experimental data. Collectively, these ten hallmarks of cancer serve as a framework for investigating the complexity of cancer biology.

1.1.2 The Warburg effect

All cells need energy in the form of adenosine-5-triphosphate (ATP) to maintain essential biological processes such as DNA synthesis and repair, protein turnover and maintenance of membranes. In the presence of oxygen, glucose is metabolized to pyruvate via glycolysis with the generation of two molecules of ATP.

The pyruvate then enters the mitochondria where it undergoes further oxidation in the citric acid cycle also known as the tricarboxylic acid (TCA) cycle.

The TCA cycle also generates reducing equivalents in the form of nicotinamide adenine dinucleotide (NADH) and flavin adenine dinucleotide ($FADH_2$). Electrons from NADH and $FADH_2$ are transferred to the Electron Transport Chain (ETC) in the inner mitochondrial membrane, and through a series of redox reactions, reach the final electron acceptor oxygen. Through the ETC, oxidative phosphorylation (OXPHOS) generates another 34 to 36 molecules of ATP per molecule of glucose, in addition to 2 ATP generated from glycolytic pathways. In the absence of oxygen, however, the ETC cannot function, and cells rely solely on glycolytic ATP production to survive.

In the 1920s, German biochemist Otto Warburg measured the amount of glycolytic and oxidative ATP production in normal kidney, liver and cancerous ascites tissues. It was discovered that even in oxygenated conditions, ascites cancer cells had almost 50% more glycolytic ATP production compared to the normal tissues [15]. Cancer cells actively metabolize glucose to produce excessive lactate even though oxygen is still consumed by the mitochondrial ETC. Warburg termed this phenomenon aerobic glycolysis and proposed that deficit in mitochondrial function may be the factor driving tumorigenesis, and that these tumor cells adapt by increasing glucose uptake for glycolytic energy production independent of the mitochondria.

The Warburg effect thus summarises drastic modifications in metabolism and cellular energetics, that agree with the emerging hallmark of metabolic shifts in cancer [3].

1.1.3 Cancer cell metabolism

As described above, cancer cells undergo uncontrolled proliferation to rapidly accumulate tumor mass. To fuel this aggressive proliferation and to sustain growth when nutrients become limited, it is paradoxical that cancer cells increase anaerobic ATP production even though aerobic ATP production is more energy efficient per glucose molecule.

Warburg initially believed cancer cells have a deficit in mitochondrial ATP production [16]. However, subsequent evidence showed that not all cancer cells had defective OXPHOS [17, 18], and that the occurrence of aerobic glycolysis was not only limited to cancers but also observed in normal cells undergoing rapid proliferation [19, 20]. Thus the shift to aerobic glycolysis is independent of mitochondrial function.

Although glycolysis is inefficient in producing ATP per molecule of glucose compared to OXPHOS [21], glycolysis has a higher turnover rate in ATP generation [22]. Therefore, given a continual supply of glucose, like having access to rich vasculature, high glycolytic rate may better meet the needs of growth and cell division [23]. Several pieces of evidence show that tumour cells indeed have higher glucose uptake [24, 25].

Moreover, cell division requires additional synthesis of cellular components, nucleic acids, proteins and lipids. Glucose catabolism in aerobic glycolysis also provides the precursors needed in these biosynthetic pathways [26, 27]. The glycolytic pathway is linked to the pentose phosphate shunt, which is the main source of nicotinamide adenine dinucleotide phosphate (NADPH) and ribose sugar for nucleic acid synthesis. TCA cycle intermediates also serve as precursors in

amino acid, lipids and nucleic acid biosynthesis [27]. Predominant use of glycolysis even in the presence of oxygen thus offers a tremendous advantage in the rate of energy production as well as the generation of biosynthetic precursors (Fig 1-3).

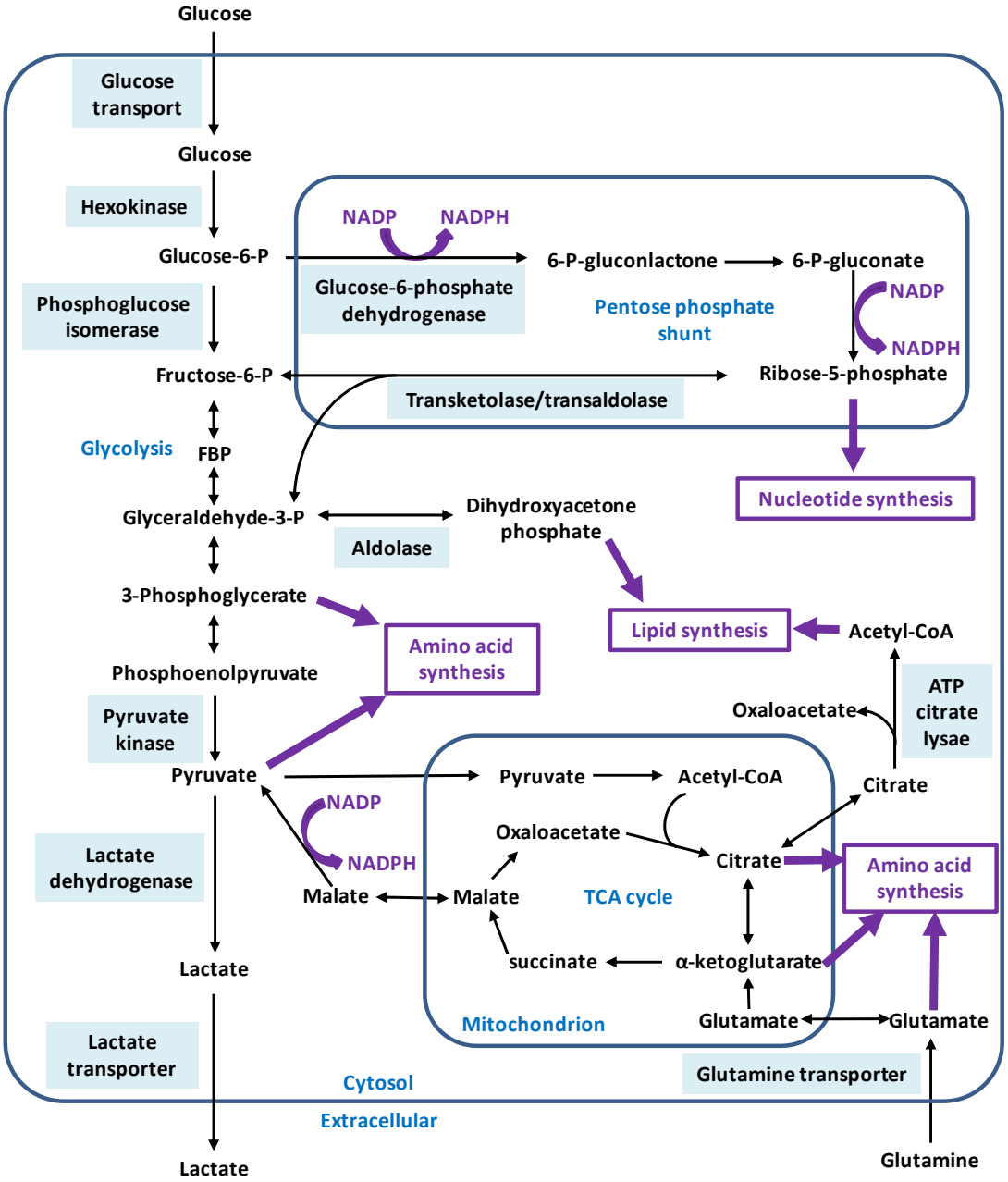

Figure 1-3: Biosynthetic precursors derived from metabolic pathways. This schematic shows how glycolysis, pentose phosphate pathway, OXPHOS and TCA cycle feed into the biosynthesis of NADPH, amino acid, lipids and nucleic acids. Main metabolic pathways are labeled in blue, cellular constituents essential for cell division are in purple. Glucose and glutamine uptake are increased in proliferating cells and excess lactate excreted. Key proteins involved are boxed in blue. Modified from Vander et. al and, Lunt and Vander [26, 27]. Intermediate steps in the pathways are omitted for clarity.

1.1.4 Mechanisms involved in altered cancer metabolism

The tumor microenvironment was believed to be the dominant driving force in metabolic transformation. During tumorigenesis, lack of blood supply due to poor vasculature and the distance of the tumor mass from the nearest blood vessels [28] often results in a hypoxic tumor microenvironment [29]. The central molecule that responds to hypoxic stress is the hypoxia-inducible factor 1 (HIF-1) [30, 31]. Being a master regulator of oxygen homeostasis and metabolism, HIF-1α targets genes associated with angiogenesis, glycolysis, cell proliferation and metastasis, and permits the survival of tumor cells under hypoxic conditions [32].

1.1.5 HIF-1α modulates cancer cell metabolism

HIF-1 activation promotes glucose uptake by increasing the expression of glucose transporter 1 (GLUT1) [33]. Many glycolytic enzymes are also regulated by HIF-1, such as phosphofructokinase, fructose-2,6-biphosphatase, aldolase, phosphoglycerate kinase and pyruvate kinase [34, 35]. On top of these, HIF-1 also regulates the processes of pyruvate conversion into lactate and lactate removal from tumor cells [36, 37]. In hypoxic conditions, HIF-1 further regulates mitochondrial activity by reducing pyruvate dehydrogenase levels, thereby limiting the use of pyruvate in the mitochondria [38, 39]. Since HIF-1 as a transcription factor directly regulates the expression of many enzymes causing the shift from OXPHOS to aerobic glycolysis, it is an attractive target for potential inhibition of the Warburg effect in cancer.

Moreover, the potential role of HIF-1 in cancer metabolism is further strengthened with reports of its activation by oncogenes and loss of tumour suppressors [40]. During normoxia, Ras/Raf/MAPK and PI3K/AKT pathways activate HIF-1. Loss of tumor suppressor PTEN also reportedly increases HIF-1

levels and cause up-regulation of its targets [41]. TCA metabolites such as succinate and fumarate in tumor cells can also regulate HIF-1 levels [42].

Although Warburg effect in cancer cells may be attributed to HIF-1 activation and transcriptional activity, other factors may also contribute to metabolic re-programming. For instance, p53 can regulate glucose metabolism through miRNA suppression of glycolytic enzymes [43], or via direct modulation of fructose-2,6-bisphosphate and cytochrome c oxidase 2 [44, 45]. Myc oncogene can also regulate an array of glycolytic enzymes such as lactate dehydrogenase, hexokinase and pyruvate dehydrogenase kinase [46, 47]. Therefore, the control of precise changes in aerobic glycolysis in cancer is likely a concerted effect of HIF-1 with other key oncogenic modulators in the cell.

1.1.6 Potential therapy targeting cancer metabolism

Elevated glucose uptake in tumors has been exploited with the use of 2-[^{18}F]-fluoro-2-deoxyglucose (FDG) positron emission tomography (PET) to detect cancerous tissue in humans [48, 49]. FDG is a labeled analogue of glucose, which is taken in and metabolized rapidly by tumors. Phosphorylation of FDG by hexokinase traps it in the cell due to charge on the phosphate group, allowing it to be detected in cancer cells. This imaging technique has been very useful in diagnosis, staging and prognosis of cancer.

Among numerous glycolytic enzymes, hexokinase is one of the key targets with two drugs reaching clinical trials. Hexokinase phosphorylation of glucose to glucose-6-phosphate is the first limiting step in glycolysis. Since glucose-6-phosphate also serves as an immediate for pentose phosphate pathway, inhibition of hexokinase likely has a profound effect on both glycolysis and the pentose

phosphate shunt. A non-metabolizable glucose analogue, 2-deoxyglucose, is phosphorylated by hexokinase, but accumulates to inhibit hexokinase via feedback mechanism. This inhibits glycolysis and eventually leads to cell death due to depletion of ATP, especially in cancer cells with defective OXPHOS [50]. An *in vivo* study showed that 2-deoxyglucose enhances anti-tumor effect of paclitaxel and adriamycin in xenograft models [51]. Based on these findings, 2-deoxyglucose had entered clinical trials for cancer treatment in combination with other drugs.

Lonidamine is another drug that also targets hexokinase 2 [52] to deplete cellular ATP in a dose dependent manner [53]. Lonidamine can enhance the killing effect of several anticancer drugs in combination treatment [54] and has begun clinical trials for treatment of early stage prostate cancer [55].

Given the importance of HIF-1α in regulating aerobic glycolysis in tumors, HIF-1α is another potential candidate in cancer therapy. Based on the mechanism of HIF-1, drugs have been developed to target transcription of HIF-1α mRNA, protein translation and degradation, or DNA binding and transcriptional activity [56].

Topotecan is an FDA approved drug able to inhibit the translation of HIF-1α. Treatment using topotecan in mouse glioma model inhibited angiogenesis and tumor growth through reducing HIF-1α protein level [57]. Topotecan is in clinical trials in various cancers and its efficacy in different drug combinations is also being evaluated. A recent phase II study on the use of oral topotecan with bevacizumab (Avastin), an angiogenesis inhibitor, in small-cell lung cancer showed promising results [58].

These drugs have shown potential in anticancer treatment but there are still concerns that need to be addressed, in particular, the specificity and associated

toxicity require further investigation. Thus more in-depth understanding of the cellular machinery is necessary and would be an important goal in the study of cancer metabolism.

1.2 A model to study alteration of cancer metabolism

The development of novel therapeutic strategies targeting cancer metabolism would require comprehensive understanding of the machineries involved. The use of a model can be beneficial by reducing the complexity of the problem. From the current literature, Frataxin (FXN) is a possible candidate given its association with the Warburg effect, its anti-tumor effect and proposed functions in the modulation of energy metabolism [59].

1.2.1 Frataxin and Friedreich's ataxia

Friedreich's ataxia (FRDA) is an autosomal hereditary ataxia caused by reduced expression of frataxin (FXN). FRDA has an early onset with the mean age of 25 and on average, patients with FRDA die by the age of 36.6, predominantly from cardiac failure [60]. The lack of FXN causes a wide range of metabolic disturbances including, but not restricted to, oxidative stress, iron metabolism and deficit in iron sulphur and heme synthesis. The effect of FXN deficiency is most severely presented in neurons and heart cells. Symptoms of FRDA include neurodegeneration, lost of reflexes in the limbs, sensory neuropathy, skeletal deformities and cardiomyopathy [61].

1.2.2 Structure of the human Frataxin

FXN is a nuclear-encoded mitochondrial protein highly conserved from gram negative bacteria to eukaryotes [62]. FXN gene likely originated from proteobacteria which was transferred to the eukaryotic genome after endosymbiosis

[63]. The nuclear magnetic resonance (NMR) [64] and crystal structures of FXN [65] were both solved in 2000. The FXN structure (Fig 1-4) consists of a large, twisted six-stranded antiparallel β-sheet (orange) flanked by N- and C-terminal α-helices (pink). The antiparallel β-sheets are mostly neutral and may be involved in protein-protein interaction, while in contrast, the α1 helix and β1 sheet are negatively charged and are believed to interact with iron [66].

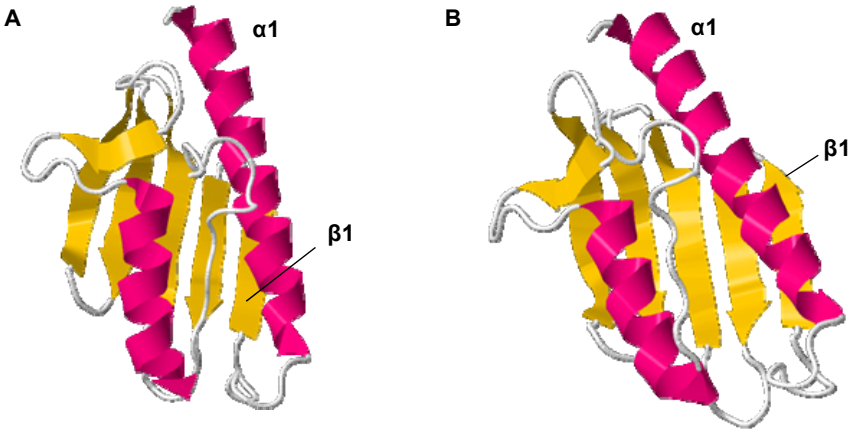

Figure 1-4: NMR and crystal structure of human FXN. A) Solution structure of human FXN. PDB ID: 1LY7[64]. **B)** Crystal structure of human FXN. PDB ID:1EKG [65]. Both structures are similar, showing large, twisted six-stranded antiparallel β-sheets in orange flanked by N- and C-terminal α-helices in pink.

1.2.3 Frataxin and its implication in metabolism

FXN was reportedly involved in the synthesis of iron sulphur clusters (ISC) [67]. ISCs are prosthetic groups required by many enzymes, including those that are involved in signaling, DNA repair, and various metabolic pathways. For example, proteins in the complexes I, II and III of the ETC, aconitase and ferredoxin [68] all required ISC for normal function. It has been observed that deficiency in FXN leads to deficit in ISC-containing proteins in FRDA patients, mouse models and

eukaryotic cells [67, 69-71]. These provide evidence that FXN is crucial for ISC biosynthesis and could probably also indirectly affect ETC function via its regulation of ISC synthesis. It was also proposed that FXN may regulate OXPHOS in the mitochondria by interacting functionally with the ETC proteins [72].

Clinical validation in patients suffering from FRDA showed defective mitochondrial ATP production [73]. Conversely, FXN over-expression increased mitochondrial membrane potential in cell line models, accompanied by increased OXPHOS [74].

1.2.4 Association of Frataxin with cancer

A few cases involving clinical onset of cancer in FRDA individuals is summarized in Table 1-1. Two cases reported in 1996 and 2001 involved FRDA siblings who developed similar cancers and highlighted possible mechanistic correlation between cancer and FXN deficiency. In addition, a recent study reported that FXN is associated with DNA repair mechanisms [75] and may be the reason behind hypersensitivity to mutagens observed in cells isolated from FRDA patients [76, 77]. However, these cases of cancer amongst FRDA patients are uncommon given the early mortality associated with the disease.

Table 1-1: Reported cancer incidents in Friedreich's ataxia cases.

No	Cancer type	Patient(s)	Year reported	References
1	Primary small bowel ganglionneuroblastoma	Female, 26	1986	Barr et. al [78]
2	Gastric carcinoma†	Female, 34 Male, 34	1996	Ackroyd et. al [79]
3	Lymphoblastic lymphoma	Male, 16	1999	De Pas et. al [80]
4	Uterine Leiomyoma	Female, 39	2011	Misiakos et. al [81]
5	Breast carcinoma†	Female, 39 Female, 42	2001	Kidd et. al [82]
6	Osteogenic sarcoma	Female, 19	2012	Deutsch et. al [83]

† These cases reported siblings developing the same type of cancer.

The association between FXN and Warburg effect in caner has been demonstrated in several *in vitro* studies. In hepatic FXN knockout mice, hepatocytes had disrupted mitochondrial function that caused defective OXPHOS. This was accompanied by high oxidative stress which stimulated hepatocyte proliferation. These hepatic FXN knockout mice also had significantly higher occurrence of multiple liver tumors [84]. Conversely, over-expression of FXN in murine fibroblast inhibited malignant transformation and tumor formation in nude mouse [85]. Over-expression of FXN in colorectal cancer cells was shown to induce OXPHOS, inhibit tumor growth and reduce tumor size in mouse xenograft [59].

However in another study, FXN level was reported to be elevated in human colon tumor tissues [86]. The authors also showed that FXN protein level in cancer cell lines may be induced during hypoxia. FXN was additionally associated with S15 phosphorylation of p53 during hypoxia. Activation of p53 first promotes cell survival, but eventually leads to cell death if left to persist. FXN was thus proposed as a tumor suppressor since it affects the adaption of tumor cell to hypoxia by modulating p53 activation.

Given the possible roles of FXN as discussed so far, FXN is a good candidate as a model to further understand the relationship between energy metabolism and cancer progression.

1.3 Omics-based approaches for study of cancer biology

An "omics"-based study refers to a large scale study of molecules relevant to biological systems in cells, tissues or organisms [87]. Depending on the nature of the molecules studied, genomics, proteomics, transcriptomics, metabolomics and many others, each in their own discipline, serve to answer complex biological questions by analysing the whole repertoire of components in its entirety [88]. High throughput "omics" approaches are widely used to study biological systems. High-throughput technology is especially powerful in association and causation studies, in the identification of genetic mutation, protein biomarkers, metabolic profiling or the integration of various omics for disease prediction or prognosis monitoring [89, 90]. It is also a good starting basis for personalized medicine in the treatment of highly heterogeneous diseases like cancer [91].

1.3.1 Metabolomics

Metabolomics is the identification and quantitation of metabolites within a cell, tissue or organism, that provides information about metabolic and bioenergetic processes [92]. Gas chromatography mass spectrometry (GC-MS) and NMR spectroscopy were traditionally used for metabolite analysis, but liquid chromatography (LC) coupled to electrospray ionization (ESI) mass spectrometry is becoming increasingly popular in metabolomics studies due to the ability to "soft ionize" large number of metabolites without much fragmentation.

In general, metabolomics studies may be classified as one of four approaches [93]. 1) Targeted metabolite analysis – the study of a primary alteration in a biological system directly, which may involve a single metabolite or a cluster of metabolites related to the biological system. 2) Metabolic profiling analysis –the measurement of a small number of pre-defined metabolites associated with a phenotype or diseased state. 3) Metabolomics – involving identification and quantitation of the entire repertoire of metabolites that reveal the state of metabolome in a biological system and in response to change. 4) Metabolic fingerprinting – a rapid high throughput screening of metabolites to differentiate samples according to their biological state, to identify unique individuals. Metabolomics approaches have been used for various applications in cancer research [94]. Various reports on the use of metabolites as potential biomarkers for both diagnostic [95, 96] and prognostic [97] applications are also increasingly common.

Although the metabolic profile of cancer cells may resemble those of rapidly proliferating cells, cancer cells may still exhibit unique metabolic signatures. Metabolomics is thus a powerful platform for understanding cancer metabolism with potential use in cancer diagnosis and prognostic monitoring.

1.3.2 Proteomics

Proteomics is the large scale study of proteins to characterize gene function and biological processes [98]. The proteome would include the entire set of protein species, protein-protein interactions, protein localization and protein complexes [99]. The workflow of proteomics can be divided into three aspects - separation, mass analysis and data processing.

Biological samples are highly complex with large dynamic range and diverse protein chemistry [100]. Sufficient separation is therefore critical to "simplify" samples for MS-based proteomics study. Depending on the proteomics approach chosen, a variety of separation techniques are used. Peptides can be resolved using reversed-phase LC, hydrophilic interaction, as well as affinity-based or ion exchange chromatography. It is also very common to separate peptides using a combination of orthogonal approaches, such as by a 2-dimensional (2-D) approach or multidimensional protein identification technology (MudPIT) [101, 102].

Separation of whole proteins may be performed on 2-D polyacrylamide gel electrophoresis (PAGE), where proteins are separated first by iso-electric point and then by molecular weight [103]. Fractionation of samples using 2-D gel preserves information regarding protein modifications such as phosphorylation, as well as truncations, which could be useful in some contexts.

Mass analysis is typically performed with mass spectrometers that consist of three main components: an ionization source, the mass analyzer and a detector. Two main ionization methods currently in use are matrix-assisted laser desorption ionization (MALDI) and ESI. MALDI uses a laser to impart energy to the analytes via the matrix, forming mostly singly positive charged ions [104]. ESI generates ions by applying a high voltage across the emitter at the inlet of the mass spectrometer. The formation of small charged droplets from the spray undergoes evaporation with the conservation of its charges. The decrease in radius of the droplets leads to fission due to charge repulsion. Repeated evaporation and fission produces very small charged particles and eventually gas-phase ions [105, 106].

Some examples of mass analyzers are the time-of-flight (TOF), quadrupole (Q), Fourier transform-ion cyclotron resonance (FT-ICR), orbitrap and ion traps. These mass analyzers used different properties to separate ions based on mass-to-charge (*m/z*) ratios. For example, TOF analyzer uses flight time of the ions travelling in an electric field; the time taken for the ions to arrive at the detector corresponds to its *m/z*. Quadrupole analyzer selects ions by varying electric fields between four rods that generate a stable trajectory only allowing ions with a desired *m/z* to pass through [107]. Orbitrap mass analyzer traps ions around a central electrode in an electrostatic field, where ions assume a circular trajectories and the *m/z* is measured based on the frequency of harmonic oscillations [108]. These mass analyzers can be stand alone or combined in tandem hybrid mass spectrometers such as the Q-TOF and Linear ion trap (LTQ)-Orbitrap mass spectrometers.

Protein abundance can be quantified in a number of approaches. 2D-PAGE and 2D Difference gel electrophoresis (2D-DIGE) are gel-based approaches where quantitation is made by comparing protein staining intensity or with fluorescence labeling. In LC-based proteomics, samples may be labelled with tags such as tandem mass tag (TMT) [109], isotope-coded affinity tags (ICAT) [110] or isobaric tags for relative and absolute quantitation (iTRAQ) [111, 112]. These tags enable concurrent identification and quantitation of proteins from different samples in a single analysis. In addition, stable isotope labeling by amino acids in cell culture (SILAC) introduced in 2002 also allows labeling of proteins in cell culture systems [113].

In recent years, label-free quantitative approaches such as spectra counting, ion intensity quantitation or selective/multiple reaction monitoring (SRM/MRM) are becoming increasingly popular [114]. MRM is a targeted approach where ions from a protein of interest are selected and measured [115]. MRM is usually performed on

a triple quadrupole MS instrument (QqQ) as only chosen peptides belonging to a targeted protein are selected and passed through the first quadrupole. Each of these peptides would enter a collision cell where they are fragmented. The pre-chosen fragmented ions are again selected to be allowed to pass through the second quadrupole and monitored by the mass detector. MRM can be used for accurate quantitation of proteins and peptides.

Two variations of MRM-like approaches are Scheduled MRM high resolution (MRM^{HR}) and the Sequential Windowed data independent Acquisition of the Total High-resolution Mass Spectra (SWATH-MS) workflow. MRM^{HR} is a targeted quantitative proteomics approach performed on a Q-TOF system. By using the knowledge of retention time of each peptide during MRM quantitation, many more peptides could be monitored in a single MS analysis. A pre-analysis run has to be performed to determine and select suitable peptides for every protein that is to be quantified. Based on the pre-analysis run, information regarding peptides and retention time on all the proteins to be monitored is used to build a method for MRM^{HR}.

SWATH-MS is a non-targeted data independent MS scan of all peptides. Instead of monitoring a single peptide, SWATH-MS monitors a windowed mass range in sequential increment [116]. During each acquisition windows, all peptides are fragmented and the resulting fragments are analyzed and recorded. This process is repeated for each sequential overlapping SWATH window until the full mass range is covered. As a result, a complete fragment ion map of a sample is recorded. With this map, post-data processing is carried out and MRM-like data extraction can be performed on any peptide observed in the analysis. In general, label-free

approaches have the advantage in compatibility with more sample types and are more economical by eliminating the need for costly labeling chemicals.

The enormous volume of data generated from high-throughput experiments is another challenge in proteomics. Mass spectrometry vendors often generate output with distinct data formats, which further complicate the burgeoning information pool. Integrated data analytical workflow or pipeline have been developed to deal with the need for ever-increasing data processing and analysis [117]. These pipelines take the forms of automated peptide and protein identification, statistical validation, peptide and protein quantitation and functional annotation [118, 119].

Cancer proteomics - Proteomics in cancer studies may be broadly classified into two categories: expression proteomics and functional proteomics studies [120]. Expression proteomics studies deal with protein abundance measurements and profiling of the proteins with associated isoforms, detecting potential biomarkers for early diagnosis and prognostic monitoring. For instance, in prostate cancer, proteomics has been used to analyse tissue samples, serum, urine and prostatic fluids to identify and validate potential biomarkers that improve specificity and sensitivity compared to prostate specific antigen (PSA) that is currently in clinical use [121]. Reported in a review, several independent studies in renal cancers commonly reported nicotinamide N-methyltransferase (NNMT) as a potential biomarker candidate [122].

Functional proteomics studies, on the other hand, answers more specific biological questions in cancer research. Proteomics has been used to unravel novel mechanisms of tyrosine kinase signaling [123]. The oncogenic fusion protein Bcr-Abl is a constitutive active tyrosine kinase involved in chronic myelogenous

leukemia [124]. The signaling partners of Bcr-Abl responsible for tumor transformation were elucidated through a protein-protein interaction proteomics study [125]. Post-translational modifications of protein also associated with important biological functions [126]. A study was performed on a large scale to quantitatively map phosphorylation events in EGF signaling using phosphoproteomics [127]. Proteomic studies of cancer cells also reveal close relationships between metabolic changes and cancer pathogenesis by characterising changes in metabolic proteins and associated functions [128-130].

Proteomics is capable of providing novel insights by visualizing the global cellular state and capturing information from the whole repertoire of the proteins. These may help resolve the complexity of cancer metabolism, and uncover patterns in the dynamic proteome indicative of disease.

1.4 Motivation of study

Metabolic alteration is a key hallmark of cancer pathogenesis. Understanding the intricate mechanisms behind cancer metabolism could lead to novel therapeutic advancements in cancer treatment. However, metabolic pathways are highly interconnected and under influence of both intrinsic and extrinsic factors. This renders the study of cancer metabolism extremely complicated. High throughput approaches like proteomics enable characterisation of the overall cell state through surveying the whole proteome.

Anti-tumor effects of FXN have been reported in cancer cell line and mouse models and postulated to be involved in modulation of cancer metabolism. Proteomics study of FXN knockout mice also showed extensive perturbation of proteins involved in energy metabolism [131]. However the mechanism of FXN

function in cancer remains largely unknown. Understanding how FXN imposes specific regulation on cancer metabolism may provide valuable insights to guide the development of novel therapeutic strategies.

1.5 Aim and Objectives

In order to unravel the complex function of FXN in cancer cells, a quantitative proteomics approach was employed to investigate the proteome changes in response to stable FXN over-expression.

The objectives of study are as follows:

- To generate stable FXN over-expression (OE) cell lines in the HCT116 cell line system.
- To profile metabolomics and proteomics changes induced by FXN OE.
- To discover meaningful biological processes perturbed by FXN over-expression using bioinformatics and pathway analysis.
- To validate functionally the effect of FXN OE using cell-based assays.
- To map the mechanisms involved in FXN OE using data generated in this study, and test how different pathways could converge and be presented at the phenotypic level.

Chapter 2: Frataxin over-expression in HCT116

2.1 Introduction

In order to investigate the proteome alterations induced by stable FXN over-expression, V5-tagged full-length FXN protein was stably over-expressed in colorectal cancer cell line HCT116. The construct harbouring FXN-V5 was introduced into HCT116 cells by electroporation. Exogenous FXN expression was validated by reverse transcriptase (RT)-PCR and immunoblotting.

2.2 Result

2.2.1 Over-expression of FXN in HCT116

2.2.1.1 Plasmid construction and transfection

To generate FXN over-expressing cells, V5-tagged full-length FXN was transfected into colorectal cancer cell line HCT116 (Section 7.1.2). FXN-V5 fusion gene was cloned into a commercially available plasmid (gift from Dr. Bi Xuezhi), containing blasticidin resistance gene as a selection marker (Fig 2-1). In parallel, a second plasmid containing chloramphenicol acetyltransferase (CAT) was used as the control. CAT is a bacterial enzyme not expressed in mammalian cells. The plasmids were delivered into HCT116 cells using electroporation, a physical transfection technique which uses short pulses of high voltage current to induce a transient period of cellular membrane permeability [132].

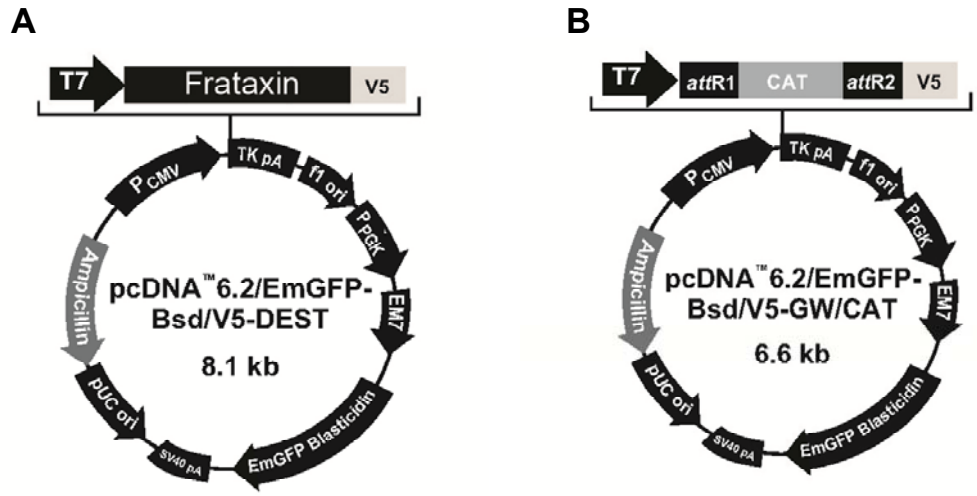

Figure 2-1: Plasmid maps of FXN-V5 and CAT gene. A) Plasmid containing FXN-V5 was transfected into HCT116. The plasmid contains a blasticidin resistance gene which was used for selection. **B)** The control plasmid contains CAT, a bacterial enzyme not found in mammalian cells.

2.2.1.2 Stable cell line selection

After transfection, the cells were maintained in media containing blasticidin for stable cell line selection (section 7.1.3 and 7.1.4). The concentration of blasticidin used was determined with a killing assay where wild type HCT116 was treated with various concentrations of blasticidin.

At a dose of 7.5 µg/ml and 10 µg/ml, no cells were found to be growing or exhibiting healthy cell morphology. When the concentration of blasticidin was reduced to 5 µg/ml, growth was partially inhibited and some features of wild type cellular morphology were retained (Fig 2-2). Based on these observations, a concentration of 7.5 µg/ml was chosen as the selection media to maintain FXN transfected HCT116.

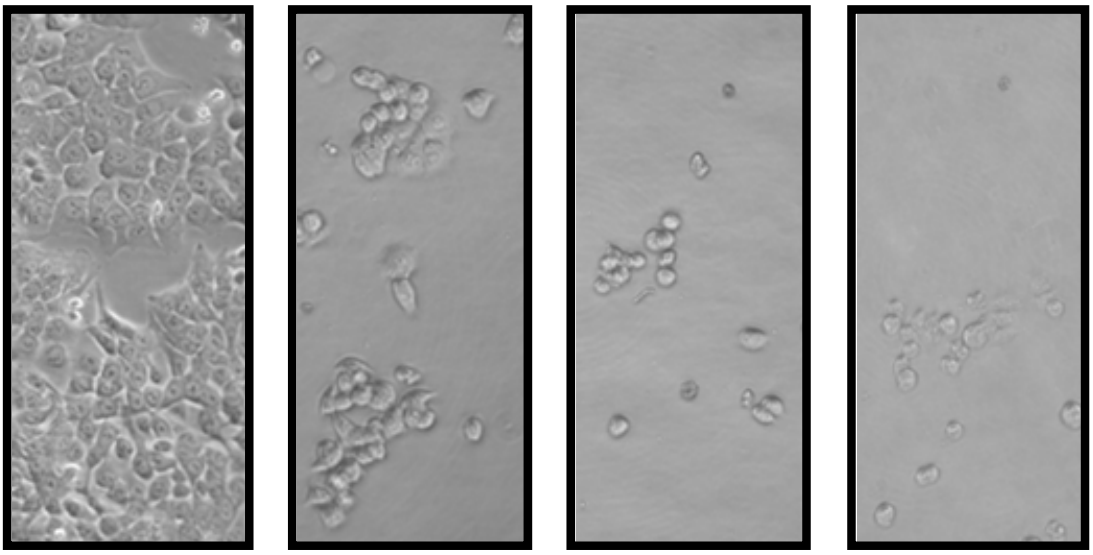

Figure 2-2: Determination of blasticidin sensitivity. The minimum inhibitory concentration of blasticidin in wild type HCT116 was determined by treating HCT116 with increasing concentrations of blasticidin. Cell growth was totally inhibited at 7.5µg/ml of blasticidin.

Transfected cells were maintained in the selection media until individual colonies of cells were visible to the naked eye. These colonies were isolated and further expanded, until sufficient cells were accumulated for validating FNX over-expression.

2.2.2 Validation of FXN over-expression

2.2.2.1 Presence of FXN-V5 fusion mRNA

The presence of FXN-V5 fusion mRNA detected with RT-PCR indicated successful transfection and integration of FXN-V5 gene (section 7.7.2). As FXN is endogenously expressed in colorectal cells, two pairs of primers were designed to distinguish between the endogenous FXN mRNA and FXN-V5 mRNA. The first pair consists of a forward primer specific to 5'-end of the FXN cDNA (FXN_F) and a reverse primer complementary to 3'-end of the FXN cDNA (FXN_R). This pair of

primers would result in the amplification of a gene product belonging to both endogenous FXN cDNA and transfected FXN-V5 fusion cDNA (Fig 2-3). The second pair of primer consists of the same FXN_F primer but a reverse primer complementary to the V5 tag (V5_R) at the 3'-end, which allows only the amplification of a region specific to FXN-V5 cDNA.

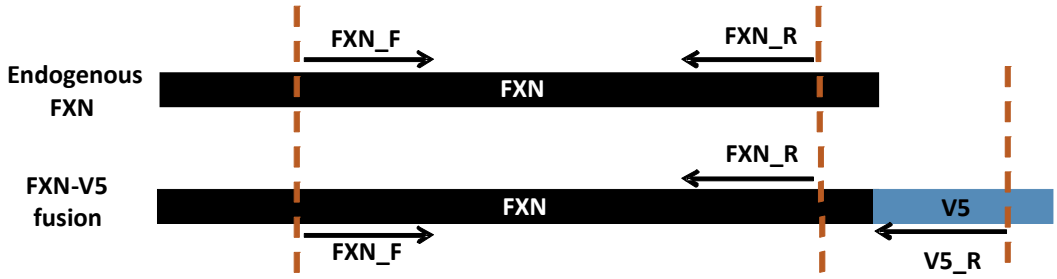

Figure 2-3: Primer design to distinguish endogenous FXN and FXN-V5 mRNA. The primer pair FXN_F and FXN_R would amplify the region corresponding to the endogenous FXN cDNA as well as the internal region of FXN-V5 fusion cDNA. The primer pair FXN_F and V5_R can only amplify the region belonging to a FXN-V5 fusion cDNA.

FXN-V5 fusion mRNA was detected in HCT116 transfected with the FXN construct and not CAT control (Fig 2-4), endogenous FXN mRNA was present in all transfected cell lines and CAT control. Genomic DNA contamination was tested to be negative by the inclusion of control RT-PCR reactions lacking the reverse transcriptase enzyme. As shown in figure 2-4, no bands were observed in lanes without reverse transcriptase enzyme.

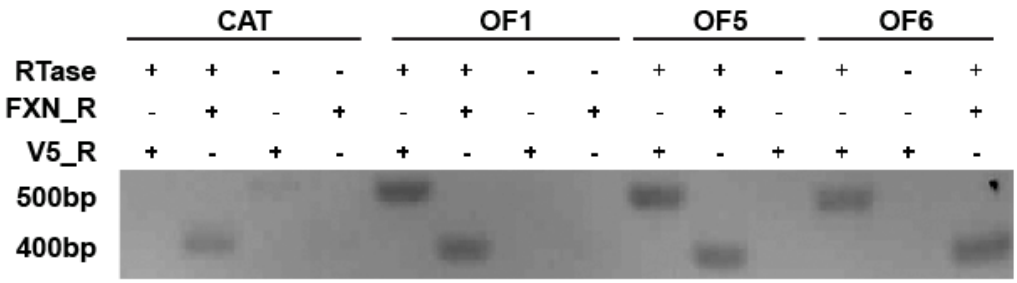

Figure 2-4: RT-PCR detects the presence of FXN-V5 fusion mRNA. Two reverse primers, FXN_R and V5_R were used to distinguish endogenous FXN and FXN-V5 mRNAs. All reactions contain FXN_F primer and either FXN_R or V5_R. Bands corresponding to FXN-V5 fusion (500bp) were detected in OF1, 5 and 6 and not in CAT control. Wild type FXN mRNA was detected in all cell lines. Negative control without reverse transcriptase confirmed the absence of genomic DNA contamination.

2.2.2.2 Detection of FXN-V5 recombinant protein

After the presence of FXN-V5 mRNA was detected, expression of the FXN-V5 fusion protein was next confirmed. FXN is synthesized as a full-length precursor (23kDa) in the cytosol and transported into the mitochondria where it is cleaved in a two-step process, resulting in an intermediate form (19kDa) and subsequently the matured form (17kDa) [133]. Fusion FXN-V5 protein could be processed into its mature/active form in a manner similar to endogenous FXN (Fig 2-5). The addition of V5 tag increases the molecular weight by 5kDa, resulting in an intermediate FXN-V5 (iFXN-V5) of 24kDa and a mature FXN-V5 (mFXN-V5) of 22kDa.

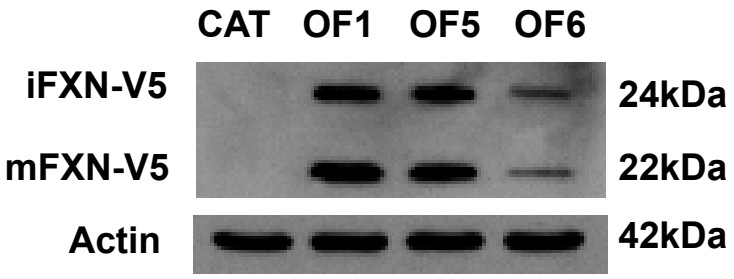

Figure 2-5: Immunoblot detection of FXN-V5 fusion protein. Using anti-V5 antibodies, recombinant FXN-V5 protein was detected in OF1, 5 and 6 and not in CAT control. FXN is synthesis as a precursor and is first cleaved into intermediate FXN-V5 (24kDa) and subsequently into mature FXN-V5 (22kDa).

2.3 Discussion

In this study, three clones containing over-expressed FXN (OF1, OF5 and OF6) were used as biological triplicates in order to minimize artefacts due to the transfection procedure (random insertion of the recombinant FXN genes into the cells) and other biological variations. Herein, only results that showed consistent and statistically significant difference in all triplicates were considered valid. This experimental setup boosts confidence and robustness in the findings involving biological changes as a result of FXN over-expression.

Secondly, non-functional protein CAT was over-expressed as a control, to account for artefacts resulting from the over-expression procedure itself and associated overload on the protein synthesis machinery in any biological system. This further strengthens the confidence in this study model.

Western blot showed the FXN-V5 protein product was also processed to its immediate and mature form, suggesting that the extent of over-expression has not overwhelmed the cellular machinery for FXN modifications and processing. The

effect of FXN over-expression in HCT116 was investigated using these three FXN over-expression clones (OF156) and CAT control.

Chapter 3: Metabolomics and proteomics profiling of FXN OE

3.1 Introduction

"Omics" approaches were employed to characterize metabolomic and proteome changes in HCT116 cells after FXN over-expression. As FXN is closely associated with metabolic pathways, a metabolomics study was performed to investigate the regulative effect of FXN on cellular metabolite levels. To enable this, metabolite extraction protocol was first optimised before a metabolomics comparison was performed between OF and CAT cells.

In addition, a quantitative proteomics analysis was also carried out to identify proteins with altered abundance for further characterization of altered biological processes. A 4-plex iTRAQ labeling approach was adopted to simultaneously annotate and quantify the CAT, OF1, OF5 and OF6 proteomes. Using proteins with altered abundance, pathway enrichment analysis was performed to highlight key biological pathways that were altered in OF cells. To verify the changes in protein levels identified by iTRAQ, SWATH-MS, a MRM-like approach was used.

3.2 Result

3.2.1 Optimization of metabolite extraction methodology

To maximize metabolites extracted from the cells, three different extraction methods were tested: i) 80% methanol, ii) 50% ACN and iii) 80% ACN (section 7.6.1). These solutions were recommended for metabolites extraction from mammalian cells in an evaluation study [134]. Extracted metabolites were separated by LC on a hydrophilic interaction chromatography (HILIC) column and analyzed using a Q-TOF MS. LC gradient was also optimized to enhance separation and increase the coverage of metabolites identified.

Among the 3 extraction methods, extracting with 50% ACN resulted in lowest total ion intensity, indicating the lowest yield while 80% ACN and 80% methanol showed similar yields and total ion chromatography (TIC) profiles (Fig 3-1). However, when metabolites were extracted in triplicate and analyzed, methanol extraction gave better reproducibility (Fig 3-2). Therefore, 80% methanol extraction was chosen as the best extraction method.

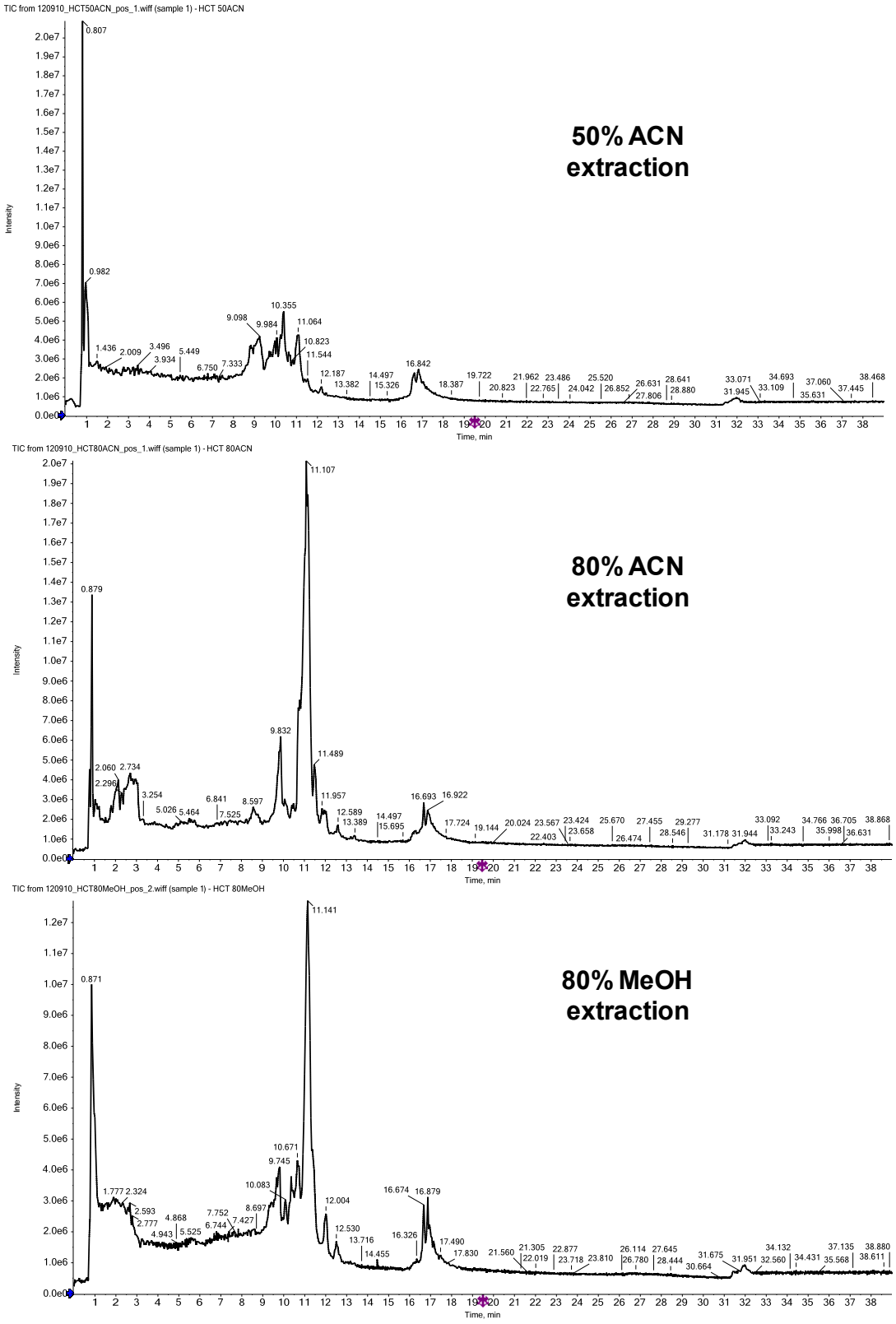

Figure 3-1: TIC profile of metabolites with different extraction methods. TIC elution profile corresponding to each extraction method as indicated on each panel. Extraction with 50% ACN produced the lowest total intensity among the three extraction methods. TIC profiles of 80% ACN and 80% methanol were similar.

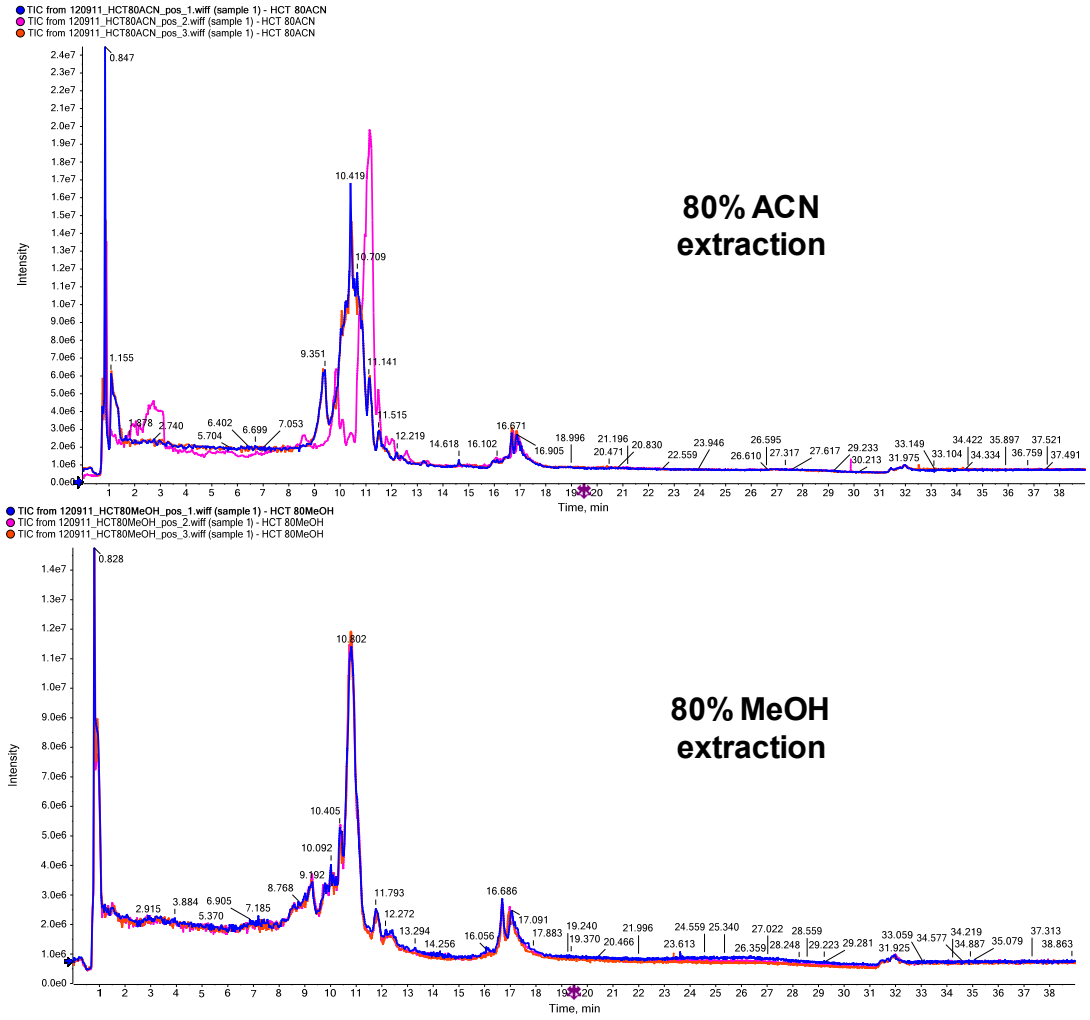

Figure 3-2: Comparisons of extraction showed difference in reproducibility. TIC profile showing 80% methanol (lower panel) had better reproducibility compared to 80% ACN (upper panel) when analysed in triplicates.

3.2.2 Metabolomics profiling of FXN OE

Metabolites from CAT and OF156 were extracted and analyzed as described in section 7.6. XCMS online was used to perform data visualization and MarkerView™ was used for peak detection, quantitation and statistical analysis (section 7.6.5).

3.2.2.1 Mirror plot shows changes in metabolite profile in OF156

A mirror plot was generated using XCMS online to compare the metabolite profile of OF156 against CAT (Fig 3-3). The mirror plot compares features across retention time and displays features that are regulated by more than 1.5 fold as circles according to mass-to-charge. Only features with significant fold change (p<0.01) were displayed. Green circles indicate fold change >1.5 while red circles indicate fold change < -1.5. The size of circle corresponds to Log[fold change], i.e., a larger circle represents a greater fold change and a smaller circle indicates a smaller fold change. Color intensity represents p-value; a darker circle represents a smaller p-value and more significant regulation.

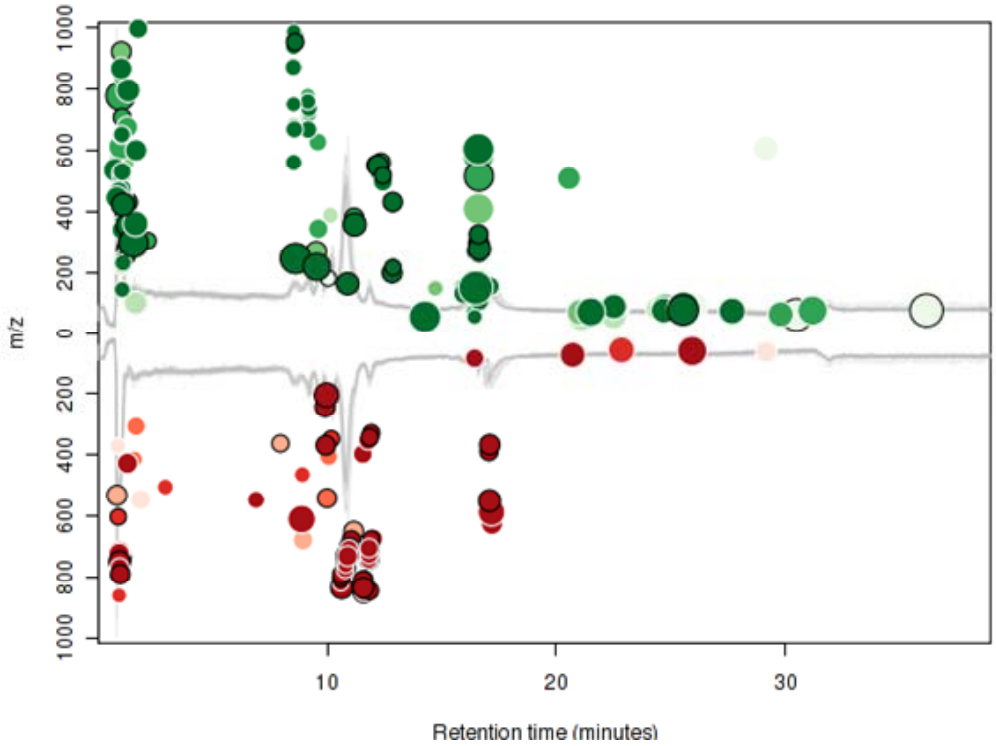

Figure 3-3: Mirror plot depicting changes in metabolite profile. The mirror plot illustrates features or peaks with fold change greater than 1.5 and $p\leq$ 0.01. Green circle represents an increased fold change; red circle indicates a decreased fold change. The size of the circle corresponds to Log[fold change], a larger circle represents a greater fold change. Color intensity represents p-value. A darker circle represents a smaller p-value.

3.2.2.2 OF156 and CAT have unique metabolic signatures

Principle component analysis (PCA) reduces complexity of metabolite information and compresses multi-dimensional data in CAT and OF156 to highlight similarities and differences between CAT and OF156 (Fig 3-4A). From the PCA plot, CAT samples were clustered in the left, away from OF1, 5 and 6 clusters in the right. The purpose of multidimensional scaling (MDS) is to provide a visual representation of the pattern of proximities (i.e., similarities or distances) within a set of samples (Fig 3-4B). From the MDS plot, it is visible that CAT and OF156 have uniquely different metabolic signatures.

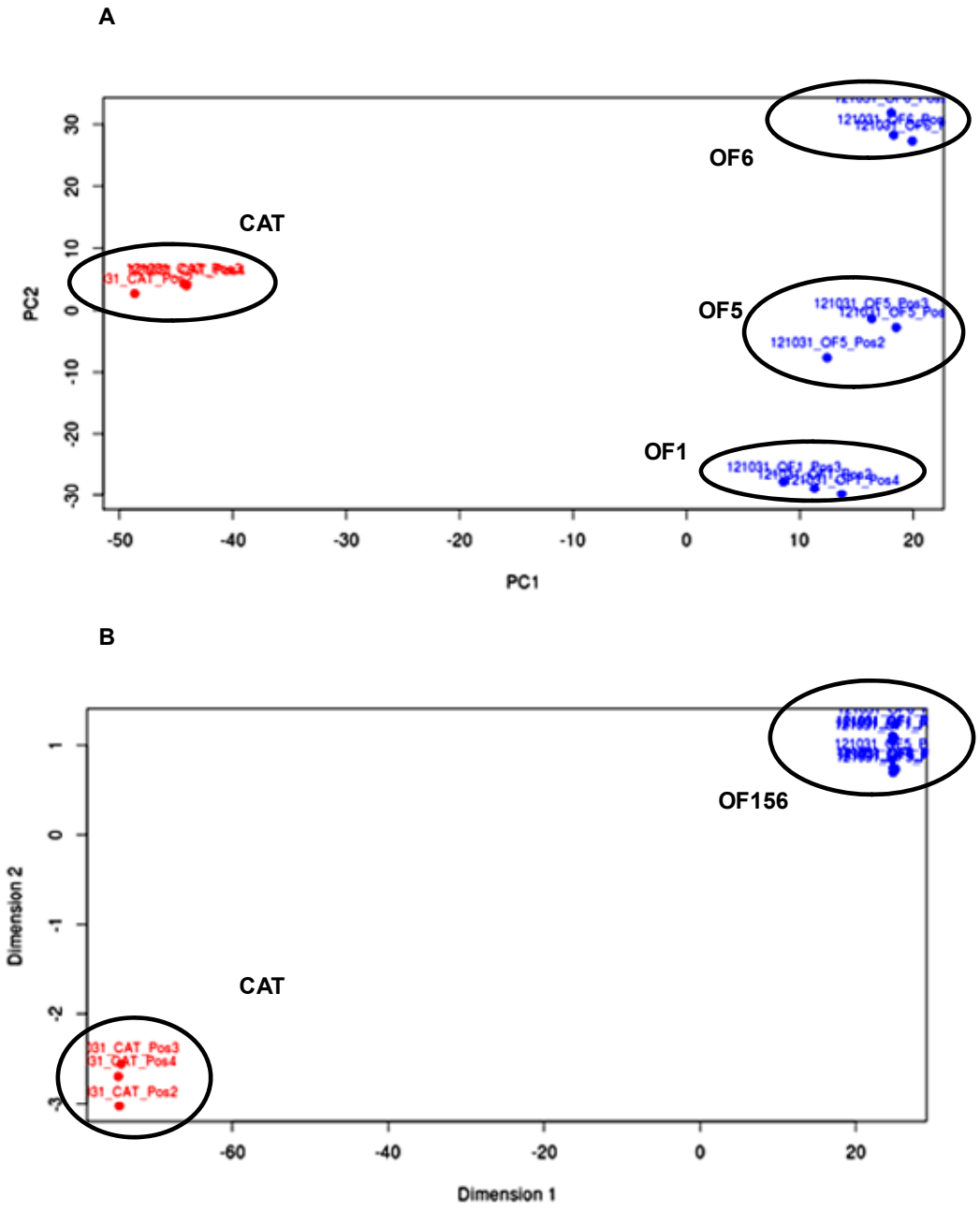

Figure 3-4: CAT and FXN OE have different metabolic signatures. **A)** Principal component analysis showed that CAT is clustered away from OF1, 5 and 6. Each sample is analyzed in triplicates; points in red represent runs from CAT and points in blue represent runs from OF1, 5 and 6. **B)** Multidimensional scaling showed CAT and FXN OE possess unique metabolic signatures. Each sample is analyzed in triplicates; points in red represent runs from CAT and points in blue represent runs from OF1, 5 and 6.

3.2.2.3 Identification of metabolites with altered concentration

MarkerView™ software was used to quantify the metabolites. A total of more than 4000 peaks were detected for each analysis combining positive and

negative modes. Within 2100 statistically significant peaks that were further analysed (p<0.05), about 1000 had good MS/MS spectra, which were manually matched using the METLIN database. Out of these, 37 peaks have good matches in the database (Fig.3-5; Appendix I).

A

METLIN ID	Name	METLIN Score (0-100)	precursor	precursor ΔPPM	Structure	Spectrum Matching
370	Glycerophosphocholine	100	M+H	0	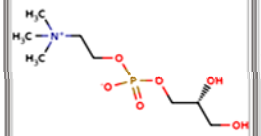	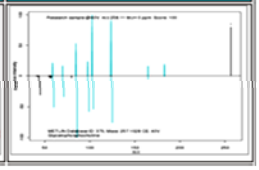

B

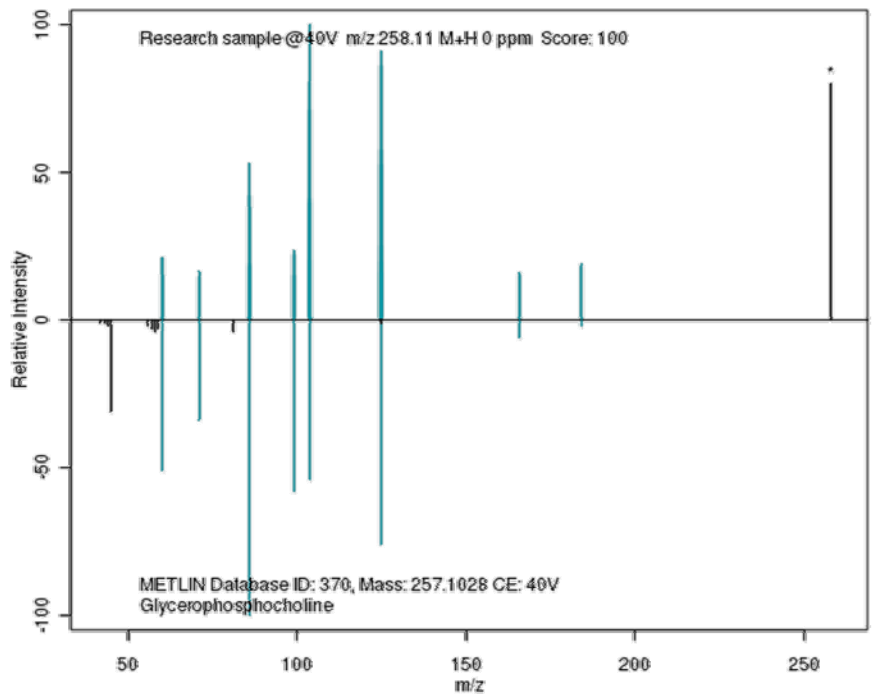

Figure 3-5: Metabolite identification in METLIN database. A) MS and MS/MS of each precursor were used for database matching. When a match is made, the database returns the matched ID and a score to measure the quality of the match, adduct of the metabolite, mass error of the precursor, structure and spectrum matching. **B)** Mirror plot of query MS/MS spectrum (Top) matched to MS/MS spectrum in the database (Bottom). Teal lines represent matched peaks.

3.2.2.4 Discussion

From the mirror plot, a number of features could be observed at the start of the gradient. As a hydrophilic column was used to separate the metabolites, these features would correspond to highly hydrophobic molecules. Most metabolites eluted around the 10 minute mark as observed in the total ion chromatography with masses spread across the whole mass range (Fig. 3-3). A smaller number of the more hydrophilic metabolites were subsequently eluted at a later time between 20 to 30 minutes and these tend to be lower molecular weight species, suggesting this group to be small polar molecules.

PCA and MDS plot demonstrated CAT and OF156 exhibited differences in metabolic profiles, implying a unique metabolic alteration had occurred as a result of FNX OE. Although MDS showed OF1, OF5 and OF6 clustered together, PCA revealed slight differences among them. Nonetheless, the small number of metabolites identified was not sufficient to conclude the extent of metabolic regulation. This could be attributed to a few reasons stated below

Firstly, available databases are far from complete. Identification of a metabolite relies on accurate mass in MS as well as knowledge of the fragmentation pattern produced during MS/MS. Existing databases often lack MS/MS spectra for many metabolite precursors and fail to capture slight differences in fragmentation pattern produced by different mass analyzers. Secondly, spectra matching software are severely lacking. Identification of metabolites in this study was performed manually for each metabolite precursor and its MS/MS spectrum individually. Thirdly, coverage of metabolites detected were limited as seen in Fig 3-1 and discussed earlier in this section. The separation of the metabolites could be improved as the highly hydrophobic species were eluted within the first minutes,

hardly with any separation. Due to the high complexity of metabolites, a pre-fractionation step would be ideal for improving coverage. High diversity of metabolite species also leads to the differential ionization efficiency issue and detection of these species.

To summarize, triplicates of FXN OE cells showed concerted differences in their metabolic profile compared to CAT control, highlighting a major shift in cellular metabolism from FXN over-expression. In addition, metabolic analysis was able to identify and quantify both oxidized and reduced form of glutathione. This finding and its associated implications will be discussed in details in section 4.2.3.

3.2.3 iTRAQ proteomics profiling of FXN OE

3.2.3.1 Reproducibility in OF156 biological triplicates

In order to determine if the biological triplicates OF1, OF5 and OF6 were reproducible in iTRAQ quantitation, a regression analysis was performed. Log fold change of all peptides identified from each sample were plotted against one another, as shown in Fig 3-6. Based on the r^2 value of 0.7507 to 0.8692, a fairly good correlation was obtained. This indicates that reproducibility in MS analysis was good within the three biological triplicates.

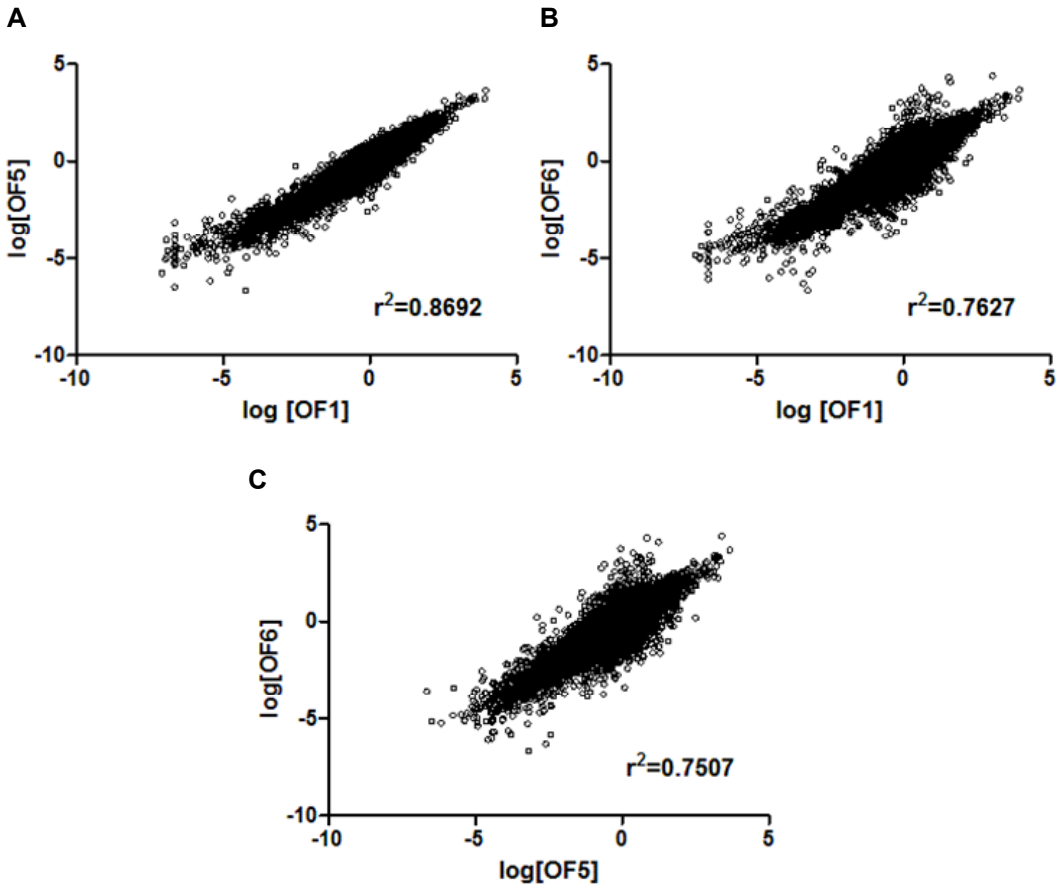

Figure 3-6: OF156 biological triplicates showed high reproducibility in iTRAQ. Regression plots of FXN OE triplicates. **A)** Log fold change of OF1against OF5, r^2 = 0.8692. **B)** Log fold change of OF1 against OF6, r^2=0.7627. **C)** Log fold change of OF5 against OF6, r^2=0.7507.

3.2.3.2 Summary statistics and cutoff threshold

In the iTRAQ analysis, a total of 2313 proteins were identified with unused protein score ≥1.3 (95% confidence). Proteins with changes in abundance were determined by the following statistical cut-offs: (i) proteins identified by a single peptide were removed from the analysis; (ii) a cut-off threshold ratio of greater than or equal to1.3, or less than or equal to the reciprocal value (0.77) was used [135]; (iii) Only proteins with ratios that met the threshold in all three biological triplicates were considered as having altered abundance (Table 3-1). By applying these selection criteria, differential abundance of 276 proteins were detected. Among these, 146 were increased while 130 had a reduction in protein level (Appendix II).

Table 3-1: iTRAQ summary statics.

Filtering criteria	Protein
Protein identified with protein score ≥ 1.3†	2313
Total protein change	276
Increased protein level (≥1.3)	146
Decreased protein level (≤0.77)	130

†False discovery rate of protein identification is less than 1%.

The coefficient of variation between biological triplicates was also calculated to determine the consistency of fold change. The average coefficient of variation was 21.46%, indicated relatively consistent fold changes among OF156. More than 90% of these 276 proteins have a coefficient of variation of less than 40%, and around 3% had a coefficient of variation of more than 50% (Fig 3-7).

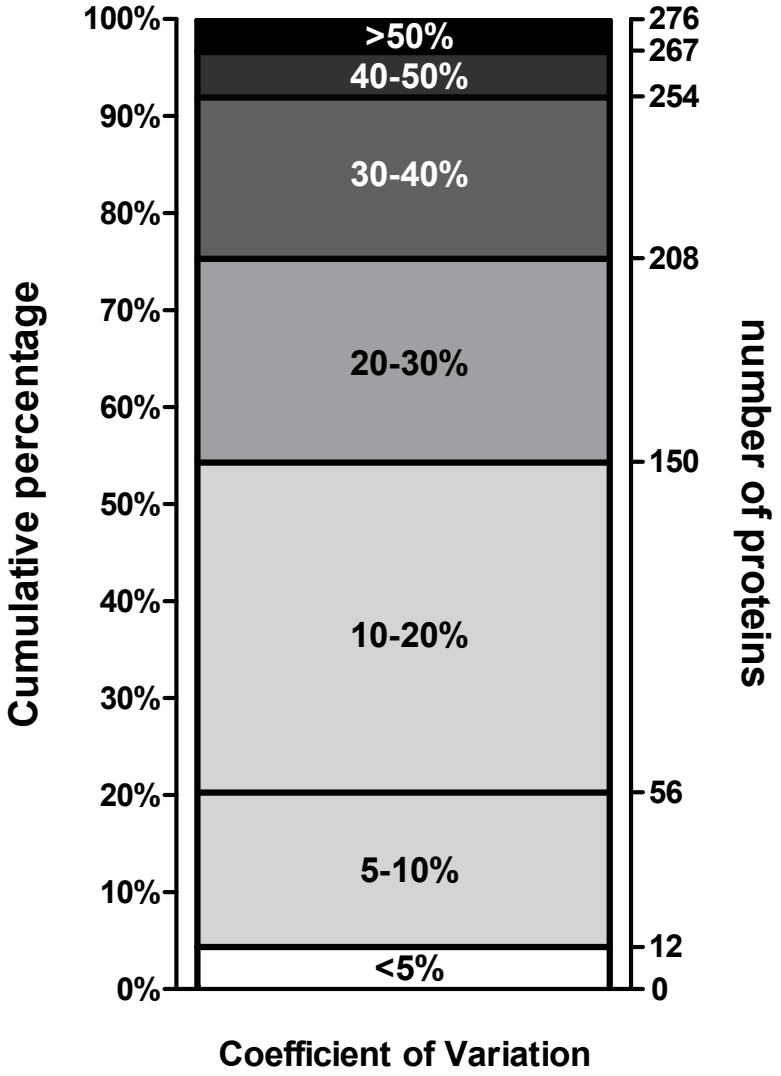

Figure 3-7: Coefficient of Variation between biological triplicates. Boxes in bar chart displaying coefficient of variation of log fold change between biological triplicates. Left axis represents the cumulative percentage of proteins with altered abundance. Right axis represents number of proteins. More than 90% of proteins have a coefficient of variation less than 40%. Average coefficient of variation is 21.46%.

3.2.3.3 Uniprot keyword of proteins with differential abundance

In order to visualize changes in protein abundance induced by FXN over-expression, these proteins were mapped using Uniprot keywords (Fig 3-8). The UniProt keyword is a set of controlled vocabulary developed to describe and assign functions to each protein. Majority of these proteins are involved in transport, transcription and mRNA processing. A smaller portion of proteins play a role in cell

cycle, DNA damage response, apoptosis and differentiation. There is also a group of proteins that are involved in a variety of metabolic processes such as protein biosynthesis, lipid metabolism, amino-acid biosynthesis. These keywords describe the function of the perturbed proteins providing insights to the effects of FXN over-expression.

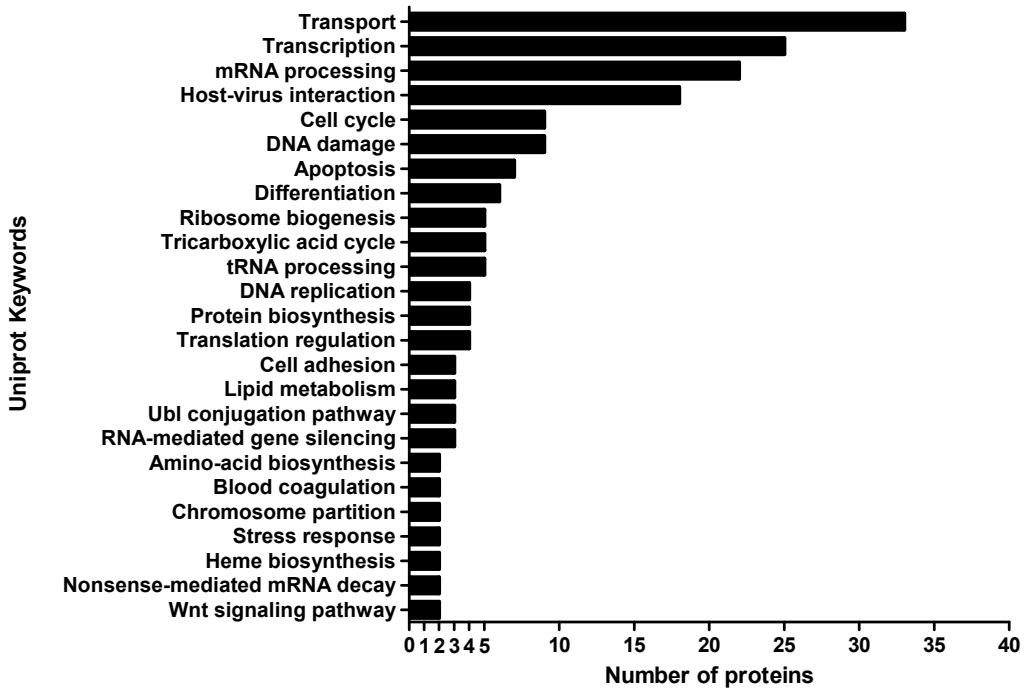

Figure 3-8: Proteins with altered abundance, stratified by Uniprot Keywords. Number of proteins with differential abundance in FXN OE annotated by each Uniprot keyword. Uniprot keywords are derived from a controlled vocabulary, similar to gene ontology.

3.2.3.4 KEGG pathway enrichment using DAVID

A pathway enrichment analysis was performed using Database for Annotation, Visualization and Intergrated Discovery (DAVID), a web-based annotation and analysis software. Using statistical tools, DAVID maps proteins that are over-represented in the present dataset to Kyoto Encyclopaedia of Genes and Genomes (KEGG) pathways (Fig 3-9).

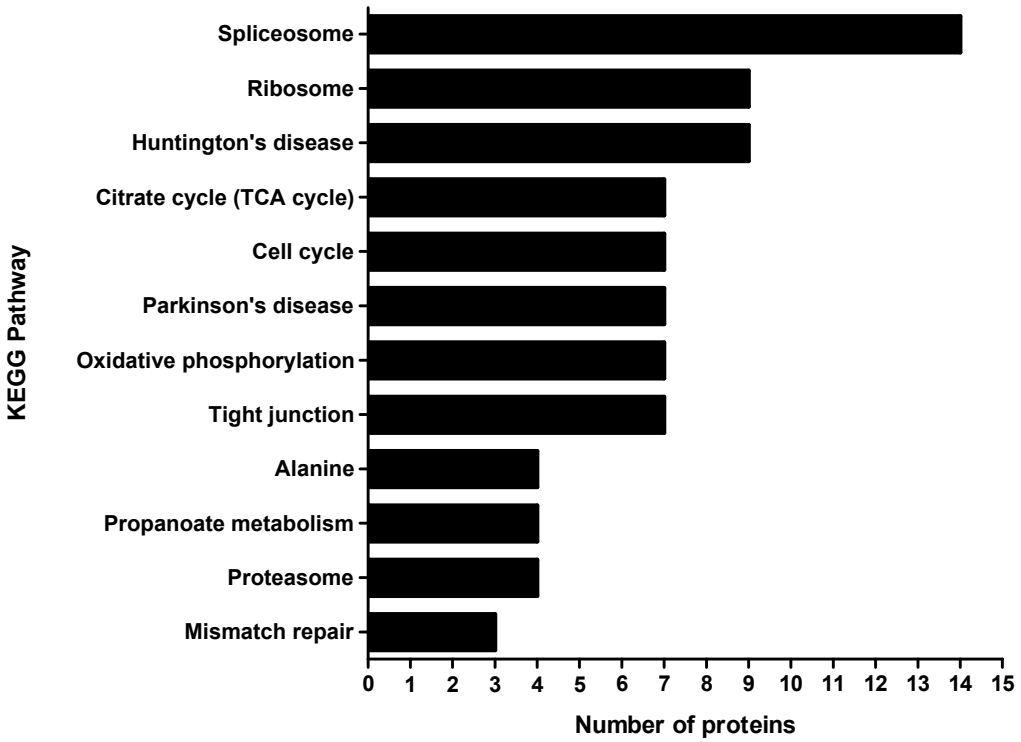

Figure 3-9: KEGG pathways over-represented by proteins with altered abundance. The pathways listed on the vertical axis are pathways which are significantly enriched (a modified Fisher's Exact test, EASE score <0.01). The horizontal axis denotes the number of proteins in each of the pathways listed.

Briefly, enrichment analysis may be understood as significantly higher number of proteins belonging to a biological pathway or process compared to an expected value of the dataset, as if the dataset were generated from random sampling of the proteome. Pathways such as TCA cycle, cell cycle and OXPHOS were significantly enriched in the present dataset, and these groups of related proteins present in our dataset were not due to random occurrences.

3.2.3.5 Verification of iTRAQ with SWATH™

Data acquired from SWATH analysis were subjected to similar cutoff criteria to shortlist proteins that have differential abundance. Proteins must have a threshold ratio of greater than 1.3 or less than its reciprocal value (0.77), and show

consistent ratio in the same trend for all triplicate OF1, OF5 and OF6. From a total of 1985 proteins identified, 331 were found to have differential abundance. This list features an overlap of 19 proteins that were also significantly changed in the iTRAQ analysis, of which, ratios of 13 proteins agree with iTRAQ data (Fig 3-10). These proteins are presented in Appendix III.

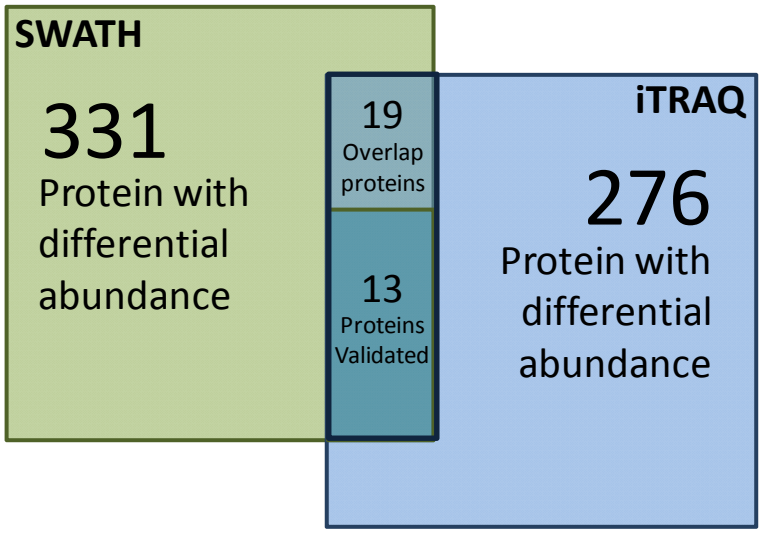

Figure 3-10: Venn diagram depicting overlap between iTRAQ and SWATH™ analyses. A total of 331 and 276 proteins were found to be differentially altered in SWATH and iTRAQ analysis respectively. 19 of these proteins were found in both methods, of which, 13 proteins were validated.

3.2.3.6 Discussion

In this study, a quantitative proteomics approach was used to elucidate the effect of FXN OE. The experimental design and method of data analysis boosted the confidence of identifying true biological changes. The use of biological replicates and only including common proteins as part of highly stringent selection criteria facilitated the identification of true biological events against background "noise" due to biological variations. OF156 had reproducibility in total peptide quantitation and the relatively low coefficient of variation in the fold changes of the shortlisted

targets demonstrated consistent biological effects which further augmented the quality and confidence of the findings.

The use of UniProt keywords is an easy and quick method to visualize the overall characteristics and functions of regulated protein targets, giving a hint into perturbed biological functions. Pathway enrichment analysis determines how these proteins relate to each other, by highlighting over-represented groups of proteins in common pathways or biological processes. Identifying biological pathways associated from these clusters of proteins provided more meaningful information than looking at individual protein functions.

From pathway enrichment analysis, pathways in cell cycle, OXPHOS and TCA cycle became the focus of this study. Considering the function of FXN, these pathways can be affected by FXN over-expression and could be the mechanism behind its anti-cancer effect. However, there is a need to further verify the iTRAQ result before any valid conclusion could be drawn.

Current MRM-like workflows available on hybrid QqTOF instrumental setup are the MRM^{HR} and SWATH-MS workflow as described in section 1.3.2. For both of these workflows, a common drawback is the lack of adequate interrogation for complex samples such as mammalian cell lysate. Both methodologies are currently performed on a 1-D LCMS platform. Without sufficient separation, desired peptides are often not detected in a complex sample, especially considering that the iTRAQ experiment was performed on a 2-D LCMS platform. However, SWATH-MS is capable of recording the maximum information regarding each sample, increasing the chance of successfully detecting desired peptides. SWATH acquisition also allows a retrospective interrogation of data in the future in the event

of new questions raised. Out of the two workflows, SWATH-MS was chosen for verification of the iTRAQ targets.

After data were acquired from SWATH acquisition, similar criteria were applied to isolate proteins with significant changes in abundance. This list of proteins was compared to the iTRAQ result. Nineteen proteins out of 276 iTRAQ targets were detected in the SWATH analysis and the abundance trend of 13 proteins were successfully verified. The low amount of overlaps could be attributed to a few reasons.

Analytical method – Firstly, iTRAQ is an information dependent acquisition whereas SWATH is a data independent approach. The algorithms for peptide selection during analysis are vastly different. Secondly, collision energy parameters used for fragmentation in iTRAQ and SWATH are different. This could lead to different fragmentation patterns even for the same peptides, resulting in a different set of total peptides identified and proteins hits from search algorithms.

Separation of samples – iTRAQ analysis was performed using 2-D LC separation while SWATH uses single reversed-phase LC separation, which likely has insufficient resolving power for complex samples. This resulted in a very different set of proteins identified.

Differences in sample – the major difference in sample would be the presence of the iTRAQ reagents linked to each peptide, which potentially changes the size of the peptides and chemistry of the sample. Loading of peptides on to the column and subsequent elution step could be affected as the iTRAQ reagent could change the hydrophobicity of peptides. Moreover, the label moiety also affects the amount of collision energy absorbed and the fragmentation patterns [136].

The changes in protein level of many iTRAQ targets were unable to be validated due to the lack of overlapping proteins identified in both methods. Therefore, presented in the next chapter of the thesis, functional assays were performed to validate the biological processes from iTRAQ findings as well as to investigate molecular mechanisms behind FXN OE.

Chapter 4: Functional validation of proteome changes in FXN OE cells

4.1 Introduction

Inhibition of tumor growth by FXN over-expression was demonstrated in various studies as discussed before. However, the exact mechanism of the anti-tumor effect was not known. In order to understand the molecular mechanism behind the phenotypic changes associated with FXN over-expression, proteome of HCT116 over-expressing FXN was characterized. HCT116 was used as a platform to investigate the changes induced by FXN over-expression since it is a well-studied colorectal cancer cell line. Based on the iTRAQ dataset, key biological networks and their protein components that are of relevance to the cancer phenotype were highlighted. In this section, changes in OXPHOS, redox status and cell cycle/cell proliferation were examined to further analyse and functionally validate the iTRAQ findings.

4.2 Results

4.2.1 Cell cycle and cell proliferation

Cell cycle progression and proliferation are key biological processes highlighted in pathway analysis of the iTRAQ data. A number of proteins related to cell cycle and growth were perturbed due to the over-expression of FXN. One such protein that is directly associated with cell cycle is cyclin dependant kinase 4 (CDK4). CDK4 was found to be elevated (2.164 ± 0.563) in OF cells. The role of CDK4 in cell cycle and cell proliferation is further explored and discussed in the subsequent section.

4.2.1.1 OF cells have increased CDK4 and cyclin D protein level

CDK 4 forms a complex with cyclin D in early G1 phase of the cell cycle. The protein level of CDK4 and cyclin D were validated independently using western blotting (Fig 4-1). Both iTRAQ and western blot data confirmed the increase in protein levels of CDK4 and cyclin D in OF1, OF5 and OF6.

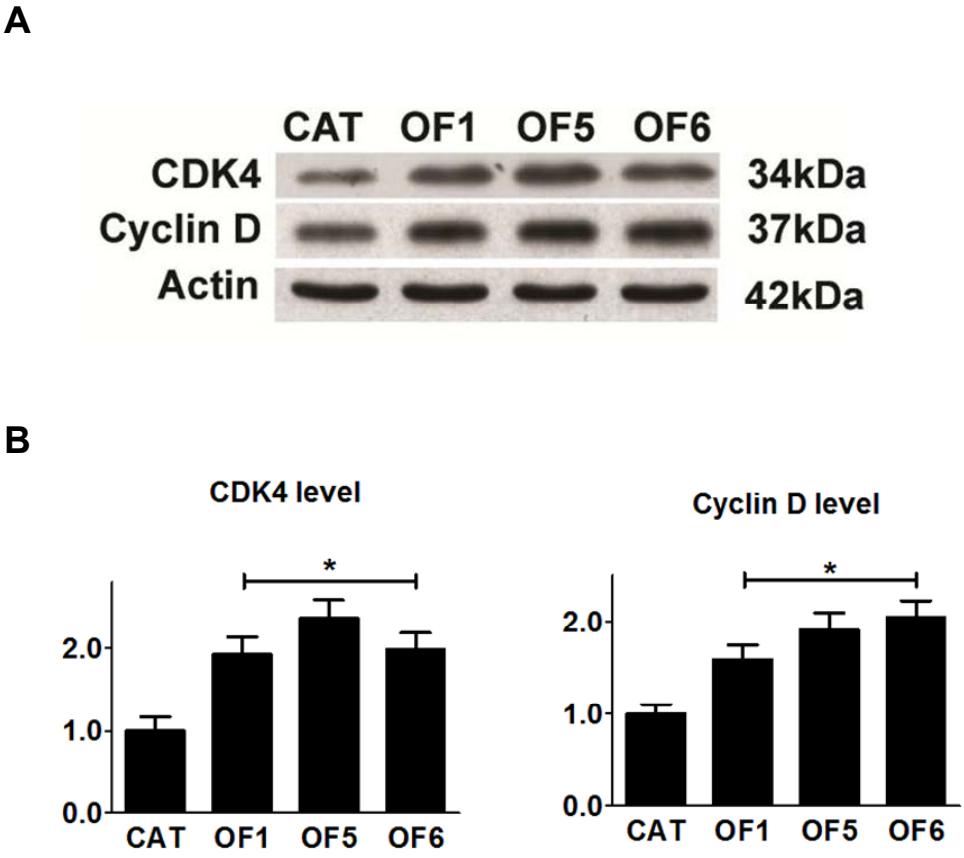

Figure 4-1: G1 phase markers are elevated in OF cells. A) Immunoblotting of cell cycle protein CDK4 and cyclin D showed higher protein level in FXN OE cells. Actin is used as the internal loading control. **B)** Histogram shows densitometric measurement of the fold change in respective cell cycle protein level compared to CAT control. * $p<0.05$

4.2.1.2 Proliferation assay shows growth inhibition in OF cells

Since changes in the levels of cell cycle markers were observed, a proliferation assay was performed to measure the growth rate of CAT and OF cells (section 7.2.2). OF cells exhibited a significantly lower proliferation rate compared to CAT (Fig 4-2) by 48 hrs after seeding. The same growth inhibition persisted to 72 hours. Growth rates of the FXN OE triplicates were similar and showed no significant differences among them.

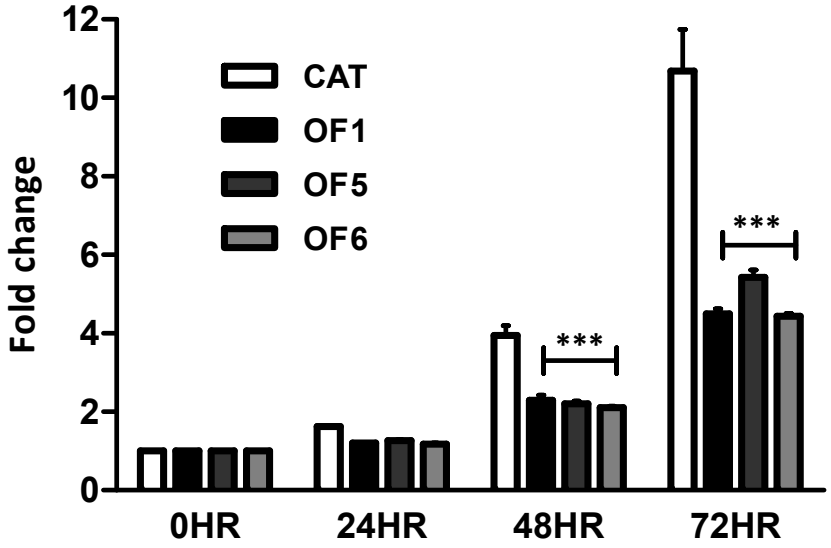

Figure 4-2: Growth inhibition of FXN OE cells. Cell proliferation assayed over a course of 72hr. FXN OE cells had a lower proliferation rate compared to CAT control cells. Columns represent mean from triplicates and error bar represents S.D.,*** $p<0.001$

4.2.1.3 FXN OE induces p21/ p27 and decreases late G1 phase proteins.

The abundance of other cell cycle proteins was determined using western blot to further elucidate the role of FXN over-expression in the perturbation of cell cycle (Fig 4-3). p21 and p27 are cell cycle inhibitors that interact and inactivate various CDKs and cyclins [137], thereby inhibiting cell cycle progression.

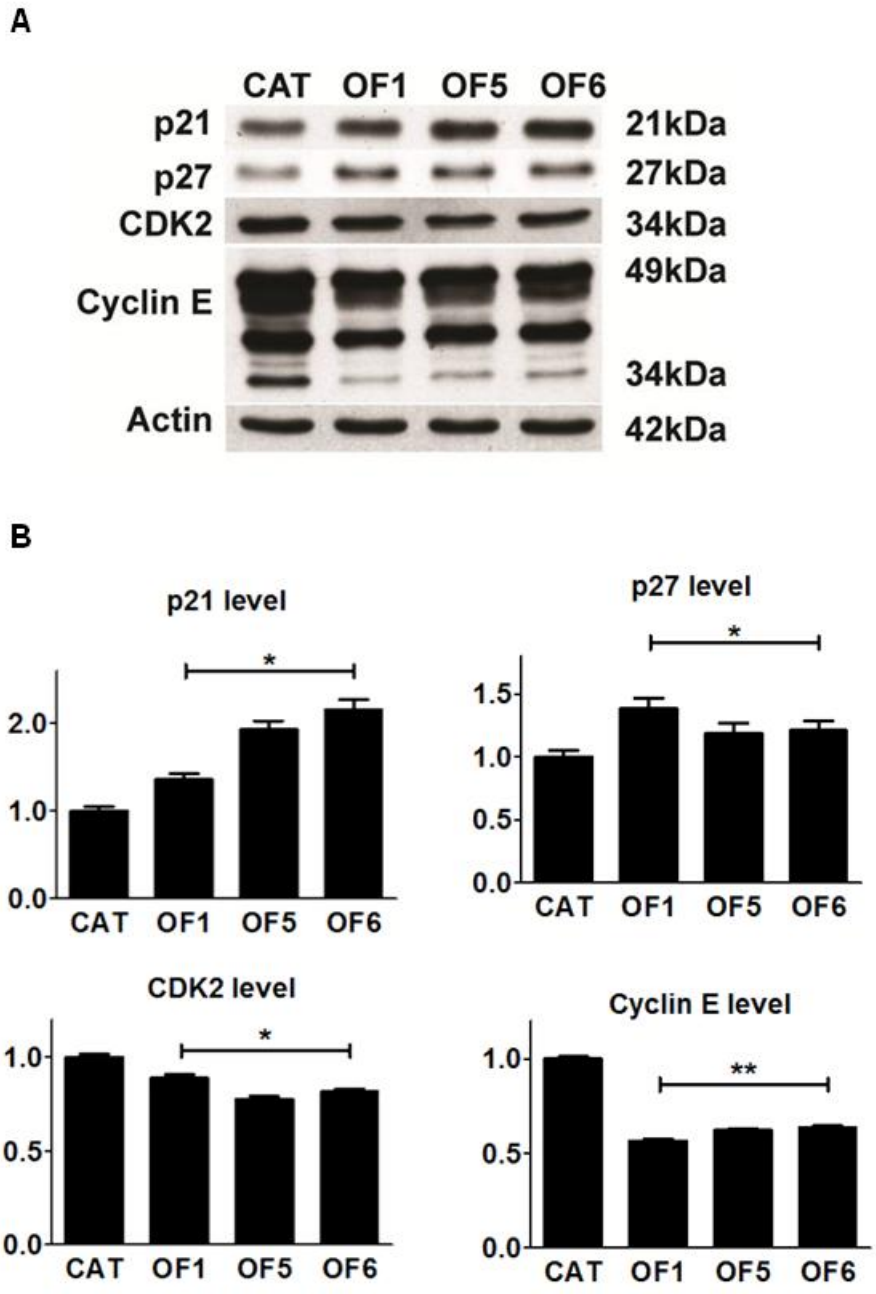

Figure 4-3: p21 and p27 inhibit expression of late G1 phase proteins. A) Immunoblot depicting higher levels of cell cycle inhibitors p21 and p27 in FXN OE cells. Late G1 phase proteins CDK2 and cyclin E are lower in FXN OE cells. **B)** Histogram shows densitometric measurement of the fold change in respective cell cycle protein level compared to CAT control. * $p<0.05$, ** $p<0.01$

Immunoblotting analysis demonstrated that the protein level of p21 and p27 were increased in OF1, OF5 and OF6, providing alternative explanation for the

inhibition of cell cycle. CDK2 and cyclin E are late G1 phase cell cycle proteins that are involved in G1 to S phase transition. Western-blot analysis also showed that FXN OE reduced the protein level of CDK2 and cyclin E compared to CAT control.

4.2.1.4 FXN OE inhibits G1 exit

Increase in cell cycle inhibitors and decrease in late G1 phase cell cycle proteins further suggest that FXN OE could modulate the cell cycle. In order to investigate perturbations to the cell cycle, cell cycle analysis was performed (section 7.3.1). Population of cells in each cell cycle phase was determined using propidium iodide (PI), which stains cellular DNA and the amount of DNA was quantified by flow cytometry. Using ModFit™, a cell cycle profile modeling software, the distribution of cells in each cell cycle phase was determined (Fig 4-4A). OF1, OF5 and OF6 showed a significant increase in the proportion of cells in G1 phase and a correspondingly lower proportion of cells in S phase, clearly suggesting a delay in G1 exit.

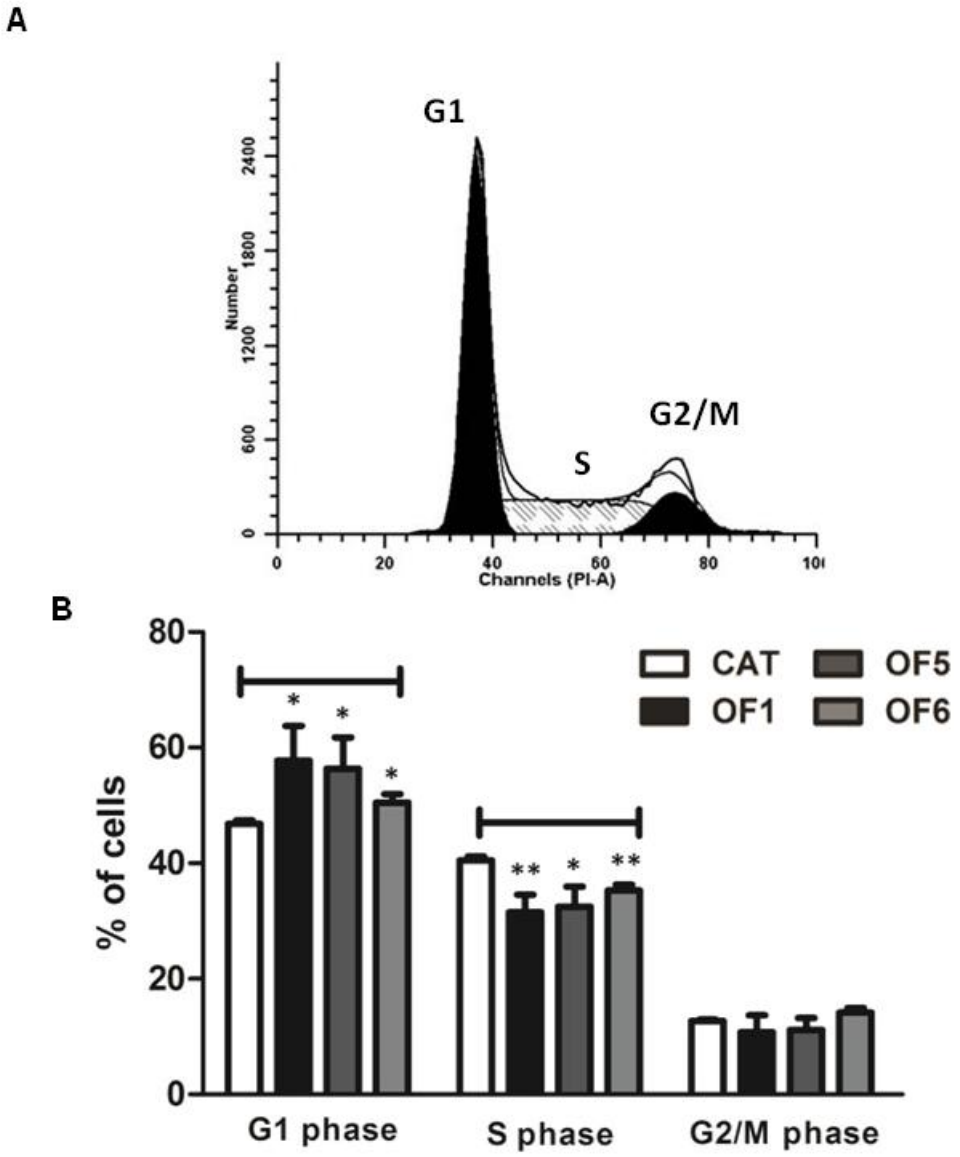

Figure 4-4: FXN OE cells had an extended G1 phase. A) Representative plot of cell cycle analysis using ModFiT™ modeling software. Percentage of cells in various cell cycle phases was determined by model fitting. **B)** Histogram shows the percentage of cells in each cell cycle phase for OF1, 5, 6 and CAT. FXN OE cells had a significantly prolonged G1 phase compared to CAT control. Columns represent mean from three flow cytometry experiments; error bar represents S.D.; * $p<0.05$, ** $p<0.01$

4.2.1.5 Decreased cell proliferation could be due to G1 inhibition

During cell division, CDK4/cyclin D complexes accumulate in G1 phase and phosphorylate the RB protein. Hyperphosphorylated RB is deactivated and no longer binds to E2F, allowing the transcription of various cell-cycle genes such as CDK2 and cyclin E. The activities of these cell cycle proteins in turn further regulate the cell cycle progression [6, 138, 139]. CDK2/cyclin E complexes further phosphorylate and maintain the hyperphosphorylated state of RB protein in late G1 phase.

Cyclin E is also reported to exist in several low molecular weight (LMW) isoforms (34-49 kDa) in cancer cells. Interestingly, these LMW cyclin E have been associated with poor prognosis and higher recurrence in clinical colorectal cancer samples [140, 141]. p21 and p27 are members of the Cip/Kip family, known to be negative regulators of cell proliferation and are considered to be tumor suppressors. LMW forms of cyclin E are hyperactive and remain functional even with the inhibition from p21 and p27, thus causing disruption of the G1/S checkpoint [142].

In section 4.2.1.1, increased CDK4 level identified in iTRAQ was verified using western blotting. Since cyclin D is closely related to the function of CDK4, protein level of cyclin D was also determined by immunoblotting. As FXN OE increases the level of both CDK4 and cyclin D, OF cells should divide more actively compared to CAT cells, resulting in higher growth. However, when a proliferation assay was performed, contradictory result was obtained, where FXN OE cells instead exhibited a lower proliferation rate. When the abundance of cell cycle inhibitor p21 and p27 were found to be up-regulated in OF cells and the late G1/S phase CDK2/cyclin E (LMW) were decreased, it became apparent that G1 phase in OF cells is likely to be extended.

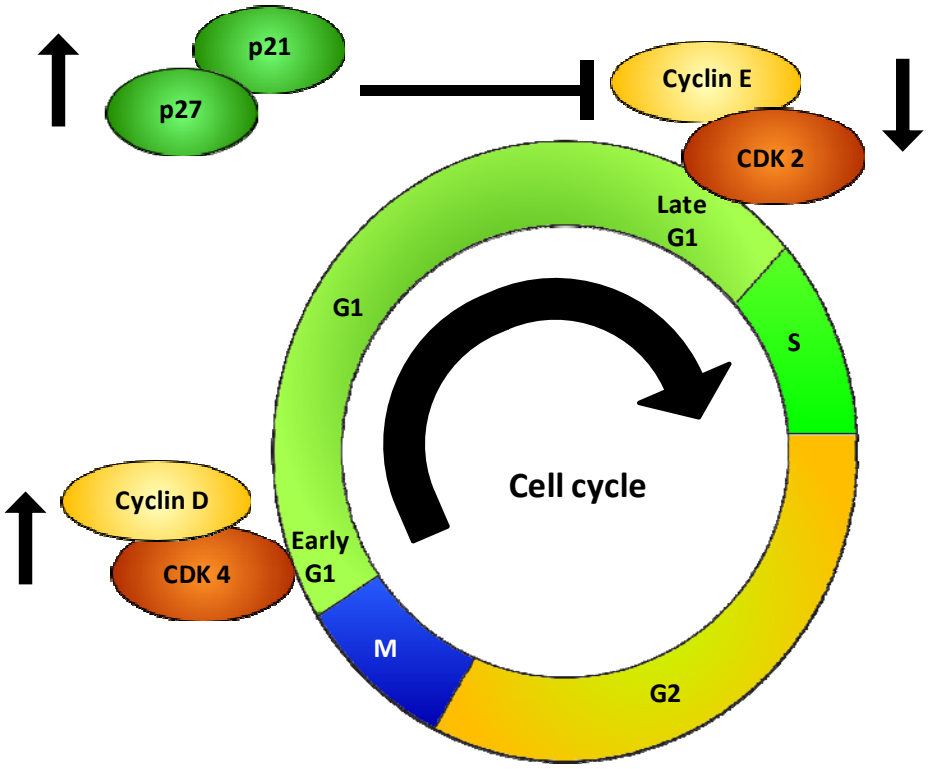

Figure 4-5: Cell cycle proteins perturbed in FXN OE. Figure shows cell cycle proteins with altered abundance in FXN OE cells. Cyclin D, CDK4, p21 and p27 protein levels were elevated while cyclin E and CDK2 protein levels were decreased. Cyclin D and CDK4 proteins are early G1 phase cell cycle proteins, while cyclin E and CDK2 are late G1 phase cell cycle proteins. p21 and p27 are cell cycle inhibitors.

Cell cycle analysis by flow cytometry was able to confirm that OF cells indeed had a prolonged G1 phase compared to CAT cells. This caused a shift in the population of OF cells, accounting for the higher proportion of cells in G1 phase and a correspondingly lower proportion progressing to the S phase. The inhibition of cell cycle thus likely occurs during the late G1 phase, delaying the transition of cells from G1 into S phase. In summary, over-expression of FXN in HCT116 cells decreases cell proliferation by inhibiting G1to S phase transition (Fig 4-5).

4.2.2 OXPHOS and TCA cycle

Data from iTRAQ also revealed changes in the level of a number of proteins associated with the ETC and TCA cycle. FXN plays an important role in the regulation of mitochondrial OXPHOS [74, 143]. In this section, the role of FXN OE in promoting OXPHOS is discussed. Specifically, the effect of FXN OE on the abundance of OXPHOS proteins is demonstrated.

4.2.2.1 iTRAQ revealed OXPHOS and TCA cycle proteins

A number of proteins involved in OXPHOS were found to be altered in OF cells, including proteins from all five complexes of the ETC (Table 4-1). Complex I, also known as NADH dehydrogenase, is involved in transferring electron from NADH to ubiquinone and translocation of H^+ across the inner mitochondrial membrane. Succinate dehydrogenase subunit B (SDHB) is a hydrophilic subunit of the complex II. Succinate dehydrogenase is involved in the transfer of electrons from succinate via $FADH_2$ to ubiquinone. In complexes III and VI, electrons are transferred to O_2 via cytochrome C with the translocation of H^+ across the inner mitochondrial membrane. Complex V, ATP synthase, utilizes the electrochemical gradient generated to drive the synthesis of ATP [21].

Based on iTRAQ data, the abundance of seven proteins involved in the TCA cycle were altered in OF clones (Table 4-2). TCA cycle connects glucose metabolism to OXPHOS. Briefly, isocitrate dehydrogenase catalyzes the conversion of isocitrate to α-ketoglutarate, which is subsequently converted to succinyl-Co-enzyme A (CoA) by 2-oxoglutarate dehydrogenase. Succinyl CoA is then catalysed to succinate by succinyl-CoA ligase while generating GTP in the process. Lastly, succinate is converted by succinate dehydrogenase to form fumarate [21].

Table 4-1: Altered proteins belonging to the electron transport chain complexes

ETC Complex	Accession No.	Protein name†	Peptides	Fold change# (±S.D.)
I	IPI00028883	NADH dehydrogenase 1 beta subcomplex subunit 8	2	1.505 ± 0.329
I	IPI00946474	NADH dehydrogenase 1 alpha subcomplex subunit 5	3	1.545 ± 0.121
I	IPI00945153	NADH dehydrogenase 1 alpha subcomplex subunit 6	2	-1.599 ± 0.033
II	IPI00294911	Succinate dehydrogenase iron-sulfur subunit	8	1.623 ± 0.174
III	IPI00029264	Cytochrome c1	9	-1.964 ± 0.167
IV	IPI00021785	Cytochrome c oxidase subunit 5B	8	-1.372 ± 0.112
V	IPI00007611	ATP synthase subunit O	11	1.840 ± 0.118

†The list contains significantly altered proteins related to electron transport chain. All these proteins have met the criteria as mentioned in section 3.2.3.1.

Fold change of protein levels in OF cells compared to CAT control

Table 4-2: Altered proteins associated with TCA cycle

Accession No.	Protein name†	Peptides	Fold change# (±S.D.)
IPI01011396	Isocitrate dehydrogenase subunit gamma	3	-1.752 ± 0.217
IPI00030702	Isocitrate dehydrogenase subunit alpha	7	-1.677 ± 0.061
IPI00945507	Succinyl-CoA ligase [GDP-forming] subunit beta	2	-1.561 ± 0.244
IPI00872762	Succinyl-CoA ligase [GDP-forming] subunit alpha	5	-1.479 ± 0.087
IPI00464979	Succinyl-CoA ligase [ADP-forming] subunit beta	3	1.714 ± 0.172
IPI00294911	Succinate dehydrogenase iron-sulfur subunit	8	1.623 ± 0.174
IPI00926925	2-oxoglutarate dehydrogenase	2	-1.664 ± 0.290

†The list contains significantly altered proteins related to TCA cycle. All these proteins have met the criteria as mentioned in section 3.2.3.1.

Fold change of protein levels in OF cells compared to CAT control

4.2.2.2 FXN OE induces OXPHOS

In order to determine the functional impact of these altered protein levels (Table 4-1 and Table 4-2), the rate of OXPHOS in FXN OE and CAT cells was measured (section 7.3.2). The mitochondrial membrane potential is an important parameter for OXPHOS in mitochondrial ATP production that directly affects the rate of OXPHOS [144, 145]. To quantify differences in OXPHOS between OF and CAT control cells, the mitochondrial membrane potential of each cell line was measured using JC10 fluorescent dye.

JC10 is a cationic, lipophilic dye which is specifically loaded into the mitochondria. A higher mitochondrial membrane potential would cause more dye to accumulate and be retained in the mitochondria. Mitochondrial accumulation of the dye causes a reversible aggregation, which shifts the emission wavelength from 520 nm to 570 nm. All three OF cell lines showed higher ratio of aggregated-red dye to green dye when compared to CAT control, indicating that FXN OE increases mitochondrial membrane potential, which can be interpreted as an increased rate of OXPHOS (Fig. 4-6).

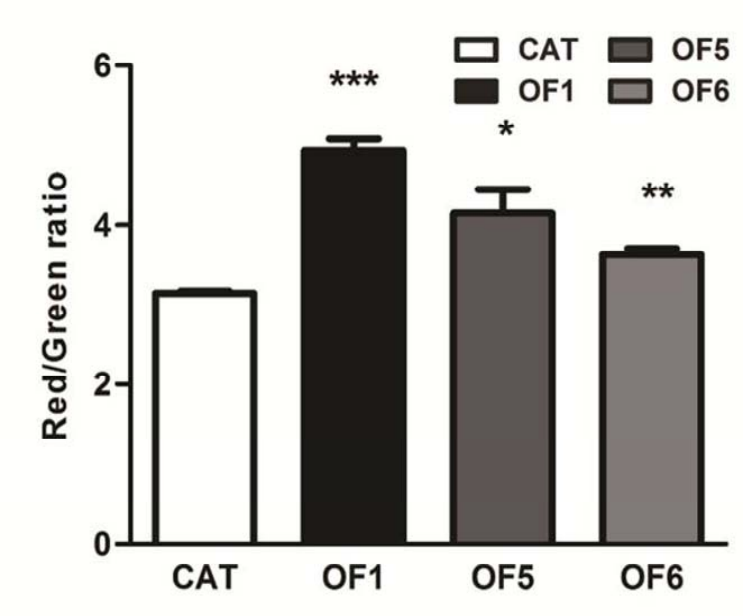

Figure 4-6: OF cells have higher OXPHOS. Histograms show the ratio of red to green signal of JC-10. JC-10 staining measures mitochondrial membrane potential, which is an indication of OXPHOS. Columns are mean from three flow cytometry experiments; bars represent S.D; *, $p< 0.05$; **,$p< 0.01$; ***,$p< 0.001$.

4.2.2.3 ATP5O and SDHB may be involved in FXN-induced OXPHOS

The iTRAQ analysis revealed changes in the level of several proteins associated with OXPHOS (Table 4-1 and Table 4-2). However, these proteins show varying trends of regulation. In order to determine the overall effect of these changes, the collective function of this group of proteins was assayed by JC10. The combined impact of these protein changes should be responsible for increasing OXPHOS in FXN OE cells. Although it is difficult to pinpoint the role of specific OXPHOS proteins or link any phenotypic change to all the proteins involved, several possible candidates that provide explanation for increased OXPHOS are highlighted below.

ATPase synthase is an ETC complex involved in the last step of ATP production during OXPHOS. ATPase synthase subunit O (ATP5O) protein level was found to be higher in FXN OE cells (1.840 ± 0.118). The role of ATP5O in

ATPase synthase in not known except for that this subunit could be involved in the regulation of glucose uptake [146], which is a factor promoting OXPHOS in FXN OE cells.

Succinate dehydrogenase (SDH) consists of four subunits (denoted as A to D) and is found on the inner mitochondrial membrane (Fig 4-7).

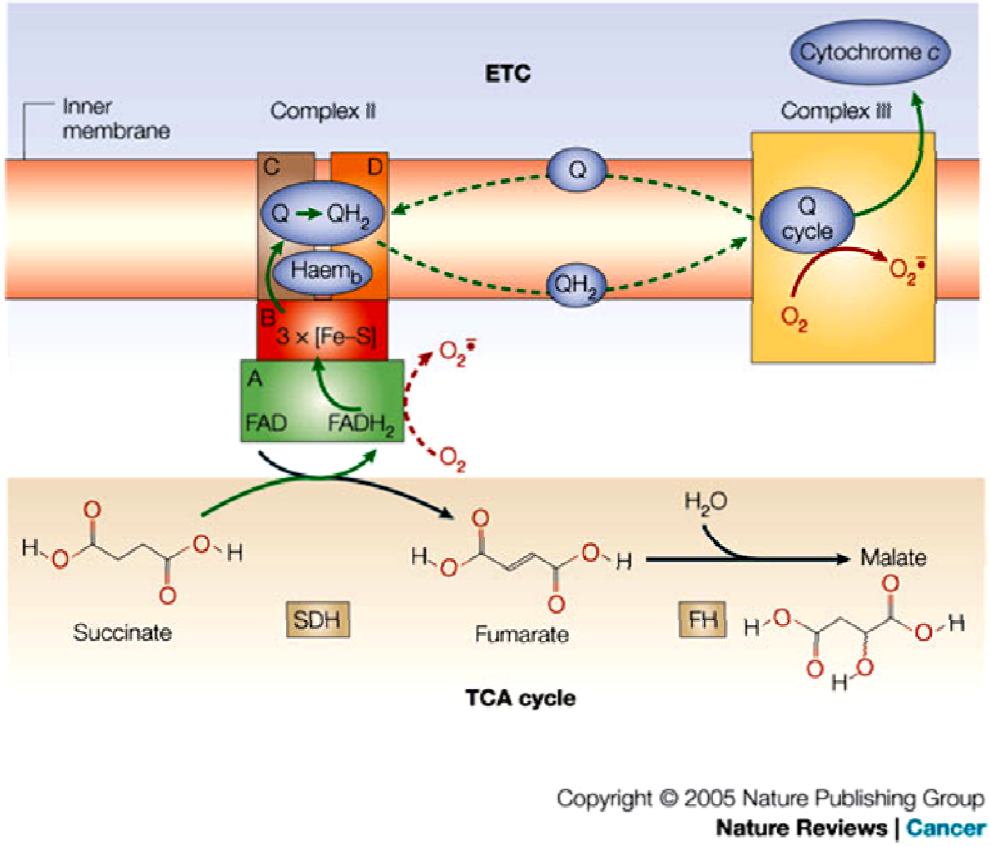

Figure 4-7: Succinate dehydrogenase functions at the crossroad of TCA cycle and ETC. Illustration showing the pivotal position of succinate dehydrogenase in OXPHOS. SDH catalyzes the conversion of succinate to fumarate. SDH is also involved in feeding electron to the electron transport chain via iron sulphur cluster and Q enzyme. Figure reproduced from Gottlieb and Tomlinson [147] with permission.

SDH is a TCA cycle enzyme, as well as complex II of the ETC, that catalyzes the dehydrogenation of succinate to fumarate, by transferring two

hydrogen atoms from succinate to FAD subunit A. In this way, FAD is reduced to $FADH_2$, which releases a pair of electrons to the three iron sulfur centers in subunit B of SDH and subsequently to ubiquinone (Q), reducing it to the ubiquinol (QH_2) [147].

SDH functions as a second ETC entry point for electrons from the TCA cycle and plays a critical role in energy metabolism through its dual function in the TCA cycle and ETC. Based on iTRAQ data, SDHB protein level was found to be elevated in OF cells (1.623 ± 0.174). This increase may be due to FXN's involvement in ISC synthesis. More data is needed to confirm this hypothesis.

4.2.3 Change of cellular redox homeostasis in OF cells

ROS may be generated as byproducts of OXPHOS, and these could cause oxidative damage to the cells. Since FXN OE increases OXPHOS, the oxidative stress associated with oxidative ATP production is in question. This section presents data supporting that over-expression of FXN leads to increased levels of anti-oxidant enzymes, and higher capacity for ROS scavenging. OF cells also have lower intracellular ROS level and increased resilience towards exogenous ROS insult.

4.2.3.1 OF cells have lower resting ROS levels

Intracellular ROS levels in OF and CAT cells were measured using a fluorescence dye 2',7'-dichlorfluorescein-diacetate (DCFH-DA) as described in section 7.3.3. After the membrane permeable DCFH-DA enters the cells, the hydrophobic diacetate group is cleaved by nonspecific intracellular esterases, thus trapping the dye within the cells. Oxidative species in the cells will then oxidize the DCFH to fluorescent DCF. The intensity of DCF fluorescence corresponds to the amount of ROS in the cells. As quantified by flow cytometry, OF cells exhibited lower DCF fluorescence intensity as compared to control CAT cells, indicating less ROS was present in FXN over-expressing cells (Fig. 4-8).

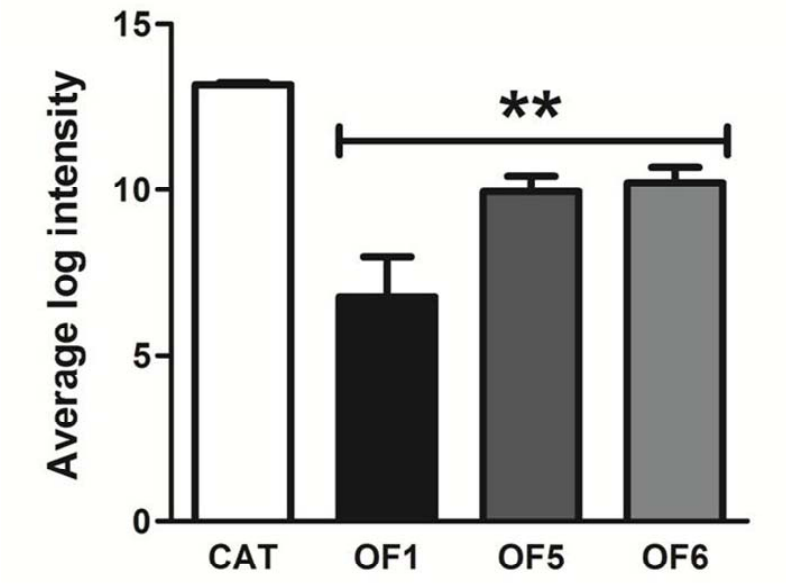

Figure 4-8: OF cells have lower intercellular ROS levels. Histograms show average fluorescence intensity of DCHF signal in OF1, 5, 6 compared to CAT. Higher intensity represents higher endogenous ROS levels. Columns represent mean from three flow cytometry experiments; bars represent S.D; **, $p< 0.001$.

4.2.3.2 FXN OE increases anti-oxidant enzymes

In the iTRAQ analysis, a number of peroxiredoxins, glutathione peroxidase and thioredoxin related proteins were identified with higher abundance in OF cells (Table 4-3).

Table 4-3: Altered proteins involved in cellular oxidative redox homeostasis

Accession No.	Protein name†	Peptides	Fold change[#] (±S.D.)
IPI00220301	Peroxiredoxin-6	6	1.311 ± 0.068
IPI00024919	Peroxiredoxin-3	38	-1.571 ± 0.119
IPI00000874	Peroxiredoxin-1	42	1.500 ± 0.051
IPI00910821	Glutathione peroxidase 8	3	1.558 ± 0.078
IPI00646689	Thioredoxin domain-containing protein 17	3	1.882 ± 0.223

†The list contains significantly altered proteins that are anti-oxidant enzymes. All these proteins have met the criteria as mentioned in section 3.2.3.1.

Fold change of protein levels in OF cells compared to CAT control

Peroxiredoxins are a family of anti-oxidant enzymes containing highly conserved cysteine active-sites and sequence. Peroxiredoxins can be found in the cytosol, nucleus and mitochondria and share the same catalytic action in the removal of peroxides [148]. Members of the glutathione peroxidase family usually contain selenium in the redox center, but newer members were found to contain cysteine in its active site [149]. Glutathione peroxidases catalyze the removal of hydrogen peroxide with the use of glutathione as co-factor [150]. Thioredoxins on the other hand are part of the thioredoxin systems involving thioredoxin reductase and co-factor NADPH. Thioredoxins mainly contain dithiol/disulfide active sites and are involved in the reduction of disulfide bonds. Thioredoxins are also essential for synthesis of deoxyribonucleotides during cell proliferation [151].

In addition to anti-oxidant properties and the ability to ameliorate oxidative stress, these enzymes have also been reported to play a significant role in signal transduction. Numerous biological processes such as inflammation, apoptosis, growth and survival also depend on peroxides such as hydrogen peroxide as signaling molecules [152, 153].

4.2.3.3 Anti-oxidant proteins in OF cells reduce intracellular ROS

In order to ascertain if the reduction of intracellular ROS is due to enhanced anti-oxidant scavenging, the glutathione redox system was investigated since it is one of the most important peroxide scavenging systems in the cell. By immunoblotting, increased abundance of glutathione peroxidase 1 (GPx1) protein was validated in FXN OE cells compared to the CAT control (Fig 4-9).

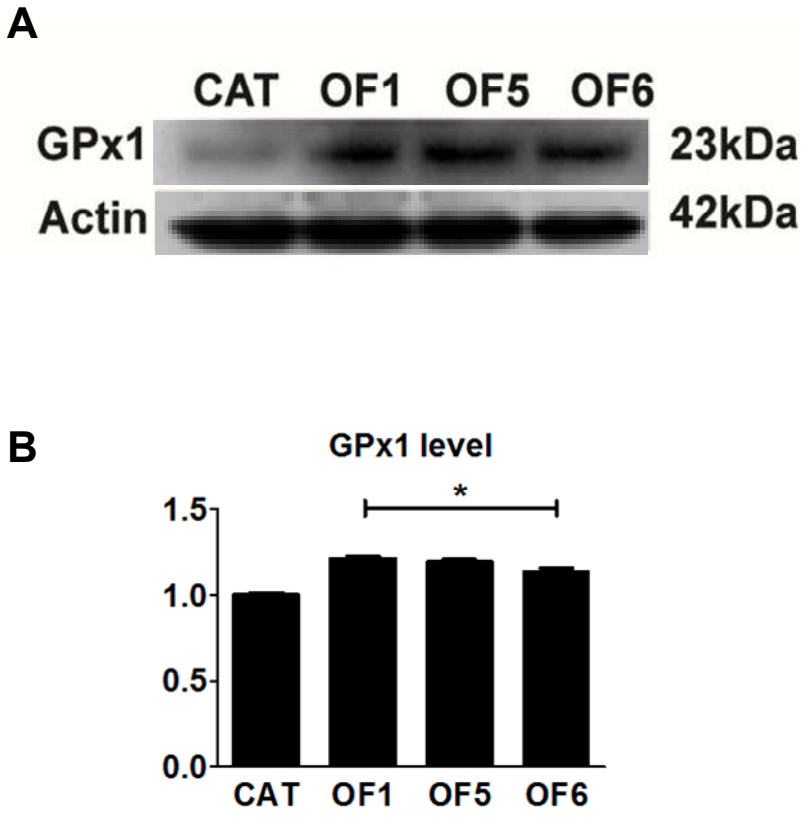

Figure 4-9: FXN OE cells have higher levels of GPx1. A) Immunoblotting shows higher levels of GPx1 protein in FXN OE cells. Actin is used as an internal loading control. **B)** Histogram shows densitometric measurement of the fold change of GPx1 in FXN OE cells compared to CAT control. * $p<0.05$.

4.2.3.4 Activated GSH redox system reduces ROS levels in OF cells

In the glutathione redox system, reduced glutathione (GSH) is a cofactor in the removal of oxidative species catalyzed by glutathione peroxidase. As byproduct, oxidized glutathione (GSSG) is generated, but it should be rapidly converted back to GSH. The ratio of GSH to GSSG reflects the activity of the glutathione redox system and constitutes a key indicator of the intracellular redox environment [154].

In section 3.2.2, a metabolomics profiling that was performed in FXN OE cells compared to CAT controls also quantified the level of GSH and GSSG as metabolites. Using these data, the ratio of GSH to GSSG was calculated. OF1, OF5 and OF6 all had lower GSH/GSSG ratios than CAT (Fig 4-10).

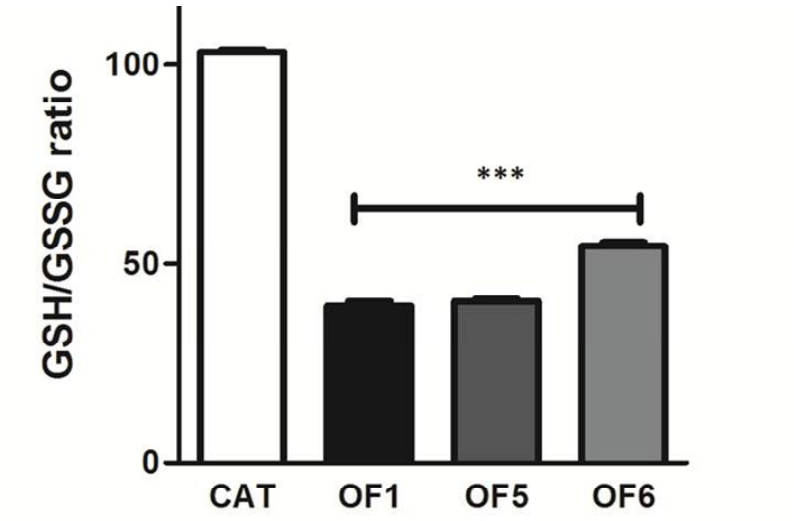

Figure 4-10: FXN OE cells have lower GSH/GSSG ratio. Histograms show average GSH/GSSG ratio calculated from XIC areas of GSH and GSSG in the metabolomics analysis. Bars represent the mean GSH/GSSG ratio from triplicate runs; error bars represent S.D; **, $p< 0.01$; ***, $p< 0.001$.

4.2.3.5 OF156 are more resistant to ROS insult

Given the different capacity to react against oxidative stress described in previous sections, the effect of exogenous ROS insult on OF cells was investigated. CAT and OF cells were treated with increasing doses of tert-butyl hydroperoxide (TBHP), a stable analogue of hydrogen peroxide (section 7.2.3). OF cells showed significantly higher resilience to TBHP compared to CAT from 40μM of TBHP onwards (Fig 4-11).

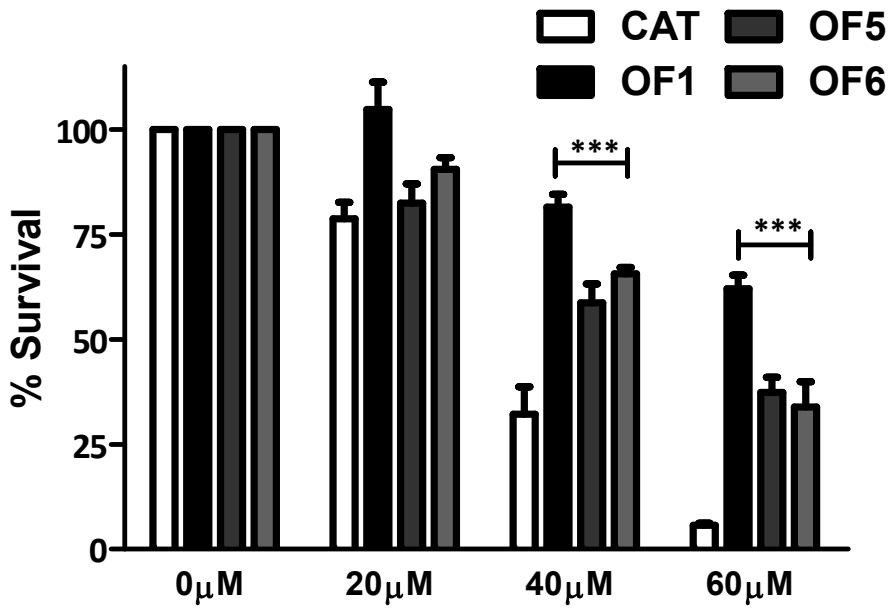

Figure 4-11: OF156 showed increased resistance to TBHP. Histograms showing percentage survival of cells after treatment with TBHP. FXN OE cells showed significantly higher survival from 40μM of TBHP onwards, columns represent mean percentage survival from three experiments; error bars represent S.D.; ***, $p< 0.001$.

4.2.3.6 FXN OE activates ROS scavenging and alters redox status

Low antioxidant defense and high oxidative status are established hallmarks of many cancers [155]. Based on iTRAQ analysis, numerous peroxiredoxins, glutathione peroxidase and thioredoxin related proteins were identified with higher abundance in OF cells (Table 4-3). This group of antioxidant enzymes play pivotal roles in oxidative homeostasis and the regulation of redox signaling [152, 156, 157], and could also in turn regulate cancer metabolism and contribute to anti-tumor effect of FXN over-expression.

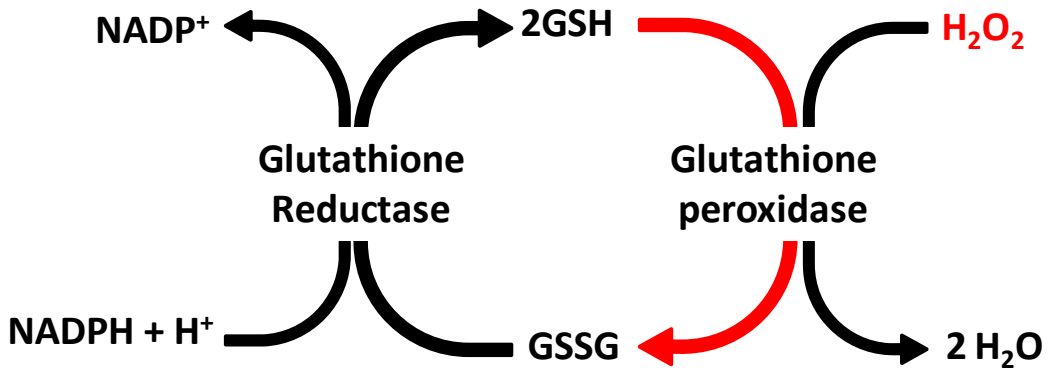

Figure 4-12: FXN OE cells possess better ROS scavenging activity. Higher level of GSSG and glutathione peroxidase enzyme coupled with lower intracellular ROS suggested the red arrow in the above pathway is more active in FXN OE cells.

OF cells have higher OXPHOS which could lead to increased generation of ROS in the ETC complexes [158]. However, the experimental observation from this study appears to contradict this proposition, since lower intracellular ROS was detected in OF cells compared to CAT. Low ROS levels could be a result of increased antioxidant enzymes such as GPx1 [85]. Indeed, this was confirmed by higher GPx1 level, suggesting that GPx1 may be catalyzing the removal of ROS such as H_2O_2, leading to an accumulation of GSSG. Enhanced resistance of OF cells to TBHP is also in support of this notion (Fig 4-12).

Chapter 5: Tumor suppressive function of FXN may be via HIF-1α destabilization

5.1 Introduction

HIF-1α is a key molecule in cancer cell metabolism. iTRAQ characterization of FXN OE seems to converge on HIF-1α as well. This section shows that OF cells have lower HIF-1α level and possible regulation of HIF-1α level in OF cells. Extracellular matrix metalloproteinase inducer (EMMPRIN) is a HIF-1 target and identified in the iTRAQ analysis. Its role in modulating metabolic changes and anti-cancer effect of FXN OE is also discussed.

5.2 Result

5.2.1 HIF-1α is destabilized in OF cells

Several pieces of evidence in this study appear to describe hypoxic changes: (i) HIF-1α is a regulator of the metabolic switch; (ii) higher SDHB should regulate HIF-1α level; and (iii) ROS play intricate roles in hypoxia.

In view of these, it was hypothesized that FXN OE could lead to a change in hypoxia state in HCT116. To substantiate this claim, the protein level of HIF-1α was measured by western blotting. As shown in Fig 5-1, FXN over-expressing cells indeed have lower endogenous HIF-1α level.

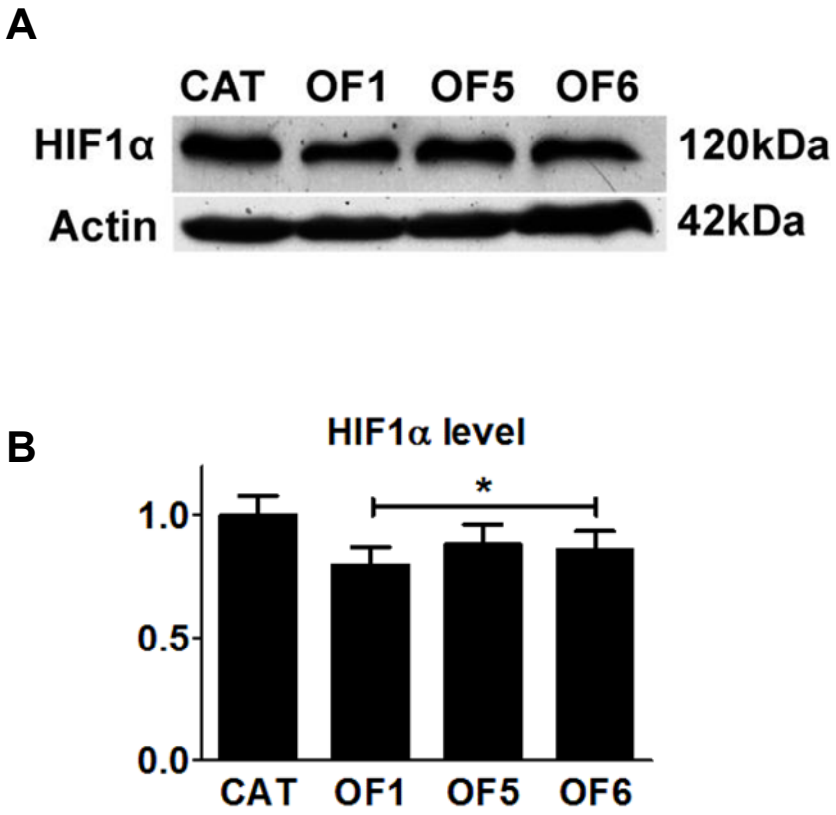

Figure 5-1: Lower HIF-1α level was detected in FXN OE cells. A) Immunoblotting showed lower HIF-1α protein levels in FXN OE cells. Actin is used as internal loading control. B) Histogram shows densitometric measurement of the fold change of HIF-1α in FXN OE cells compared to CAT control. * $p<0.05$

5.2.2 Western-blot and MRM validation of decreased EMMPRIN level

The reduced protein level of EMMPRIN (-1.612 ± 0.035) was verified in OF cells by immunoblotting. A lower level of EMMPRIN protein was consistently detected in all OF1, OF5 and OF6 (Fig 5-2). As EMMPRIN may be glycolysated, several bands are detected in western blots. The abundance of EMMPRIN in FXN clones and CAT was further verified by SWATH in section 3.2.3.5. Three peptides belonging to EMMPRIN were quantified based on the area under the curve (AUC) of three transitions from each peptide (Fig 5-3 and Fig 5-4).

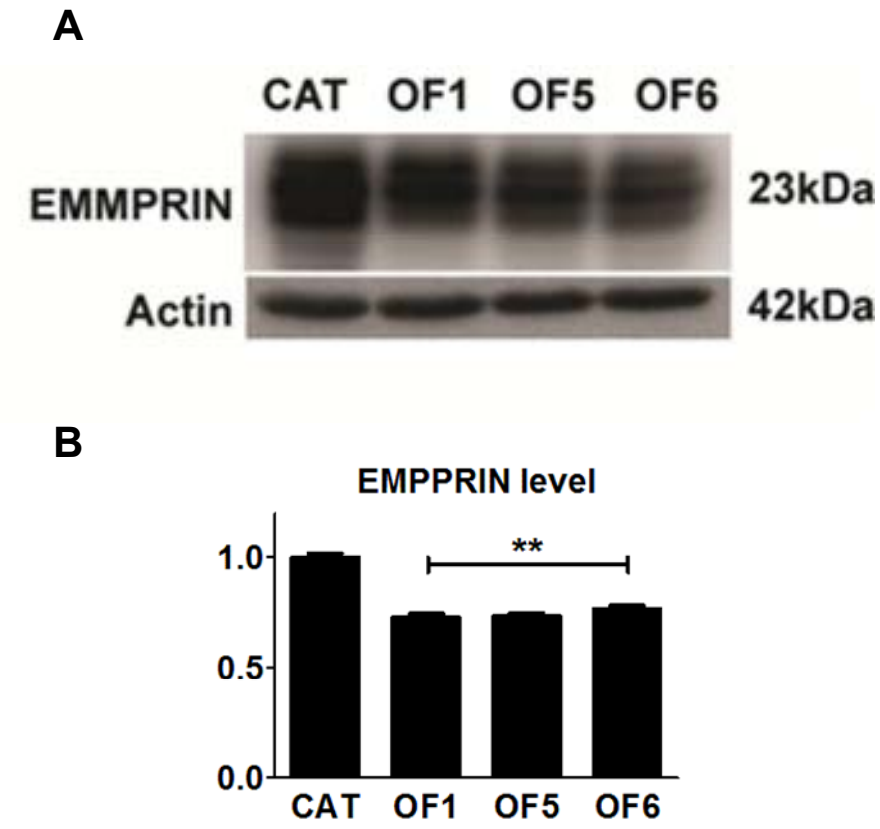

Figure 5-2: FXN OE cells had lower EMMPRIN levels. A) Immunoblotting showed lower EMMPRIN protein levels in FXN OE cells. Actin is used as an internal loading control. **B)** Histograms show densitometric measurement of the fold change of EMMPRIN in FXN OE cells compared to CAT control. ** $p<0.01$

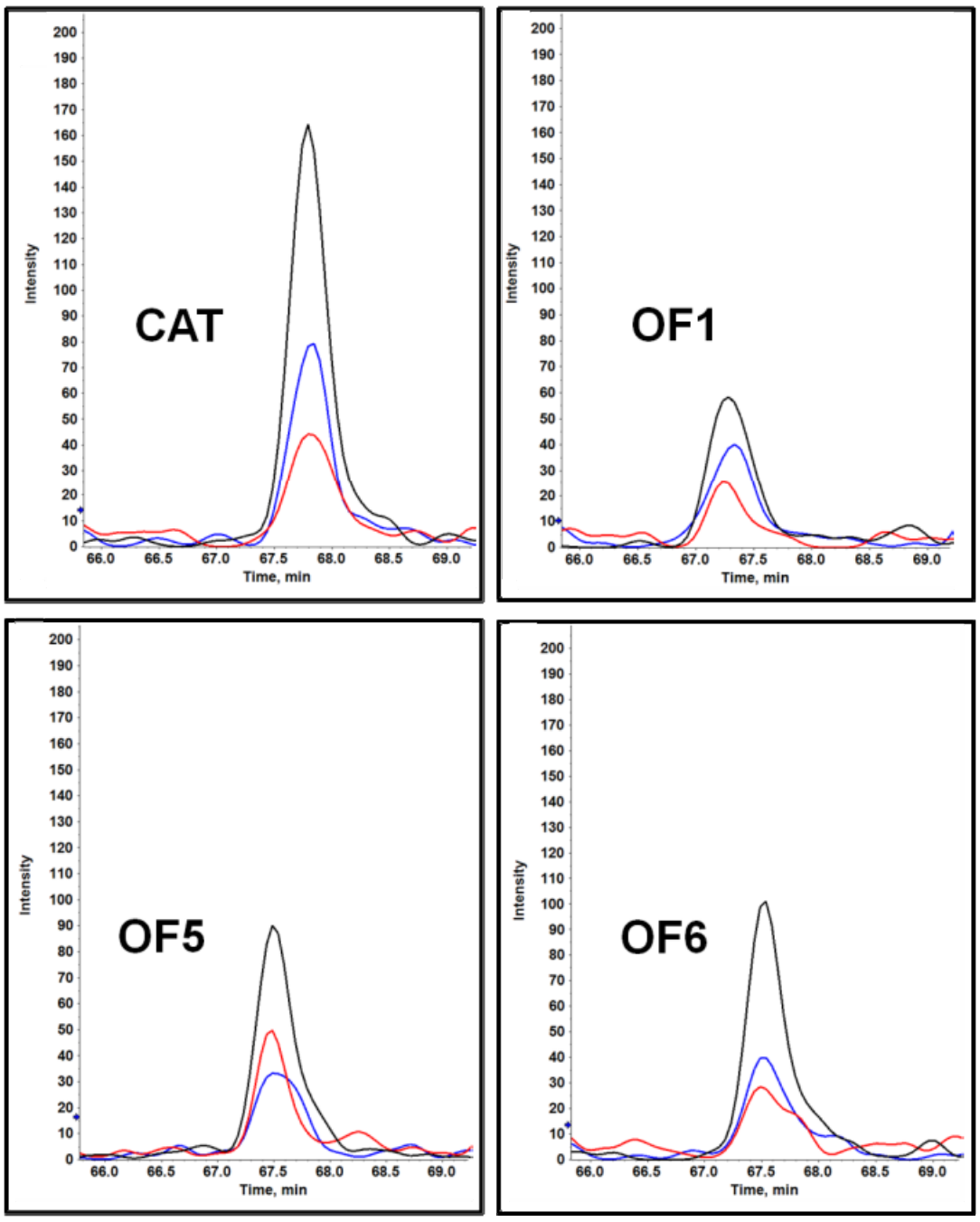

Figure 5-3: Representative XICs showing lower EMMPRIN in FXN OE cells. Each panel shows the overlay of three transitions of the peptide AAGTVFTTVEDLGSK from the protein EMMPRIN. The scales of the axis in all four panels are standardised. CAT shows the highest peak compared to OF1, OF5 and OF6.

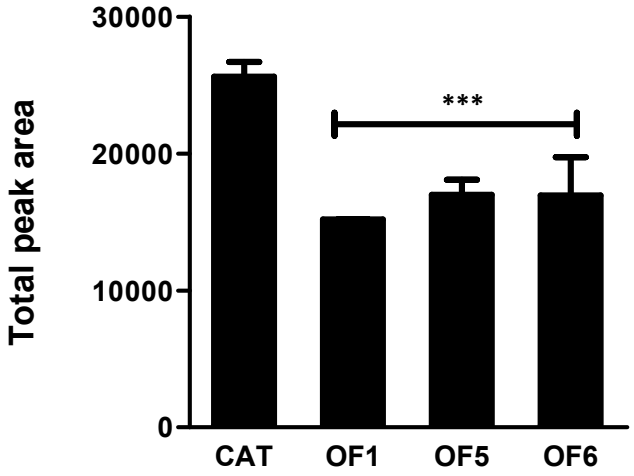

Figure 5-4: Total peak area of EMMPRIN. Histograms show total peak area of EMMPRIN in FXN OE and CAT cells as identified and quantified in SWATH. Columns represent mean from triplicate runs; error bars represent S.D.; *** $p<0.001$

5.3 Discussion

Experimentally, reduction in HIF-1α level in OF cells was observed, and it could be rationalised by numerous changes at protein and metabolite levels. This section discusses how FXN over-expression could lead to reduced HIF-1α levels and how lower HIF-1α could explain phenotypic changes observed in OF cells.

5.3.1 Succinate dehydrogenase B may play a role in HIF-1α regulation

As discussed in section 4.2.2.4, SDHB potentially affects TCA cycle as well as OXPHOS. SDH is a well-established mitochondrial tumor suppressor, loss-of-function mutation in SDH subunits leads to an accumulation of succinate which may leak into the cytosol to cause inhibition of prolyl hydroxylases (PHD) [159]. Inactivating PHD leads to the stabilization of HIF-1α in a pseudo-hypoxia condition. Defective SDH is associated with a number of malignancies such as gastrointestinal stromal cell tumor, renal carcinoma, as well as gastric cancer, and familial head and neck paragangliomas [160-164]. The anti-tumor effect of SDHB subunit was

recently observed in colorectal cancer [165], where lower SDHB expression in human colorectal cancer tissues was reported. It was demonstrated that restoration of SDHB expression inhibited cancer growth both *in vitro* and *in vivo.*

In summary, FXN aids in the synthesis of ISC which could account for the increasing abundance of SDHB, a protein containing ISC. Over-expression of FXN may increase the availability of ISC, and lead to higher assimilation of ISC into SDHB during protein synthesis. High SDHB level in turn promotes dehydrogenation of succinate to lower the level of succinate inside the cell. This relieves the negative regulation on PHDs, thereby promoting the degradation of HIF-1α through PHDs. This explains the changes of SDHB and HIF-1α levels observed in FXN OE cells.

5.3.2 Lower intracellular ROS in OF cells could lower HIF-1α

In section 4.2.3, over-expression of FXN was shown to lower intracellular ROS level. The effect of ROS in the regulation of HIF-1α and hypoxia is controversial. While some studies claim that ROS generated by the mitochondrial complex III can stabilize HIF-1α [166-168], it may well be due to ROS oxidization of the non-heme iron center within PHDs, which inhibits PHD activity, leaving HIF-1α to accumulate, instead of active HIF-1α induction. In support of this, more recent evidence proposed that HIF-1α stabilization may be independent of ROS generated from complex III of the mitochondria [169].

In the context of findings presented herein, the reduction in ROS level upon FXN OE was not a result of diminished mitochondrial function, since OXPHOS was higher in OF cells. Instead, lower intracellular ROS was due to higher ROS scavenging activity. Since drug-induced ROS production could induce stabilization of HIF-1α, it thus follows that ROS can regulate HIF-1α levels independently

without involvement of the mitochondria [170]. Over-expression of GPx1 on the other hand was also shown to suppress HIF-1α stabilization [171]. Therefore, lower intracellular ROS and higher GPx1 expression induced by FXN OE may both contribute to suppression of HIF-1α stabilization.

The role of ROS in HIF-1α accumulation is still largely under debate [172, 173], yet it is undeniable that ROS generation and detoxification play important roles in regulation of tumorigenesis and cancer metabolism [174].

5.3.3 Reduced EMMPRIN could induce metabolic changes in FXN OE

In normal cells, glycolysis without ATP production through the ETC is energetically inefficient. Cancer cells on the other hand are reported to rely heavily on glycolytic ATP generation, even in the presence of oxygen [175]. One of the models explaining this phenomenon is the need to provide essential biosynthetic materials for rapid cell division [23].

Glycolysis is interconnected with several metabolic pathways, and glycolytic intermediates are precursors for amino acid, nucleic acid and lipid synthesis. The pentose phosphate shunt, on the other hand, also provides the essential reducing equivalents in the form of NADPH, required for many biochemical reactions in the cell [23, 176]. Large amount of lactate produced at the end of glycolysis are eventually secreted, which may also benefit the tumor cells by inhibiting immune response in the surrounding environment [177, 178]. Acidic tumor microenvironment is also associated with increased metastasis and invasion [179, 180]. Lactic acid is mainly transported by monocarboxylate transporter (MCT) 1 and 4 [181], which require EMMPRIN for proper function. EMMPRIN interacts

with MCT1/4, and act as a chaperone to promote MCT1/4 translocation and distribution to the plasma membrane.

Reported to be up-regulate by HIF-1α during hypoxia [182], EMMPRIN is a transmembrane glycoprotein that is usually over-expressed in the tumor cells [183]. EMMPRIN induces matrix metalloproteinase production from nearby stromal fibroblast, and is involved in tumor-stroma cell interaction and metastatic progression [184-186]. Increased level of EMMPRIN is highly correlated with increased tumor progression [187-189] and lower survival rate [190-192] in various cancers including colorectal cancer. EMMPRIN expression is critical for tumor cells to maintain malignancy and tumor progression and is also reported to promote glycolysis in cancer cells [182, 193].

Lower EMMPRIN expression is associated with numerous benefits. Silencing of EMMRIN inhibits glycolysis and lactate secretion, thereby leading to decreased cell proliferation, vascular endothelial growth factor production, invasiveness and tumorigenicity [193, 194]. Blocking EMMPRIN function with specific antibodies similarly down-regulated glycolysis and quickly induced cell death in colorectal cancer cells [195].

Given the intricate role of EMMPRIN in glucose metabolism and cancer, the reduced protein level of EMMPRIN in FXN OE cells may potentially be one of the key proteins potentiating the anti-tumor effect as a result of FXN over-expression and lower HIF-1α levels.

5.3.4 Destabilization of HIF-1α explains the effect of FXN OE

Under normoxia, PHDs catalyze the hydroxylation of proline residues on HIF-1α, which are signals for von Hippel-Lindau (VHL) binding, to target HIF-1α

for degradation. HIF-1α can be stabilized when PHDs are inhibited by hypoxia, succinate or ROS. HIF-1α then dimerizes with HIF-1β, to cause activation of genes associated with the metabolic switch such as promoting glycolysis and inhibiting mitochondrial ATP production (Fig 5-5).

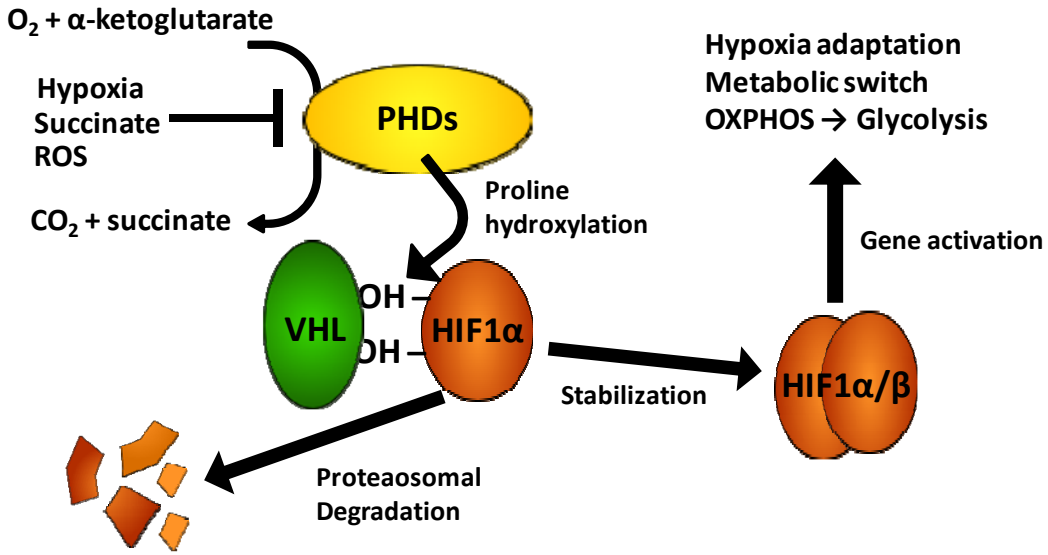

Figure 5-5: Function and regulation of HIF-1α. HIF-1α levels depend on the activity of PHDs, which can be inhibited by hypoxia, succinate and potentially ROS. The stabilization of HIF-1α leads to hypoxia adaptation and a metabolic switch to favour glycolysis [196].

Inhibition on PHDs may be relieved by lower succinate and ROS levels in OF cells, leading to higher degradation of HIF-1α. Increased OXPHOS observed in OF cells could thus be one intermediate effect of lower HIF-1α, a sign of reversed Warburg effect. Decreased HIF-1α may also be responsible for lower proliferation rate in OF from the inhibition of cell cycle. A study had shown HIF-1α depletion could induce p21 and p27 mRNA and protein levels, resulting in higher number of cells in G1 phase [197]. In this thesis, similar findings were demonstrated in FXN over-expression. The direct effect of lower HIF-1α was presented as a reduction of HIF-1 regulated gene EMMPRIN, and validated in OF cells.

Chapter 6: Conclusion and Future studies

6.1 Conclusion

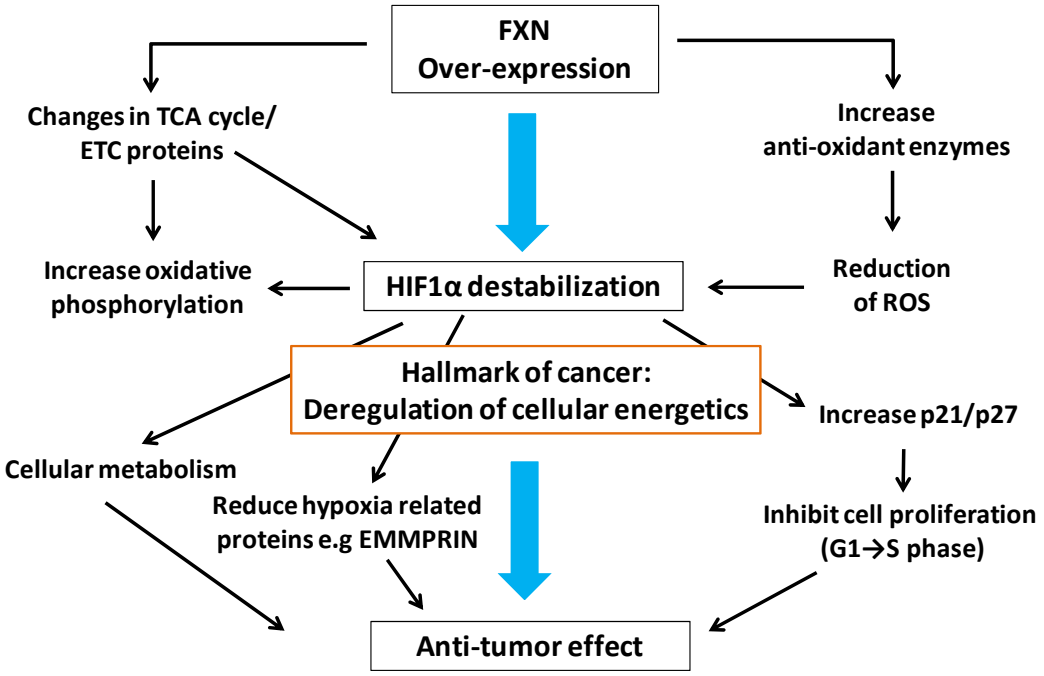

Figure 6-1: Flowchart depicting overall effect of FXN over-expression in cancer cells. Many key changes observed in FXN over-expressions resulted in decreased HIF-1α, an important regulator of metabolic switch in altering cancer cell metabolism.

In this study, the anti-tumor effect of FXN over-expression in HCT116 was investigated. It was found that OF cells had a reduction in cell proliferation due to cell cycle inhibition by p21 and p27. This likely was the result of lower HIF-1α levels. The reduction of HIF-1α could be due to a combination of decreased succinate levels due to alteration of TCA cycle protein levels and changes in the redox status in the cell due to higher antioxidant enzymes, promoting the activity of PHDs. Other effects of HIF-1α in OF cells were the shift of metabolism by increasing OXPHOS and regulation of HIF-1α downstream targets (Fig 6-1).

6.2 Future studies

6.2.1 Validation of HIF-1α induced effect in OF cells

Based on this study, FXN OE lowers HIF-1α level. In the next stage of investigation, the effect of HIF-1α induction during hypoxic stress should be studied. This should involve assessing cell survival and HIF-1α protein level, as well as measuring the abundance of targets downstream of HIF-1α by using targeted proteomics and functional assays. Some of these candidates should include GLUT1, which is involved in uptake of glucose into the cell [33]; monocarboxylate transport 4 (MCT4), which is associated with EMMPRIN and involved in removal of lactate from the cells [37]; as well as pyruvate dehydrogenase kinase (PDK), that phosphorylates and inactivates pyruvate dehydrogenase (PDH) catalyzing the conversion of pyruvate to acetyl-coA [39]. All these HIF-1α regulated genes are important nodes in the cancer metabolic switch.

6.2.2 Measurement of succinate levels in OF cells

Protein level of SDHB was found to be increased in OF cells and could potentially reduce the level of succinate, that in turn regulates the activity of PHDs. To fully substantiate this claim, succinate level should be measured directly in OF and CAT cells. This would further strengthen the linkage between FXN, oxidative phosphorylation and HIF-1α levels.

6.2.3 Measurement of iron level and the effect of iron chelation on OF cells

Iron is an essential element required for life [198]. The importance of iron in cell metabolism is highlighted by its presence in numerous crucial enzymes such as those in the cytochrome p450 family, ribonucleotide reductase and prolyl hydroxylase, which perform critical functions in regulating cell growth, metabolism

and hypoxia [199, 200]. However, free iron is highly toxic to cells due to its redox properties. Without protective mechanisms in place, iron can catalyze detrimental production of ROS [201].

Mitochondria are key organelles involved in the synthesis of ISC and heme, and involved in cellular iron storage [202, 203]. Previous works have suggested that FXN may act as a sensor of intracellular iron level, as well as regulate iron metabolism in the mitochondria [204]. FXN also binds iron and may act as an iron chaperone that releases iron during ISC biosynthesis (Fig 6-2).

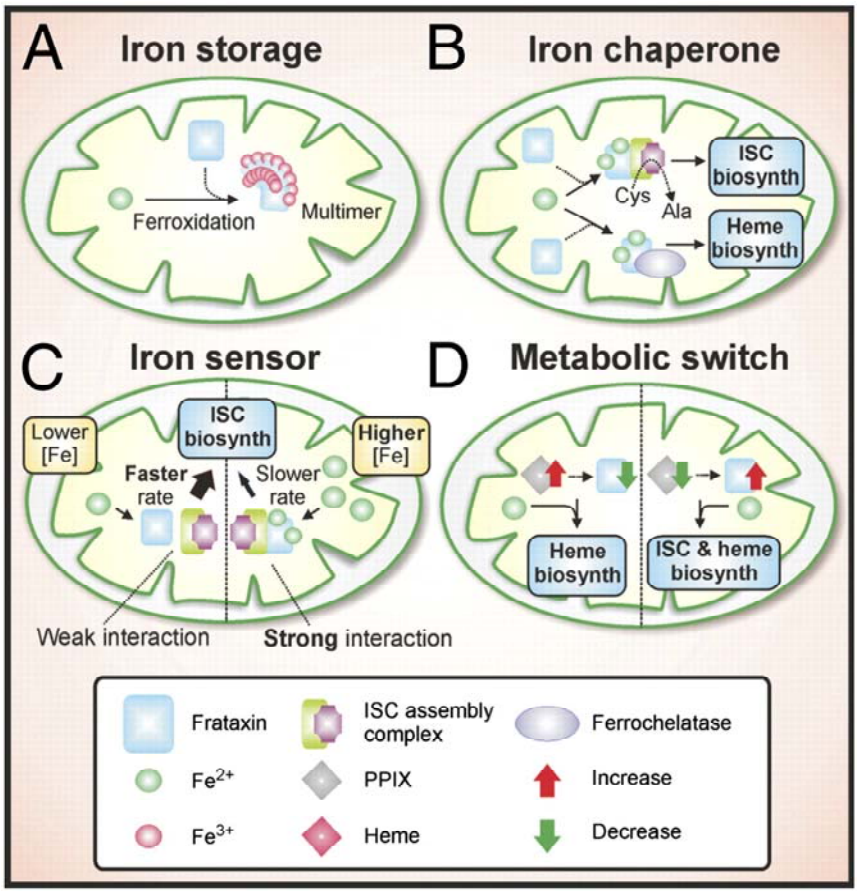

Figure 6-2: Possible function of FXN. Frataxin may act as a A) iron storage protein similar to ferritin. B) An iron chaperone protein by bind to iron and delivering it to heme and ISC synthesis. C) A negative regulator of ISC synthesis during high iron level to limit ISC over-production. D) As a metabolic switch between ISC and heme synthesis. Figure reproduced from Richardson et al. [205]. Copyright © 2010 PNAS

It is also postulated that FXN may function as a mitochondrial iron storage protein by assembling into oligomers that possess ferroxidase activity, catalysing Fe^{2+} to Fe^{3+} and sequestering these ions in a higher order complex. This prevents the iron from taking part in unwanted redox reactions [206]. However, these studies were done on yeast and bacteria homologue and evidence have been lacking in human FXN.

Association of iron metabolism and cancer has been reported in cell lines as well as animal models [207]. A clinical trial evaluated the efficacy of iron chelator with radiotherapy in pancreatic cancer showed promising result [208]. Regulation of iron metabolism can further affect HIF-1α levels as PHDs that cause HIF-1α degradation are also iron-dependent enzymes. PHDs can be inhibited if intracellular iron levels are low, resulting in stabilization of HIF-1α. Given the intricate link between iron metabolism, FXN and hypoxia, it is intuitive to further investigate level of free and bound iron, as well as the effect of iron chelation in FXN OE cells.

Measurement of labile iron pool in CAT and OF cells - The labile iron pool (LIP) is a chelatable and redox-active iron pool in the cell [209] that must be tightly regulated to restrict the oxidative damage induced by Fenton chemistry [210]. LIP is dynamic and its level is representative of total iron level in the cell and its regulation [211]. In order to determine if the over-expression of FXN indeed affects intracellular iron level, the LIP in CAT and OF156 cells should be quantified directly.

Effect of iron chelation on FXN OE cells – Treatment with membrane-permeable iron chelator Dp44mt inhibits proliferation. At 35nM concentration, Dp44mt causes a 50% reduction in wild type HCT116 proliferation after 48 hours (Fig 6-3). Using these parameters, the following should be investigated: (i) whether FXN OE affects the efficacy of Dp44mt treatment, as well as (ii) whether Dp44mt treatment modulates cell cycle of OF cells.

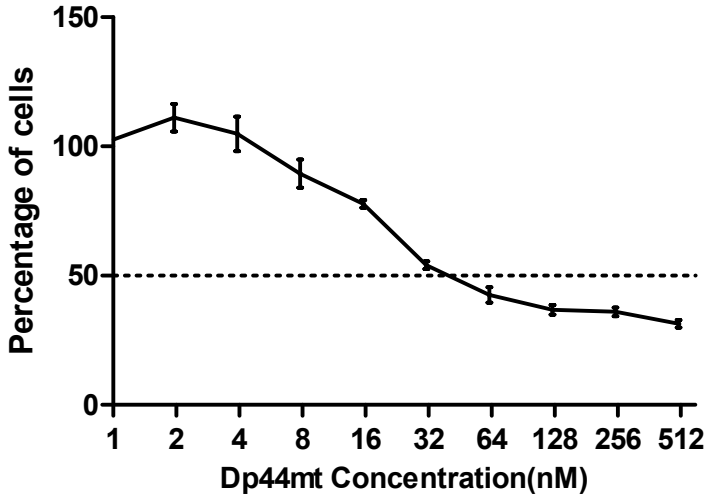

Figure 6-3: Dp44mt inhibits proliferation of HCT116. HCT116 cells were treated with increasing concentration of Dp44mt, an iron chelator for 48 hours. The number of cells remaining at each concentration was expressed as a percentage of the untreated control. IC_{50} of Dp44mt at 48hr is approximately 35nM.

Chapter 7: Materials and methods

7.1 Cell lines and constructs

7.1.1 HCT116 cell line and cell culture

Human Colorectal Carcinoma Cell Line HCT116 was purchased from American Type Culture Collection (ATCC; Manassas, VA). HCT116 was cultured in McCoy's 5A media [modified] with L-glutamine (Sigma Aldrich, St Louis, MO) supplemented with 7.5% (w/v) sodium bicarbonate (Sigma Aldrich), 10% fetal bovine serum (Gibco, Life Technologies, Carlsbad, CA) and 1% antibiotic/antimycotic (Life Technologies), in a humidified incubator at 37 $^{\circ}$C in 5% (v/v) CO_2. Culture reached sub-confluency every 2-3 days and was sub-cultured.

7.1.2 Transfection

Plasmid vector containing Frataxin gene (a gift from Dr. Bi Xuezhi), was constructed using Vivid Colors™ pcDNA™ 6.2 / EmGFP-Bsd / V5-DEST Mammalian Expression Vector (Life Technologies). Control plasmid containing Chloramphenicol acetyltransferase (CAT) gene was provided with the kit. Transfection of FXN-V5 and CAT control into HCT116 was carried out using electroporation (Cell Line Nucleofector® Kit V, Amaxa Biosystem) according to manufacturer's protocol.

7.1.3 Determination of blasticidin sensitivity

35,000 wild-type HCT116 cells were seeded in 24-well plates for 24 h. The cells were treated with McCoy's 5A medium containing 0 μg/ml, 5 μg/ml, 7.5 μg/ml, 10 μg/ml and 12.5 μg/ml of blasticidin (Life Technologies). After 72 h, the minimum concentration of blasticidin which inhibited the growth of normal HCT116 was determined.

7.1.4 Stable cell line selection

After transfection, cells were diluted in McCoy's 5A media containing 7.5 µg/ml blasticidin. Transfected cells were sparsely seeded with the ratio of 1:20 in 60 mm plates to allow colony amplification from single cells over a period of 5 – 7 days. Visible colonies were trypsinized individually and re-cultured in each well of a 24-well plate. Eventually six colonies showed healthy growth and were expanded and screened using V5 antibodies to check for FXN over-expression.

7.1.5 Preparation of whole cell lysate

Cells were trypsinized and spun down at 500 g for 5min. The supernatant was removed and the cell pellets were washed thrice with 1× Phosphate Buffered Saline (PBS). The cells were lysed using RIPA buffer (1% Sodium Deoxycholate, 0.1% SDS, 1% Triton X -100, 0.01 M Tris-HCL pH 8.0, 0.14 M NaCl) with 1× Halt^{TM} protease inhibitor cocktail, EDTA free (Pierce). After a brief vortex, lysates were centrifuged at 14,500 g at 4 ^{o}C for 20 min, and the supernatant was aspirated into a clean tube. Protein concentrations were determined using Coomassie Plus Protein Assay Reagent kit (Pierce) with modifications. Proteins were then stored at −80 ^{o}C.

7.2 Cell based assays

7.2.1 Crystal Violet staining

Each well was washed twice with PBS. Adherent cells were incubated with 0.5% crystal violet in 20% methanol for 10 min, and each well was washed with PBS to remove residual crystal violet stain. The plate was left to dry overnight, and cells stained with crystal violet were solubilized using 500 µl of 1% SDS for 15 min.

Absorbance was read at 520 nm by a spectrometer (Infinite M200, TECAN, Männedorf, Switzerland).

7.2.2 Proliferation assay

Cells were seeded at 2,000 cells per well, in triplicates, in four 96-well plates. Every 24 h, one plate was removed and proliferation was terminated. After washing the cells with PBS, the amount of cells was quantified by crystal violet staining. Cell proliferation was followed over a course of 96 h.

7.2.3 TBHP treatment

For TBHP survival assay, 35,000 cells were seeded in triplicate in 24-well plates. Cells were treated with 0 μM, 10 μM, 20 μM, 30 μM, 40 μM, 50 μM, 60 μM and 70 μM TBHP (Sigma Aldrich) 24 h after seeding and cultured for another 24 h. Adherent cells were quantified using crystal violet staining.

7.3 Flow cytometry

Flow cytometry was performed on FacsAria II (BD Biosciences, San Jose, CA) and data collected using FACS Diva v6 software (BD Biosciences). Cells were fixed by adding −20 °C 100% ethanol dropwise with shaking to a cell suspension in 1 ml PBS to a final concentration of 70% ethanol.

7.3.1 Cell cycle analysis

250,000 cells were seeded in 6 well plates for 48 h before harvesting. It was ensured that the cells had not reached more than 90% confluency. Collected cells were washed twice with ice-cold PBS before fixing with 70% ethanol at −20 ^{o}C overnight. After fixing, cells were washed twice with PBS and incubated with 50 μg/mL PI, 50 ug/mL RNase in PBS for 3 h before flow cytometry analysis. Data

from 20,000 singlets were recorded. Analysis of cell cycle was carried out using ModFIT LT software version 3.3 (Verity Software House Inc., Topsham, ME).

7.3.2 Mitochondrial membrane potential measurement

250,000 cells were seeded in 6 well plates for 48 h, before being harvested, fixed in 70% cold ethanol and stained using the JC10 mitochondrial membrane potential assay kit (Abcam). Data from 10,000 singlets were recorded and analysis was carried out using Cyflogic version 1.2.1 (CyFlo Ltd)

7.3.3 ROS measurement

250,000 cells were seeded in 6 well plates for 48 h. After 48 h, cells were loaded with 5 mM 2′,7′Dichloro-dihydro-fluorescein diacetate (DCFH, Life Technologies) in growth media for 30 min before the cells were harvested, washed and fixed for 30 min and analyzed using FACS. Data from 10,000 singlets were recorded. Data analysis was carried out using Cyflogic version 1.2.1 (CyFlo Ltd, Turku, Finland).

7.4 iTRAQ proteome profiling

7.4.1 iTRAQ labeling chemistry

Isobaric Tags for Relative and Absolute Quantitation (iTRAQ) uses up to four or eight different isobaric labels for relative quantification of protein expression. The technology lies in the design of the isobaric labels (Fig 7-1), where each label consists of a reporter group, balance group and a peptide reactive group. In four-plex iTRAQ, the reporter groups have masses of 114, 115, 116 and 117, however the overall mass of each label is kept constant by balancing it with a neutral loss group. During chemical labeling, the peptide reactive groups link covalently with lysine side chain amine groups as well as the N-termini of all peptides, ensuring complete

coverage of the entire proteome. As each iTRAQ label adds the same mass to every peptide, peptide precursors from different samples would still appear as a single peak in MS. During fragmentation, the reporter group is released along with the usual fragmentation of peptides. The intensity of the reporter indicates the relative abundance of that peptide in each sample and the MS/MS spectra of the peptides identify the peptide sequence.

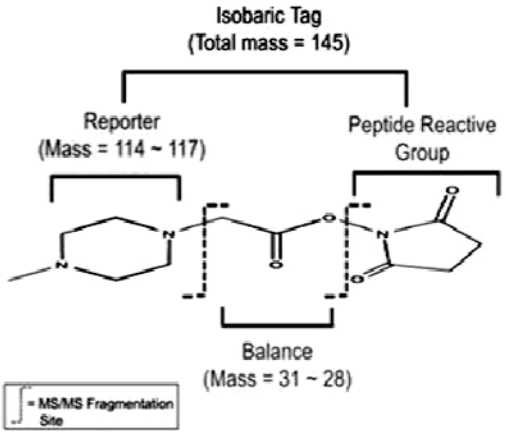

Figure 7-1: Chemistry of the iTRAQ Label. Equal mass of each label is maintained with neutral loss of the balance group. This ensures the same peptide with different label would only appear as a single peak in MS. The reporter group quantifies peptides from respective sample in MS/MS.

7.4.2 Protein extraction for iTRAQ

Control and OF cells were harvested and lysed with 500 mM triethylammonium bicarbonate (TEAB; Sigma), 1.0% (w/v) SDS and boiled at 100 ^{o}C for 10 min. Supernatant was retained after centrifugation at 14,500g for 30 min at 4°C. Estimation of protein content was carried out using RC-DC protein assay kit (Bio-Rad, Hercules, CA).

7.4.3 iTRAQ labeling and sample preparation

100 µg of each sample was reduced with tris-(2-carboxyethyl) phosphine (TCEP) and alkylated with methyl methane-thiosulfonate (MMTS). After cysteine blocking, the samples were trypsinized for 16 h at 37°C. After digestion, each sample was dried and reconstituted with 0.5M TEAB. Each digested sample was labeled for 2 h at room temperature with one of the four isobaric amine-reactive tags, 114 for CAT control and 115, 116, 117 for OE cells OF1, OF5 and OF6 respectively. The four iTRAQ-derivatized samples were then pooled and passed through a strong cation exchange cartridge following manufacturer's protocol (Applied Biosystems, Foster City, CA) to remove interfering substance such as excess iTRAQ regents, organic solvent and SDS. The samples after clean-up were desalted using a C-18 Sep-Pak cartridge (Merck Millipore) and lyophilized, before reconstitution in 95% H_2O, 5% acetonitrile (ACN) and 0.1% formic acid (FA) for 2D-LC separation.

7.4.4 2D-LC separation

The first dimension peptide separation was performed using the Ultimate LC system (Dionex-LC-Packings, Sunnyvale, CA) connected to a strong cation-exchange (SCX) column. Ninety-six microgram (via multiple injections) of the labeled peptide mixture was injected using the micro-pickup mode into a Zorbax Bio-SCX II column (Agilent, SantaClara, CA). SCX mobile phase A was 5% ACN and 0.05% FA and mobile phase B was 5% ACN, 500 mM NaCl and 0.05% FA. The flow rate was set at 10µl/min. A total of 43 fractions were eluted (2 min each) and collected on a 96 well v-bottom plates using step gradients of mobile B as follows: 5% for 1 min, 5-12% for next 29 min, 12-30% for next 90 min, 30-90% for next 2 min, hold at 90% for next 7 min and 90-5% for last 5 min and continued at 5% for another 12 min. The eluted fractions were subsequently combined to 9 fractions

and then desalted with Sep-Pak® tC18 µElution Plate (186002318, Waters Corp., Milford, MA) using a vacuum manifold (Merck Millipore) in accordance to the manufacturer's recommendations, before second-dimension reversed-phase (RP) chromatography. From RP separation of each fraction, 5 µg was trapped on a pre-column (200 µm x 0.5 mm) and then eluted on an analytical column (75 µm x 150 mm). Both columns were packed with Reprosil-Pur C18-AQ 3 µm 120 Å phase (Eksigent, Dublin, CA). The RP mobile phase A was 98% H2O (with 0.1% FA) while RP mobile phase B was 98% ACN (with 0.1% FA). The peptides were separated by a linear gradient of 12-30% of mobile B in 90 min at a flow rate of 300 nl/min.

7.4.5 Tandem mass spectrometry

The tandem MS analysis was performed using a 5600 TripleTOF analyzer (QqTOF; AB SCIEX, Framingham, MA) in Information Dependent Mode. Precursor ions were selected across the mass range of 400-1800 m/z using 250 ms accumulation time per spectrum. A maximum of 20 precursors per cycle from each MS spectra were selected for MS/MS analyses with 100 ms accumulation time for each precursor and dynamic exclusion for 15 s. Tandem mass spectrometry was recorded in high sensitivity mode with rolling collision energy on and iTRAQ reagent collision energy adjustment on.

Precursor ions were selected across the mass range of 350-1250 m/z using 250 ms accumulation time per spectrum. A maximum of 20 precursors per cycle from each MS spectra were selected for MS/MS analyses with 100 ms accumulation time for each precursor and dynamic exclusion for 8 s. Tandem mass spectrometry was recorded in high sensitivity mode with rolling collision energy on.

7.4.6 Peptide and protein identification

Protein identification and relative iTRAQ quantification were performed with ProteinPilot™ Software 4.1 (AB SCIEX) using the Paragon™ algorithm for the peptide identification, which was further processed by Pro Group™ algorithm where isoform-specific quantification was adopted to trace the differences between expressions of various isoforms. The Pro Group Algorithm calculates protein ratios using only ratios from the spectra that are distinct to each protein or protein form and thus eliminates any masking of changes in expression because of peptides that are shared between proteins. User defined search parameters were as follows: (1) Sample Type: iTRAQ 4 plex (Peptide Labeled); (2) Cysteine Alkylation: MMTS; (3) Digestion: Trypsin; (4) Instrument: TripleTOF5600; (5) Special Factors: None; (6) Species: Homo sapiens; (7) ID Focus: Biological modifications; (8) Database: ipi.HUMAN.v3.87.fasta (182888 proteins searched); (9) Search Effort: Thorough; (10) the False Discovery Rate Analysis: Yes; (11) User Modified Parameter Files: Yes. For iTRAQ quantitation, the peptide for quantification was automatically selected by Pro Group™ algorithm to calculate the reporter peak area, error factor (EF) and *p*-value. The resulting data set was auto bias-corrected to remove any variations resulting from unequal mixing when combining labeled samples. Each modified peptide was counted as a unique peptide. The peak areas and the signal-to-noise (S/N) ratios were extracted from the database by Protein Pilot to process the raw data for quantification. A reverse database search strategy was adopted to estimate the false discovery rate for peptide identification. A strict unused score above 1.3 was used as the qualification criteria, which corresponds to a peptide confidence level of 95%. With this filter, the corresponding false discovery rate of 0% was calculated from the decoy hits.

7.4.7 Protein annotation, data representation and enrichment analysis

For determination of consistency within biological triplicates, log ratio of all peptides from OF1, OF5 and OF6 were plotted pair wise and their r-square values were calculated with MS EXCEL. Coefficient of variation for proteins with differential abundance was calculated using MS EXCEL. Proteins with differential abundance were annotated using UniprotKB Protein Knowledgebase (http://www.uniprot.org/). The proteins were classified based on Uniprot keywords under the category of Biological process. Significantly altered protein list was uploaded into Database for Annotation, Visualization and Intergrated Discovery (DAVID v6.7, http://david.abcc.ncifcrf.gov) for functional annotation and enrichment analysis [212, 213]. Enriched targets were mapped onto KEGG pathway using the Functional Annotation Tool.

7.5 SWATH™ MS proteome profiling

7.5.1 Protein extraction and sample preparation

Control and OF cells were harvested and lysed in 8M Urea, 25mM TEAB, 2% Triton X-100, 0.1% SDS supplemented with 1× HALT protease inhibitor cocktail (Thermo scientific), 50 µg/ml DNase I (Sigma) and 50 µg/ml RNase A (Sigma). Supernatant was acquired after centrifugation at 14,500g for 30 min at 15°C. Protein estimation was carried out using RC-DC protein assay kit (Bio-Rad, Hercules, CA).

7.5.2 LC separation

Four microgram of each sample was separated on the same RP LC setup (Section 7.4.4, second dimension separation). Mobile phase A: 0.1% FA in 2% ACN. Mobile phase B: 0.1% FA in 98% ACN. Flow rate was set to 300 nL/min. LC

gradient: 1 min of 95% A, 29 min of 95-88% A, 90 min of 88-70% A, 2 min of 70-10% A, 7 min of 10% A, 3 min of 10-95% and 14 min of 95% A.

7.5.3 SWATH™ acquisition mass spectrometry

Samples were analyzed on a TripleTOF 5600® system (QqTOF; AB SCIEX,) in SWATH mode. Each acquisition method had a cycle time of 3 s, consisting of 36 acquisition window of 25 Da, each with 80 ms accumulation time and 50 ms of TOF/MS survey scan from 350 to 1250 Da. Each MS/MS acquisition window consisted of a scan of 100 to 1,800 Da and was performed using collision energy of 35 V with a spread of 15 V.

7.5.4 SWATH™ ion library generation

An ion library was generated using a pool of all samples in equal proportion that was separated using the same LC gradient (Section 7.5.2) and analyzed on a TripleTOF 5600® system (QqTOF; AB SCIEX,) in Information Dependent Mode. Precursor ions were selected across the mass range of 350-1250 m/z using 250 ms accumulation time per spectrum. A maximum of 20 precursors per cycle from each MS spectra were selected for MS/MS analyses with 100 ms accumulation time for each precursor and dynamic exclusion for 8 s. Tandem mass spectrometry was recorded across the mass range of 100-1800 m/z in high sensitivity mode with rolling collision energy on.

7.5.5 Protein identification and quantitation

Protein identification was performed with ProteinPilot™ Software 4.1 (AB SCIEX) as previously described (Section 7.4.6). User defined search parameters were as follows: (1) Sample Type: Identification; (2) Cysteine Alkylation: MMTS; (3) Digestion: Trypsin; (4) Instrument: TripleTOF5600; (5) Special Factors: None;

(6) Species: Homo sapiens; (7) ID Focus: Biological modifications; (8) Database: ipi.HUMAN.v3.87.fasta (182888 proteins searched); (9) Search Effort: Thorough; (10) the False Discovery Rate Analysis: Yes; (11) User Modified Parameter Files: No. The proteins identified were used to generate an ion library for SWATH™. Peak alignment and data interrogation was done using PeakView software V1.2.0.3(AB SCIEX) supplement with MS/MS(ALL) with SWATH Acquisition Microapp, version 1.0.0.653 add-on with the following filter: Peptide confidence: 99%, Exclude modifications: Yes, Exclude Shared: Yes.

7.6 Metabolomics profiling

7.6.1 Metabolite extraction

Metabolites were extracted from control and OF cells using 80% methanol. Cells from OF1, 5, 6 and CAT were seeded in 15 mm dish and grown to 70% confluency. Cells were lysed by adding -80°C 80% methanol and scraped down. Cell debris was pelleted at 16,000 *g* for 10 min at 4°C and the supernatants were retained for LC-MS analyses. To obtain similar concentration of metabolites within samples, the amount of 80% methanol used was 1 mL per 10^6 cells. Cell numbers were determined using a counting plate, seeded alongside the triplicate plates.

7.6.2 LC separation

10 µl of extracted metabolite samples were separated on Agilent1290 Infinity LC (Agilent, Santa Clara, CA) with Phenomenex (Torrance, CA) Kinetex HILIC column (2.6 µm ID x 5 cm). Mobile phase A: H_2O with 0.1% FA. Mobile phase B: ACN with 0.1% FA. Flow rate is set at 0.3 mL/min. LC gradient: 5 min of 5% A, 19 min of 5-50% A, 4 min of 50-80% A, 2 min of 80% A, 1 min of 80%-20% A, 8 min of 20% A.

7.6.3 Tandem mass spectrometry

Samples were analyzed on a TripleTOF 5600 system (QqTOF; AB SCIEX) in an Information Dependent Acquisition (IDA) LC/MS/MS method. Each IDA method consisted of a high-resolution TOF/MS survey scan of 50-1000 m/z mass range for 100 ms accumulation time, followed by the selection of up to 20 singly-charged precursors for MS/MS analyses. Each MS/MS acquisition was performed using rolling collision energy and acquired for 100 ms. Dynamic exclusion for 3 s was performed.

7.6.4 Metabolite quantitation and identification

Data processing and interpretation were performed using PeakView software (AB SCIEX). Peak alignment and peak area integration was performed with MultiQuant software (AB SCIEX). Triplicate runs from OF1, OF5 and OF6 were averaged. Triplicate runs from CAT were averaged. Comparison was done within all OF samples versus CAT samples. Differential peaks with fold change ≥1.5 and p value < 0.05 were selected for peak identification. For metabolite identification, MS and MS/MS spectra of each peak was searched using MS/MS spectrum Match tool (http://metlin.scripps.edu/spec_search.php) available from the METLIN database (http://metlin.scripps.edu/index.php).

7.6.5 Data representation

For visualization of data, metabolite dataset were uploaded to XCMS online (https://xcmsonline.scripps.edu/), a web-based metabolomics data processing platform. XCMS performs feature detection, which are peaks with retention time corrected and aligned across all dataset. Using these features, XCMS then annotates, quantifies and performs statistical analyses. XCMS online also generates visualization plot of the data, providing a clearer picture of the metabolic differences

between CAT and OF156. A comparison analysis was carried out with predefined settings with the closest match of the instrumentation used. MarkerView™ software was used for quantitation of the metabolomics data. MarkerView™ also performs peak detection, retention time alignment as well as quantitation. Importantly, MarkerView™ also offers various methods for data normalization during quantification providing a more reliable relative abundance of metabolites.

7.7 Molecular methods

7.7.1 Western blot

Twenty microgram of whole cell lysate (Section 7.1.5) was separated with 12.5% SDS-PAGE. Proteins were electroblotted onto PVDF membrane (Bio-Rad) at 50V for one hour at 4 ^{o}C. Blocking and subsequent antibody incubation were performed with 5% and 1% non-fat milk in PBS with 0.05% Tween-20 respectively. The primary antibodies used were anti-FXN (Merck Millipore, Billerica, MA), anti-V5, (Life Technologies), cyclin D and cyclin E (Cell Signaling Technology, Danvers, MA), p21, p27, cdk2, cdk4, EMMPRIN, HIF-1α (Santa Cruz, Dallas, TX), GPx1, ATP5O (Abcam, Cambridge, UK) and actin (GE Healthcare, Buckinghamshire, UK). The secondary antibodies used were anti-mouse antibody conjugated with HRP (BD biosciences), anti-goat antibody conjugated with HRP (Thermo scientific) and anti-rabbit antibody conjugated with HRP (GE Healthcare).

7.7.2 Reverse transcriptase PCR

Total RNA was isolated from control and FXN over-expressing cell using RNeasy Plus minikit (Qiagen, Chatworth, CA) according to manufacturer's protocol. SuperScript® III kit was used to perform a two step reverse transcription PCR on the isolated RNA using the following primers: FXN forward primer 5'-

GCCTCAACCAGATTTGGAAT-3', FXN reverse primer 5'-CTGGACTTGTCTTCCTTGGC-3' or V5 Reverse primer 5'-ATCCCTAACCCTCTCCTCGGT-3'. Negative control for presence of genomic DNA was carried out without reverse transcriptase in the reaction mix.

7.8 Statistical analysis

All experiments were carried out in triplicate unless stated otherwise. Student's *t*-test was performed using GraphPad Prism Version 5 (GraphPad Software, Inc., La Jolla, CA).

Appendix I: Metabolites with altered concentrations in OF cells.

Compound	m/z	Retention time in mins	Fold change[#]	*p*-value
5′-Deoxy-5′-(methylthio)adenosine	298.0976	18.66	2.698	0.0169
Butenoyl PAF	550.386	12.18	2.521	0.00988
L-Carnitine	162.1117	10.47	2.319	0.00057
PC(16:0/0:0)[U] / PC(16:0/0:0)[rac]	496.3382	12.45	2.268	0.00616
PAF C-16	546.3554	12.29	2.236	0.01294
Thr Cys Gly	280.0903	16.57	2.191	0.01818
Choline	104.1054	11.42	2.024	6.4249E-05
Phosphocholine	184.0733	16.58	1.963	0.00391
Glutathione, oxidized	613.161	14.54	1.825	0.01129
Glycerophosphocholine	292.0726	16.58	1.771	0.01234
Lyso-PAF C-16	482.3602	12.65	1.755	0.00068
L-Arginine	175.1183	15.95	1.704	0.0001
Elaidylphosphocholine	434.3402	12.64	1.610	0.00712
D-Lysine	147.1118	15.93	1.599	0.00031
L-Methionine S-oxide	166.0524	12.6	1.537	6.4764E-06
3-Methyl-L-histidine	170.0899	16.67	1.462	0.0111
L-Valine	118.085	9.49	1.412	9.1302E-07
L-Tyrosine	182.0802	9.2	1.387	0.03751
L-Methionine	150.0579	9.42	1.348	5.9789E-06
(R)-(+)-2-Pyrrolidone-5-carboxylic acid	130.05	11.15	1.299	0.00021
Betaine	118.0856	11.87	1.277	5.8829E-05

Compound	m/z	Retention time in mins	Fold change[#]	*p*-value
L-proline	116.0696	10.78	1.209	0.00026
D-Glutamine	145.0618	11.1	1.195	0.0425
L-Phenylalanine	166.0853	8.89	1.174	0.00589
Creatine	130.0622	9.73	1.067	0.00805
L-Asparagine	131.045	10.83	-1.079	0.04898
cGMP	366.0153	9.93	-1.094	0.01684
Isobutyryl carnitine	232.1538	8.79	-1.124	0.03287
Trans-4-Hydroxy-L-proline	130.0503	10.8	-1.148	0.03602
Dihomo-γ-Linolenoyl PAF C-16	792.5896	10.7	-1.184	0.00182
Glutathione	306.076	10.15	-1.242	0.00026
Eicosapentaenoyl PAF C-16	766.5669	10.77	-1.252	0.0067
L-Glutamate	146.0451	9.54	-1.261	5.3322E-05
PC(18:3(6Z,9Z,12Z)/18:3(6Z,9Z,12Z))	778.5375	10.82	-1.314	0.00297
SM(d18:1/16:0)	725.5591	11.84	-1.330	0.00025
Acetylcarnitine	204.1212	9.76	-1.467	0.03115
1-Octadecyl Lysophosphatidic Acid	425.3102	11.5	-1.646	0.00095

Fold change of metabolite levels in OF cells compared to CAT control

Appendix II: Altered proteins in FXN OE as identified by iTRAQ

Accession No.	Gene name	Protein name	Peptides	Fold change[#] (±S.D.)
IPI00925572	ASNS	Asparagine synthetase [glutamine-hydrolyzing] isoform b	4	3.971 ± 0.794
IPI00425562	SCRIB	Isoform 2 of Protein scribble homolog	3	3.033 ± 0.345
IPI00335069	PSMD12	26S proteasome non-ATPase regulatory subunit 12 isoform 2	2	3.007 ± 0.217
IPI00900380	MCTS1	Isoform 2 of Malignant T cell-amplified sequence 1	2	2.563 ± 0.284
IPI00759832	YWHAB	Isoform Short of 14-3-3 protein beta/alpha	15	2.594 ± 0.316
IPI00007811	CDK4	Cyclin-dependent kinase 4	2	2.146 ± 0.563
IPI00289159	GLS	Glutaminase kidney isoform, mitochondrial	8	2.117 ± 0.388
IPI00927799	CTNNB1	Beta-catenin	3	2.078 ± 0.435
IPI00003704	RBM4	RNA-binding protein 4	10	2.298 ± 0.11
IPI00019359	KRT9	Keratin, type I cytoskeletal 9	2	3.041 ± 0.839
IPI00845507	RPL21	60S ribosomal protein L21	4	2.236 ± 0.599
IPI01022431	ALDH2	Aldehyde dehydrogenase, mitochondrial	3	2.029 ± 0.436
IPI00965445	FIP1L1	Pre-mRNA 3'-end-processing factor FIP1	3	2.514 ± 0.897
IPI01013106	BAG2	BAG family molecular chaperone regulator 2	3	1.956 ± 0.328
IPI00021258	ARFIP1	Isoform B of Arfaptin-1	2	1.827 ± 0.43
IPI01010990	LGALS3BP	Galectin-3-binding protein	4	1.583 ± 0.451
IPI00017339	SF3B4	Splicing factor 3B subunit 4	6	2.09 ± 0.208
IPI00646689	TXNDC17	Thioredoxin domain-containing protein 17	3	1.882 ± 0.223
IPI00890727	SPATA5	Isoform 2 of Spermatogenesis-associated protein 5	2	1.839 ± 0.225
IPI00641157	CTSA	lysosomal protective protein isoform c precursor	2	1.846 ± 0.331
IPI01009918	PRSS1	Trypsin-1	16	2.492 ± 0.884

Accession No.	Gene name	Protein name	Peptides	Fold change[#] (±S.D.)
IPI00967716	Sep 11	Septin-11	4	1.965 ± 0.342
IPI00549296	SAP30BP	SAP30-binding protein	2	2.095 ± 0.448
IPI00954530	OCIAD1	OCIA domain-containing protein 1 isoform 4	7	2.241 ± 0.231
IPI00329801	ANXA5	Annexin A5	9	1.767 ± 0.191
IPI00956296	APOPT1	Kinesin light chain 1	3	2.126 ± 0.317
IPI00797126	NACA	Nascent polypeptide-associated complex subunit alpha	5	1.74 ± 0.377
IPI00007611	ATP5O	ATP synthase subunit O, mitochondrial	11	1.84 ± 0.118
IPI00795751	RPL23	60S ribosomal protein L23	14	1.817 ± 0.134
IPI00221093	RPS17	40S ribosomal protein S17	5	1.948 ± 0.085
IPI00909812	B4DTS6	CD97 antigen	2	1.818 ± 0.078
IPI00964364	EEF1E1	Eukaryotic translation elongation factor 1 epsilon-1	3	1.998 ± 0.407
IPI00156689	VAT1	Synaptic vesicle membrane protein VAT-1 homolog	11	1.694 ± 0.185
IPI00946558	ALDH5A1	Succinate-semialdehyde dehydrogenase, mitochondrial	2	1.717 ± 0.144
IPI00922336	TBL1XR1	F-box-like/WD repeat protein TBL1XR1	3	2.01 ± 0.221
IPI01015990	Sep 7	Septin-7	2	1.607 ± 0.215
IPI00216691	PFN1	Profilin-1	17	1.991 ± 0.326
IPI00024320	RBM3	RNA-binding protein 3	8	1.822 ± 0.102
IPI01024943	CLASP1	CLIP-associating protein 1	2	1.852 ± 0.239
IPI00182373	P4HA2	Prolyl 4-hydroxylase subunit alpha-2	2	1.723 ± 0.1
IPI00021267	EPHA2	Ephrin type-A receptor 2	4	1.735 ± 0.264
IPI00017469	SPR	Sepiapterin reductase	3	1.721 ± 0.271
IPI00646762	NUDT5	ADP-sugar pyrophosphatase	8	1.854 ± 0.086
IPI00845446	PDS5B	Isoform 2 of Sister chromatid cohesion protein PDS5 homolog B	5	1.629 ± 0.183
IPI00009276	PROCR	Endothelial protein C receptor precursor	2	1.568 ± 0.207

Accession No.	Gene name	Protein name	Peptides	Fold change[#] (±S.D.)
IPI00410026	LUC7L	Isoform 2 of Putative RNA-binding protein Luc7-like 1	5	1.753 ± 0.408
IPI00746438	RPL11	Isoform 2 of 60S ribosomal protein L11	8	1.951 ± 0.314
IPI00171665	NUP37	Nucleoporin Nup37	2	1.641 ± 0.124
IPI00216044	RALY	RNA-binding protein Raly	9	1.684 ± 0.072
IPI00021405	LMNA	soform A of Prelamin-A/C	90	1.825 ± 0.108
IPI00464979	SUCLA2	Succinyl-CoA ligase [ADP-forming] subunit beta, mitochondrial	3	1.714 ± 0.172
IPI00472442	PSMA1	Isoform Long of Proteasome subunit alpha type-1	7	1.58 ± 0.146
IPI00019912	HSD17B4	Peroxisomal multifunctional enzyme type 2	3	1.486 ± 0.198
IPI00910593	CNN2	Calponin-2	2	2.005 ± 0.45
IPI01026232	NAP1L1	Nucleosome assembly protein 1-like 1	9	1.741 ± 0.148
IPI00293425	FXN	Frataxin, mitochondrial	3	1.781 ± 0.428
IPI00978887	RAB11B	Ras-related protein Rab-11B	3	1.619 ± 0.12
IPI00746165	WDR1	WD repeat-containing protein 1	5	1.637 ± 0.144
IPI00909097	CIRBP	Cold-inducible RNA-binding protein	3	1.711 ± 0.129
IPI00908949	TARS	Threonyl-tRNA synthetase, cytoplasmic	2	1.691 ± 0.04
IPI00856098	RRBP1	p180/ribosome receptor	21	1.641 ± 0.09
IPI00788849	TFG	Protein TFG isoform 2	6	1.716 ± 0.066
IPI00294911	SDHB	Succinate dehydrogenase [ubiquinone] iron-sulfur subunit, mitochondrial	8	1.623 ± 0.174
IPI01009326	CCT8	T-complex protein 1 subunit theta	25	1.602 ± 0.031
IPI00930174	HIST2H2BF	Histone H2B type 2-F isoform b	46	1.72 ± 0.323
IPI00021327	GRB2	Growth factor receptor-bound protein 2	2	1.517 ± 0.099
IPI00515061	HIST1H2BJ	Histone H2B type 1-J	41	1.665 ± 0.15
IPI00465151	RAB11FIP1	Isoform 2 of Rab11 family-interacting protein 1	3	1.613 ± 0.058
IPI00014808	PAFAH1B3	Platelet-activating factor acetylhydrolase IB subunit gamma	3	1.747 ± 0.117

Accession No.	Gene name	Protein name	Peptides	Fold change[#] (±S.D.)
IPI00942092	ADSL	Adenylosuccinate lyase	3	1.598 ± 0.189
IPI00418497	TIMM50	Isoform 2 of Mitochondrial import inner membrane translocase subunit TIM50	3	1.793 ± 0.157
IPI00946474	NDUFA5	NADH dehydrogenase [ubiquinone] 1 alpha subcomplex subunit 5	3	1.545 ± 0.121
IPI00967869	CAMK2D	Calcium/calmodulin-dependent protein kinase type II subunit delta	3	1.651 ± 0.174
IPI00017334	PHB	Prohibitin	25	1.574 ± 0.139
IPI00941463	NAP1L4	Nucleosome assembly protein 1-like 4	7	1.69 ± 0.213
IPI00010415	ACOT7	Cytosolic acyl coenzyme A thioester hydrolase	2	1.595 ± 0.027
IPI00099996	RG9MTD1	Mitochondrial ribonuclease P protein 1	7	1.61 ± 0.091
IPI00019755	GSTO1	Glutathione S-transferase omega-1	5	1.647 ± 0.261
IPI00100748	HSPBP1	Hsp70-binding protein 1	2	1.634 ± 0.264
IPI00647491	KIAA0391	Mitochondrial ribonuclease P protein 3	2	1.613 ± 0.056
IPI00922214	RDBP	Negative elongation factor E	2	1.657 ± 0.399
IPI00013683	TUBB3	Tubulin beta-3 chain	65	1.675 ± 0.223
IPI01018641	SNRPB	Small nuclear ribonucleoprotein-associated proteins B	5	1.507 ± 0.083
IPI00980165	MANF	Mesencephalic astrocyte-derived neurotrophic factor	6	1.54 ± 0.044
IPI00011996	UBE2Z	Ubiquitin-conjugating enzyme E2 Z	2	1.639 ± 0.104
IPI00647286	FAM129B	Niban-like protein 1	3	1.608 ± 0.125
IPI00291467	SLC25A6	ADP/ATP translocase 3	4	1.597 ± 0.049
IPI00440727	BRD4	Bromodomain-containing protein 4	3	1.61 ± 0.097
IPI00024911	ERP29	Endoplasmic reticulum resident protein 29	8	1.48 ± 0.047
IPI00021700	PCNA	Proliferating cell nuclear antigen	9	1.586 ± 0.08
IPI00382869	FDPS	Farnesyl pyrophosphate synthetase like-4 protein (Fragment)	3	1.607 ± 0.091
IPI00900366	KIAA0564	von Willebrand factor A domain-containing protein 8	3	1.507 ± 0.1
IPI00910821	GPX8	Glutathione peroxidase 8	3	1.558 ± 0.078

Accession No.	Gene name	Protein name	Peptides	Fold change[#] (±S.D.)
IPI00218606	RPS23	40S ribosomal protein S23	2	1.531 ± 0.051
IPI00002134	PSMD5	26S proteasome non-ATPase regulatory subunit 5	2	1.424 ± 0.09
IPI00890837	SMCHD1	Structural maintenance of chromosomes flexible hinge domain-containing protein 1	3	1.471 ± 0.051
IPI00166749	PMPCA	Mitochondrial-processing peptidase subunit alpha	4	1.532 ± 0.047
IPI00829819	C9orf80	Isoform 2 of SOSS complex subunit C	3	1.529 ± 0.158
IPI00001639	KPNB1	Importin subunit beta-1	11	1.607 ± 0.102
IPI00003217	PSMB7	Proteasome subunit beta type-7	5	1.472 ± 0.056
IPI00216695	BAZ1B	Isoform 2 of Tyrosine-protein kinase BAZ1B	7	1.522 ± 0.108
IPI00016342	RAB7A	Ras-related protein Rab-7a	6	1.438 ± 0.115
IPI00021766	RTN4	Reticulon-4	5	1.508 ± 0.199
IPI00001589	TIMM13	Mitochondrial import inner membrane translocase subunit Tim13	2	1.544 ± 0.246
IPI00337494	SLC25A24	Calcium-binding mitochondrial carrier protein SCaMC-1	5	1.577 ± 0.083
IPI00007320	TCF25	Transcription factor 25	3	1.782 ± 0.278
IPI00020418	RRAS	Ras-related protein R-Ras	2	1.492 ± 0.189
IPI00376215	PRKDC	Isoform 2 of DNA-dependent protein kinase catalytic subunit	2	1.433 ± 0.041
IPI00000816	YWHAE	14-3-3 protein epsilon	23	1.476 ± 0.029
IPI00216057	SORD	Sorbitol dehydrogenase	2	1.667 ± 0.345
IPI00000874	PRDX1	Peroxiredoxin-1	42	1.5 ± 0.051
IPI00026970	SUPT16H	FACT complex subunit SPT16	7	1.575 ± 0.114
IPI00301323	DDX18	ATP-dependent RNA helicase DDX18	5	1.398 ± 0.071
IPI00027252	PHB2	Prohibitin-2	26	1.55 ± 0.121
IPI00646813	TROVE2	60 kDa SS-A/Ro ribonucleoprotein isoform 1	4	1.392 ± 0.059
IPI00916229	MAT2A	S-adenosylmethionine synthase	4	1.539 ± 0.158
IPI00020021	DEK	Protein DEK	9	1.436 ± 0.02

Accession No.	Gene name	Protein name	Peptides	Fold change[#] (±S.D.)
IPI00006442	COIL	Coilin	3	1.479 ± 0.064
IPI00017289	SNRNP27	U4/U6.U5 small nuclear ribonucleoprotein 27 kDa protein	2	1.396 ± 0.059
IPI01013413	ACTR3	Actin-related protein 3	7	1.587 ± 0.341
IPI00183508	TWF1	Twinfilin-1	2	1.616 ± 0.314
IPI00984332	CD58	Isoform 2 of Lymphocyte function-associated antigen 3	2	1.614 ± 0.345
IPI00939917	SMARCD2	Isoform 3 of SWI/SNF-related matrix-associated actin-dependent regulator of chromatin	2	1.466 ± 0.047
IPI00644108	BUB3	Mitotic checkpoint protein BUB3	12	1.442 ± 0.053
IPI00746062	PPP4R2	Isoform 2 of Serine/threonine-protein phosphatase 4 regulatory subunit 2	2	1.54 ± 0.117
IPI00555593	PDLIM5	Enigma homolog (Fragment)	10	2.281 ± 1.367
IPI00952607	CCT7	T-complex protein 1 subunit eta isoform d	10	1.454 ± 0.137
IPI00298111	SNX6	Sorting nexin-6 isoform b	2	1.442 ± 0.046
IPI01021277	DCTN2	Dynactin subunit 2	5	1.555 ± 0.297
IPI00646917	NUDT21	Cleavage and polyadenylation specificity factor subunit 5	4	1.418 ± 0.052
IPI00015897	CHORDC1	Cysteine and histidine-rich domain-containing protein 1	6	1.497 ± 0.11
IPI00373882	RFC3	Replication factor C subunit 3 isoform 2	2	1.521 ± 0.226
IPI00797421	SDAD1	Isoform 2 of Protein SDA1 homolog	2	1.443 ± 0.119
IPI00941907	STRAP	Serine-threonine kinase receptor-associated protein	5	1.411 ± 0.12
IPI00013930	STX6	Syntaxin-6	2	1.405 ± 0.059
IPI00384967	ALDH1A3	Aldehyde dehydrogenase family 1 member A3	2	1.462 ± 0.217
IPI00386803	LASP1	Isoform 2 of LIM and SH3 domain protein 1	8	1.464 ± 0.208
IPI00465248	ENO1	Alpha-enolase	58	1.352 ± 0.038
IPI00374657	VAPA	Isoform 2 of Vesicle-associated membrane protein-associated protein A	17	1.436 ± 0.088
IPI00004968	PRPF19	Pre-mRNA-processing factor 19	6	1.418 ± 0.07
IPI00644220	HTATSF1	HIV TAT specific factor 1	4	1.541 ± 0.189

Accession No.	Gene name	Protein name	Peptides	Fold change[#] (±S.D.)
IPI00465028	TPI1;TPI1P1	Triosephosphate isomerase isoform 2	32	1.318 ± 0.008
IPI00843876	TNPO1	Isoform 2 of Transportin-1	6	1.399 ± 0.123
IPI00028883	NDUFB8	NADH dehydrogenase [ubiquinone] 1 beta subcomplex subunit 8, mitochondrial	2	1.505 ± 0.329
IPI00395627	CACYBP	Calcyclin-binding protein	20	1.443 ± 0.195
IPI00003362	HSPA5	78 kDa glucose-regulated protein	110	1.35 ± 0.044
IPI00069309	LRWD1	Leucine-rich repeat and WD repeat-containing protein 1	2	-1.39 ± 0.155
IPI00718940	PRKRA	Isoform 2 of Interferon-inducible double stranded RNA-dependent protein kinase activator A	4	-1.549 ± 0.214
IPI00093057	CPOX	Coproporphyrinogen-III oxidase, mitochondrial	35	-1.51 ± 0.281
IPI00001734	PSAT1	Phosphoserine aminotransferase	4	-1.414 ± 0.096
IPI00216492	HNRNPH3	Isoform 2 of Heterogeneous nuclear ribonucleoprotein H3	5	-1.48 ± 0.135
IPI00916892	NUP35	Nucleoporin NUP53	2	-1.467 ± 0.136
IPI00027107	TUFM	Elongation factor Tu, mitochondrial precursor	31	-1.468 ± 0.211
IPI00967000	CHCHD6	Coiled coil helix cristae morphology protein 1	2	-1.474 ± 0.22
IPI00396967	FHL2	Four and a half LIM domains protein 2	2	-1.394 ± 0.064
IPI00607723	OGT	UDP-N-acetylglucosamine--peptide N-acetylglucosaminyltransferase 110 kDa subunit	2	-1.375 ± 0.024
IPI01014026	LAMTOR1	Ragulator complex protein LAMTOR1	3	-1.525 ± 0.224
IPI00336094	HSD17B10	Isoform 2 of 3-hydroxyacyl-CoA dehydrogenase type-2	2	-1.553 ± 0.171
IPI00177716	HMGA1	High mobility group protein HMG-I/HMG-Y	3	-1.368 ± 0.026
IPI00030131	TMPO	Isoform Beta of Lamina-associated polypeptide 2, isoforms beta/gamma	37	-1.434 ± 0.094
IPI01011752	DNAJB12	Isoform 2 of DnaJ homolog subfamily B member 12	4	-1.333 ± 0.026
IPI00465256	AK3	GTP:AMP phosphotransferase, mitochondrial	4	-1.544 ± 0.193
IPI01021818	PPHLN1	Periphilin-1	3	-1.354 ± 0.012
IPI00554711	JUP	Junction plakoglobin	7	-1.376 ± 0.064
IPI00216659	RBM8A	Isoform 2 of RNA-binding protein 8A	2	-1.461 ± 0.104

Accession No.	Gene name	Protein name	Peptides	Fold change[#] (±S.D.)
IPI00007001	MRPL11	39S ribosomal protein L11, mitochondrial	5	-1.438 ± 0.056
IPI00872762	SUCLG1	Succinyl-CoA ligase [GDP-forming] subunit alpha, mitochondrial	5	-1.479 ± 0.087
IPI00293350	TSNAX	Translin-associated protein X	3	-1.604 ± 0.347
IPI00443909	CNPY2	Protein canopy homolog 2	6	-1.39 ± 0.053
IPI00783250	TRIP12	E3 ubiquitin-protein ligase TRIP12	2	-1.542 ± 0.145
IPI00789428	MCCC2	Isoform 2 of Methylcrotonoyl-CoA carboxylase beta chain, mitochondrial	2	-1.515 ± 0.236
IPI00101163	MTERFD1	mTERF domain-containing protein 1, mitochondrial	2	-1.417 ± 0.027
IPI00297579	CBX3	Chromobox protein homolog 3	11	-1.373 ± 0.035
IPI00641924	MRPS9	28S ribosomal protein S9, mitochondrial	5	-1.657 ± 0.466
IPI00917908	PPIG	Peptidyl-prolyl cis-trans isomerase G	2	-1.368 ± 0.057
IPI00018098	PRPF38B	Pre-mRNA-splicing factor 38B	2	-1.459 ± 0.109
IPI00221106	SF3B2	Splicing factor 3B subunit 2	41	-1.379 ± 0.037
IPI00218448	H2AFZ	Histone H2A.Z	12	-1.49 ± 0.188
IPI00827857	ABI1	Isoform 9 of Abl interactor 1	2	-1.418 ± 0.064
IPI00011913	HNRNPA0	Heterogeneous nuclear ribonucleoprotein A0	8	-1.449 ± 0.127
IPI00852584	RBM33	RNA-binding protein 33	2	-1.367 ± 0.075
IPI00025176	SMNDC1	Survival of motor neuron-related-splicing factor 30	3	-1.5 ± 0.05
IPI00744507	CSNK2A1	Casein kinase II subunit alpha	11	-1.371 ± 0.069
IPI00013830	SNW1	SNW domain-containing protein 1	6	-1.475 ± 0.174
IPI00025285	ATP6V1G1	V-type proton ATPase subunit G 1	3	-1.495 ± 0.1
IPI00060107	CHCHD1	Coiled-coil-helix-coiled-coil-helix domain-containing protein 1	2	-1.819 ± 0.357
IPI00328619	COQ6	Ubiquinone biosynthesis monooxygenase isoform b	2	-1.401 ± 0.074
IPI00009943	TPT1	Tumor protein, translationally-controlled 1	6	-1.461 ± 0.036
IPI00007729	NOL7	Nucleolar protein 7	6	-1.447 ± 0.046

Accession No.	Gene name	Protein name	Peptides	Fold change[#] (±S.D.)
IPI00163644	OSBPL8	Oxysterol-binding protein	3	-1.656 ± 0.247
IPI00290460	EIF3G	Eukaryotic translation initiation factor 3 subunit G	5	-1.469 ± 0.038
IPI00807545	HNRNPK	Isoform 3 of Heterogeneous nuclear ribonucleoprotein K	27	-1.549 ± 0.153
IPI00019380	NCBP1	Nuclear cap-binding protein subunit 1	2	-1.997 ± 0.816
IPI00433048	CREB1	Cyclic AMP-responsive element-binding protein 1	2	-1.859 ± 0.639
IPI01014074	PPP2R1A	Serine/threonine-protein phosphatase 2A 65 kDa regulatory subunit A alpha isoform	10	-1.4 ± 0.101
IPI00304187	RBM28	RNA-binding protein 28	7	-1.532 ± 0.156
IPI00006052	PFDN2	Prefoldin subunit 2	5	-1.475 ± 0.046
IPI00044761	PUS7	Pseudouridylate synthase 7 homolog	2	-1.425 ± 0.094
IPI00789551	MATR3	Matrin-3	28	-1.484 ± 0.149
IPI00410360	NGDN	Isoform 2 of Neuroguidin	3	-1.436 ± 0.103
IPI00916489	COPS8	COP9 signalosome complex subunit 8	2	-1.467 ± 0.091
IPI00026167	NHP2L1	NHP2-like protein 1	10	-1.487 ± 0.144
IPI00019906	BSG	Isoform 2 of Basigin	16	-1.612 ± 0.035
IPI00924935	TFRC	Transferrin receptor protein 1	5	-1.467 ± 0.12
IPI00641640	LSR	Lipolysis-stimulated lipoprotein receptor isoform 1	2	-1.742 ± 0.328
IPI00942760	MRPS27	28S ribosomal protein S27, mitochondrial	5	-1.829 ± 0.284
IPI00550689	RTCB	tRNA-splicing ligase RtcB homolog	5	-1.54 ± 0.062
IPI00024551	EMC7	ER membrane protein complex subunit 7	2	-1.541 ± 0.147
IPI00855924	EIF5AL1	Eukaryotic translation initiation factor 5A-1-like	28	-1.488 ± 0.104
IPI00024919	PRDX3	Thioredoxin-dependent peroxide reductase, mitochondrial	38	-1.571 ± 0.119
IPI00030363	ACAT1	Acetyl-CoA acetyltransferase, mitochondrial	13	-1.675 ± 0.051
IPI00945153	NDUFA6	NADH dehydrogenase [ubiquinone] 1 alpha subcomplex subunit 6	2	-1.599 ± 0.033
IPI00304493	SRFBP1	Serum response factor-binding protein 1	2	-1.505 ± 0.107

Accession No.	Gene name	Protein name	Peptides	Fold change[#] (±S.D.)
IPI00434623	MBD2	Methyl-CpG-binding domain protein 2	2	-1.445 ± 0.165
IPI00304692	RBMX	Heterogeneous nuclear ribonucleoprotein G	13	-1.528 ± 0.099
IPI00012199	CCDC86	Coiled-coil domain-containing protein 86	9	-1.537 ± 0.114
IPI00030702	IDH3A	Isocitrate dehydrogenase [NAD] subunit alpha, mitochondrial	7	-1.677 ± 0.061
IPI00395527	MINA	Isoform 4 of MYC-induced nuclear antigen	6	-1.689 ± 0.072
IPI00001541	TIMM9	Mitochondrial import inner membrane translocase subunit Tim9	2	-1.64 ± 0.217
IPI00382733	LRRFIP1	Isoform 3 of Leucine-rich repeat flightless-interacting protein 1	7	-1.541 ± 0.125
IPI00328170	MOGS	Mannosyl-oligosaccharide glucosidase	2	-1.57 ± 0.135
IPI00303568	PTGES2	Prostaglandin E synthase 2	3	-1.474 ± 0.193
IPI00334282	FAM3C	FAM3C Protein FAM3C	5	-1.694 ± 0.169
IPI00477842	SRSF8	Serine/arginine-rich splicing factor 8	2	-1.507 ± 0.18
IPI00219148	CSDA	Isoform 3 of DNA-binding protein A	14	-1.538 ± 0.21
IPI00000811	PSMB6	Proteasome subunit beta type-6	2	-1.745 ± 0.366
IPI00010346	NLN	Neurolysin, mitochondrial	3	-1.5 ± 0.226
IPI00795482	STAT1	Signal transducer and activator of transcription 1	3	-1.535 ± 0.196
IPI00893933	MSH2	DNA mismatch repair protein n	2	-1.517 ± 0.227
IPI00902976	WRNIP1	ATPase WRNIP1	2	-1.73 ± 0.131
IPI00926925	OGDH	2-oxoglutarate dehydrogenase, mitochondrial	2	-1.664 ± 0.29
IPI00328987	Bystin	Bystin	7	-1.669 ± 0.118
IPI00658000	IGF2BP3	Insulin-like growth factor 2 mRNA-binding protein 3	7	-1.618 ± 0.166
IPI00011253	RPS3	40S ribosomal protein S3	5	-1.735 ± 0.118
IPI00022648	EIF5	Eukaryotic translation initiation factor 5	6	-1.789 ± 0.049
IPI00305668	MRPS6	28S ribosomal protein S6, mitochondrial	2	-2.316 ± 0.701
IPI01010055	ANXA11	Annexin A11	4	-1.572 ± 0.211

Accession No.	Gene name	Protein name	Peptides	Fold change[#] (±S.D.)
IPI00930241	EBNA1BP2	rRNA-processing protein EBP2 isoform 1	9	-1.781 ± 0.045
IPI00945375	CUTA	Acetylcholinesterase-associated protein	2	-1.7 ± 0.267
IPI00945507	SUCLG2	Succinyl-CoA ligase [GDP-forming] subunit beta, mitochondrial isoform 1 precursor	2	-1.561 ± 0.244
IPI00397571	NSFL1C	Isoform 3 of NSFL1 cofactor p47	5	-1.67 ± 0.173
IPI00106491	MRTO4	mRNA turnover protein 4 homolog	2	-1.755 ± 0.14
IPI00642457	APRT	Adenine phosphoribosyltransferase isoform b	2	-1.786 ± 0.184
IPI00793997	IPO8	Importin-8 isoform 2	2	-1.995 ± 0.404
IPI00003327	ARL3	ADP-ribosylation factor-like protein 3	2	-1.67 ± 0.214
IPI00307591	ZNF609	Zinc finger protein 609	2	-1.704 ± 0.181
IPI00293078	DDX27	ATP-dependent RNA helicase DDX27	6	-1.99 ± 0.153
IPI00966829	ALB	Afamin	2	-1.94 ± 0.045
IPI00029264	CYC1	Cytochrome c1, heme protein, mitochondrial	9	-1.964 ± 0.167
IPI00922178	KIAA1598	Isoform 5 of Shootin-1	3	-1.767 ± 0.256
IPI00971018	TARDBP	TAR DNA-binding protein 43	3	-1.837 ± 0.161
IPI00375462	SREK1	Isoform 2 of Splicing regulatory glutamine/lysine-rich protein 1	7	-1.87 ± 0.151
IPI01011396	IDH3G	Isocitrate dehydrogenase [NAD] subunit gamma, mitochondrial isoform b precursor	3	-1.752 ± 0.217
IPI01013183	COPE	Coatomer subunit epsilon	2	-1.989 ± 0.011
IPI00902914	TM9SF2	Transmembrane 9 superfamily member 2	2	-1.64 ± 0.366
IPI00242630	HEATR2	HEAT repeat-containing protein 2	3	-1.978 ± 0.266
IPI00060627	CCDC124	Coiled-coil domain-containing protein 124	3	-1.803 ± 0.311
IPI00027172	CLIP1	Isoform 2 of CAP-Gly domain-containing linker protein 1	4	-2.154 ± 0.131
IPI00171798	MTA2	Metastasis-associated protein MTA2	2	-1.664 ± 0.403
IPI00742943	NUP43	Nucleoporin Nup43	4	-2.153 ± 0.487
IPI00748354	CHCHD4	Mitochondrial intermembrane space import and assembly protein 40	2	-2.248 ± 0.344

Accession No.	Gene name	Protein name	Peptides	Fold change[#] (±S.D.)
IPI00549248	NPM1	Nucleophosmin	29	-2.012 ± 0.165
IPI00470870	TRIP6	Thyroid receptor-interacting protein 6	2	-2.111 ± 0.134
IPI00449112	OGFR	Opioid growth factor receptor	3	-2.117 ± 0.138
IPI00026268	GNB1	Guanine nucleotide-binding protein G(I)/G(S)/G(T) subunit beta-1	6	-2.865 ± 1.104
IPI00784224	ZFR	Zinc finger RNA-binding protein	9	-2.139 ± 0.214
IPI00647528	EXOSC2	Exosome complex component RRP4	4	-1.773 ± 0.525
IPI00879460	SPTY2D1	Isoform 2 of Protein SPT2 homolog	2	-2.13 ± 0.352
IPI00026230	HNRNPH2	Heterogeneous nuclear ribonucleoprotein H2	10	-2.319 ± 0.301
IPI00217354	ARFGAP1	Isoform 2 of ADP-ribosylation factor GTPase-activating protein 1	3	-2.311 ± 0.144
IPI00719622	RPS28	40S ribosomal protein S28	2	-2.068 ± 0.715
IPI00031109	NDUFAF2	Mimitin, mitochondrial	3	-2.646 ± 0.285
IPI00411706	ESD	S-formylglutathione hydrolase	2	-3.162 ± 0.209
IPI00013774	HDAC1	Histone deacetylase 1	18	-2.059 ± 1.059
IPI01010080	STRN4	Striatin-4	3	-2.555 ± 0.756
IPI00031612	UTP23	rRNA-processing protein UTP23 homolog	2	-2.422 ± 0.961

Fold change of protein level in OF cells compared to CAT control

Appendix III: Commonly altered proteins identified by iTRAQ and SWATH

Accession No.	Gene name	Protein name	Fold change[#] in iTRAQ(±S.D.)	Fold change[#] in SWATH (±S.D.)	Same Trend
IPI00009276	PROCR	Endothelial protein C receptor precursor	1.568 ± 0.207	2.088 ± 0.506	Y
IPI00015897	CHORDC1	Cysteine and histidine-rich domain-containing protein 1	1.497 ± 0.11	1.531 ± 0.192	Y
IPI00019906	BSG	Isoform 2 of Basigin	-1.612 ± 0.035	-1.57 ± 0.102	Y
IPI00024320	RBM3	RNA-binding protein 3	1.822 ± 0.102	1.606 ± 0.245	Y
IPI00182373	P4HA2	Prolyl 4-hydroxylase subunit alpha-2	1.723 ± 0.1	3.271 ± 1.7	Y
IPI00289159	GLS	Glutaminase kidney isoform, mitochondrial	2.117 ± 0.388	2.016 ± 0.665	Y
IPI00418497	TIMM50	Isoform 2 of Mitochondrial import inner membrane translocase subunit TIM50	1.793 ± 0.157	-1.638 ± 0.117	N
IPI00550689	RTCB	tRNA-splicing ligase RtcB homolog	-1.54 ± 0.062	-1.448 ± 0.157	Y
IPI00641924	MRPS9	28S ribosomal protein S9, mitochondrial	-1.657 ± 0.466	3.453 ± 0.428	N
IPI00746438	RPL11	Isoform 2 of 60S ribosomal protein L11	1.951 ± 0.314	1.849 ± 0.337	Y
IPI00759832	YWHAB	Isoform Short of 14-3-3 protein beta/alpha	2.594 ± 0.316	-1.841 ± 0.432	N
IPI00789428	MCCC2	Isoform 2 of Methylcrotonoyl-CoA carboxylase beta chain, mitochondrial	-1.515 ± 0.236	1.558 ± 0.122	N
IPI00900380	MCTS1	Isoform 2 of Malignant T cell-amplified sequence 1	2.563 ± 0.284	1.618 ± 0.127	Y
IPI00910593	CNN2	Calponin-2	2.005 ± 0.45	1.598 ± 0.192	Y
IPI00924935	TFRC	Transferrin receptor protein 1	-1.467 ± 0.12	-1.409 ± 0.111	Y
IPI00945153	NDUFA6	NADH dehydrogenase [ubiquinone] 1 alpha subcomplex subunit 6	-1.599 ± 0.033	4.472 ± 1.103	N
IPI00966829	ALB	Afamin	-1.94 ± 0.045	-4.716 ± 3.516	Y
IPI00967869	CAMK2D	Calcium/calmodulin-dependent protein kinase type II subunit delta	1.651 ± 0.174	-1.674 ± 0.242	N
IPI00980165	MANF	Mesencephalic astrocyte-derived neurotrophic factor	1.54 ± 0.044	1.518 ± 0.161	Y

Fold change of protein levels in OF cells compared to CAT control.

List of publications

1. **Tan XF**, Wu W, Lim TK, Ghosh D, Bi X, Lin Q. Elucidating tumor suppressive function of frataxin in colorectal cancer with a quantitative proteomics approach. Manuscript in preparation

2. Wang J*, **Tan XF***, Nguyen VS, Yang P, Zhou J, Gao M, Li Z, Lim TK, He Y, Ong CS, Lay Y, Ghosh D, Mok YK, Shen HM, Lin Q. A Quantitative Chemical Proteomics Approach to Profile the Specific Cellular Targets of Andrographolide, a Promising Anticancer Agent that Suppresses Tumor Metastasis. Revised manuscript resubmitted to Molecular and Cellular Proteomics. *Equal contributions.

3. Ghosh D, Li Z, **Tan XF**, Lim TK, Mao Y, Lin Q. iTRAQ based quantitative proteomics approach validated the role of calcyclin binding protein (CacyBP) in promoting colorectal cancer metastasis. Mol Cell Proteomics. 2013;12:1865-80.

4. Ghosh D, Yu, H, **Tan XF**, Lim TK, Zubaidah RM, Tan HT, Chung MCM, Lin Q. Identification of key players for colorectal cancer metastasis by iTRAQ quantitative proteomics profiling of isogenic SW480 and SW620 cell lines. J Proteome Res. 2011;10:4373-87.

Conference Presentations

1. 6th International Structural Biology and Functional Genomics (SBFG) Conference
   Singapore, 2010

2. 16th Biological Sciences Graduate Congress
   Singapore, 2011

3. 6th Asia-Oceanic Human Proteome Organisation (AOHUPO) Congress
   Beijing, China, 2012

4. Human Proteome Organisation (HUPO) 12th Annual World Congress
   Yokohama, Japan, 2013

5. Proteomic Forum 2013
   Berlin, Germany, 2013

6. 7th International Structural Biology and Functional Genomics (SBFG) Conference
   Singapore, 2013

Awards

1. Best poster presentation
16th Biological Sciences Graduate Congress
Singapore, 2012

2. Best poster prize
6th Asia-Oceanic Human Proteome Organisation (AOHUPO) Congress
Beijing, China, 2012

3. DBS travel award
Proteomic Forum 2013
Berlin, Germany, 2013

Bibliography

[1] Jemal A, Bray F, Center MM, Ferlay J, Ward E, Forman D. Global cancer statistics. CA Cancer J Clin. 2011;61:69-90.
[2] Hanahan D, Weinberg RA. The hallmarks of cancer. Cell. 2000;100:57-70.
[3] Hanahan D, Weinberg Robert A. Hallmarks of Cancer: The Next Generation. Cell. 2011;144:646-74.
[4] Evan GI, Vousden KH. Proliferation, cell cycle and apoptosis in cancer. Nature. 2001;411:342-8.
[5] Henley SA, Dick FA. The retinoblastoma family of proteins and their regulatory functions in the mammalian cell division cycle. Cell Div. 2012;7:10.
[6] Weinberg RA. The retinoblastoma protein and cell cycle control. Cell. 1995;81:323-30.
[7] Fernald K, Kurokawa M. Evading apoptosis in cancer. Trends Cell Biol. 2013;23:620-33.
[8] Shay JW, Bacchetti S. A survey of telomerase activity in human cancer. Eur J Cancer. 1997;33:787-91.
[9] Hanahan D, Folkman J. Patterns and emerging mechanisms of the angiogenic switch during tumorigenesis. Cell. 1996;86:353-64.
[10] Geiger TR, Peeper DS. Metastasis mechanisms. Biochim Biophys Acta. 2009;1796:293-308.
[11] Pages F, Galon J, Dieu-Nosjean MC, Tartour E, Sautes-Fridman C, Fridman WH. Immune infiltration in human tumors: a prognostic factor that should not be ignored. Oncogene. 2010;29:1093-102.
[12] Grivennikov SI, Greten FR, Karin M. Immunity, inflammation, and cancer. Cell. 2010;140:883-99.
[13] Yang L, Pang Y, Moses HL. TGF-beta and immune cells: an important regulatory axis in the tumor microenvironment and progression. Trends Immunol. 2010;31:220-7.
[14] Oleinika K, Nibbs RJ, Graham GJ, Fraser AR. Suppression, subversion and escape: the role of regulatory T cells in cancer progression. Clin Exp Immunol. 2013;171:36-45.
[15] Warburg O. On the origin of cancer cells. Science. 1956;123:309-14.
[16] Warburg O. On respiratory impairment in cancer cells. Science. 1956;124:269-70.
[17] Moreno-Sanchez R, Rodriguez-Enriquez S, Marin-Hernandez A, Saavedra E. Energy metabolism in tumor cells. FEBS J. 2007;274:1393-418.
[18] Zu XL, Guppy M. Cancer metabolism: facts, fantasy, and fiction. Biochem Biophys Res Commun. 2004;313:459-65.
[19] Wang T, Marquardt C, Foker J. Aerobic glycolysis during lymphocyte proliferation. Nature. 1976;261:702-5.
[20] Steck TL, Kaufman S, Bader JP. Glycolysis in chick embryo cell cultures transformed by Rous sarcoma virus. Cancer Res. 1968;28:1611-9.
[21] Voet D, Voet JG. Biochemistry. 4th ed. Hoboken, NJ: John Wiley & Sons; 2011.
[22] Pfeiffer T, Schuster S, Bonhoeffer S. Cooperation and competition in the evolution of ATP-producing pathways. Science. 2001;292:504-7.
[23] Lunt SY, Vander Heiden MG. Aerobic glycolysis: meeting the metabolic requirements of cell proliferation. Annu Rev Cell Dev Biol. 2011;27:441-64.

[24] Younes M, Lechago LV, Somoano JR, Mosharaf M, Lechago J. Wide expression of the human erythrocyte glucose transporter Glut1 in human cancers. Cancer Res. 1996;56:1164-7.
[25] Brown RS, Wahl RL. Overexpression of Glut-1 glucose transporter in human breast cancer. An immunohistochemical study. Cancer. 1993;72:2979-85.
[26] Lunt S, Vander Heiden M. Aerobic glycolysis: meeting the metabolic requirements of cell proliferation. Annual review of cell and developmental biology. 2011;27.
[27] Vander Heiden MG, Cantley LC, Thompson CB. Understanding the Warburg Effect: The Metabolic Requirements of Cell Proliferation. Science. 2009;324:1029-33.
[28] Brown JM, Giaccia AJ. The unique physiology of solid tumors: opportunities (and problems) for cancer therapy. Cancer Res. 1998;58:1408-16.
[29] Milosevic M, Fyles A, Hedley D, Hill R. The human tumor microenvironment: invasive (needle) measurement of oxygen and interstitial fluid pressure. Semin Radiat Oncol. 2004;14:249-58.
[30] Huang LE, Gu J, Schau M, Bunn HF. Regulation of hypoxia-inducible factor 1alpha is mediated by an O2-dependent degradation domain via the ubiquitin-proteasome pathway. Proc Natl Acad Sci U S A. 1998;95:7987-92.
[31] Semenza GL. Hypoxia-inducible factor 1: master regulator of O2 homeostasis. Curr Opin Genet Dev. 1998;8:588-94.
[32] Semenza GL. Targeting HIF-1 for cancer therapy. Nat Rev Cancer. 2003;3:721-32.
[33] Chen C, Pore N, Behrooz A, Ismail-Beigi F, Maity A. Regulation of glut1 mRNA by hypoxia-inducible factor-1. Interaction between H-ras and hypoxia. J Biol Chem. 2001;276:9519-25.
[34] Semenza GL, Roth PH, Fang HM, Wang GL. Transcriptional regulation of genes encoding glycolytic enzymes by hypoxia-inducible factor 1. J Biol Chem. 1994;269:23757-63.
[35] Minchenko O, Opentanova I, Caro J. Hypoxic regulation of the 6-phosphofructo-2-kinase/fructose-2,6-bisphosphatase gene family (PFKFB-1-4) expression in vivo. FEBS Lett. 2003;554:264-70.
[36] Firth JD, Ebert BL, Ratcliffe PJ. Hypoxic regulation of lactate dehydrogenase A. Interaction between hypoxia-inducible factor 1 and cAMP response elements. J Biol Chem. 1995;270:21021-7.
[37] Ullah MS, Davies AJ, Halestrap AP. The plasma membrane lactate transporter MCT4, but not MCT1, is up-regulated by hypoxia through a HIF-1alpha-dependent mechanism. J Biol Chem. 2006;281:9030-7.
[38] Papandreou I, Cairns RA, Fontana L, Lim AL, Denko NC. HIF-1 mediates adaptation to hypoxia by actively downregulating mitochondrial oxygen consumption. Cell Metab. 2006;3:187-97.
[39] Kim JW, Tchernyshyov I, Semenza GL, Dang CV. HIF-1-mediated expression of pyruvate dehydrogenase kinase: a metabolic switch required for cellular adaptation to hypoxia. Cell Metab. 2006;3:177-85.
[40] Bardos JI, Ashcroft M. Hypoxia-inducible factor-1 and oncogenic signalling. Bioessays. 2004;26:262-9.
[41] Zundel W, Schindler C, Haas-Kogan D, Koong A, Kaper F, Chen E, et al. Loss of PTEN facilitates HIF-1-mediated gene expression. Genes Dev. 2000;14:391-6.
[42] Gottlieb E, Tomlinson IPM. Mitochondrial tumour suppressors: a genetic and biochemical update. Nature Reviews Cancer. 2005;5:857-66.

[43] Kim HR, Roe JS, Lee JE, Cho EJ, Youn HD. p53 regulates glucose metabolism by miR-34a. Biochem Biophys Res Commun. 2013;437:225-31.
[44] Bensaad K, Tsuruta A, Selak MA, Vidal MN, Nakano K, Bartrons R, et al. TIGAR, a p53-inducible regulator of glycolysis and apoptosis. Cell. 2006;126:107-20.
[45] Won KY, Lim SJ, Kim GY, Kim YW, Han SA, Song JY, et al. Regulatory role of p53 in cancer metabolism via SCO2 and TIGAR in human breast cancer. Hum Pathol. 2012;43:221-8.
[46] Shim H, Dolde C, Lewis BC, Wu CS, Dang G, Jungmann RA, et al. c-Myc transactivation of LDH-A: implications for tumor metabolism and growth. Proc Natl Acad Sci U S A. 1997;94:6658-63.
[47] Kim JW, Gao P, Liu YC, Semenza GL, Dang CV. Hypoxia-inducible factor 1 and dysregulated c-Myc cooperatively induce vascular endothelial growth factor and metabolic switches hexokinase 2 and pyruvate dehydrogenase kinase 1. Mol Cell Biol. 2007;27:7381-93.
[48] Fong Y, Saldinger PF, Akhurst T, Macapinlac H, Yeung H, Finn RD, et al. Utility of 18F-FDG positron emission tomography scanning on selection of patients for resection of hepatic colorectal metastases. Am J Surg. 1999;178:282-7.
[49] Nieweg OE, Kim EE, Wong WH, Broussard WF, Singletary SE, Hortobagyi GN, et al. Positron emission tomography with fluorine-18-deoxyglucose in the detection and staging of breast cancer. Cancer. 1993;71:3920-5.
[50] Maher JC, Krishan A, Lampidis TJ. Greater cell cycle inhibition and cytotoxicity induced by 2-deoxy-D-glucose in tumor cells treated under hypoxic vs aerobic conditions. Cancer Chemother Pharmacol. 2004;53:116-22.
[51] Maschek G, Savaraj N, Priebe W, Braunschweiger P, Hamilton K, Tidmarsh GF, et al. 2-deoxy-D-glucose increases the efficacy of adriamycin and paclitaxel in human osteosarcoma and non-small cell lung cancers in vivo. Cancer Res. 2004;64:31-4.
[52] Floridi A, Paggi MG, Marcante ML, Silvestrini B, Caputo A, De Martino C. Lonidamine, a selective inhibitor of aerobic glycolysis of murine tumor cells. J Natl Cancer Inst. 1981;66:497-9.
[53] Floridi A, Bruno T, Miccadei S, Fanciulli M, Federico A, Paggi MG. Enhancement of doxorubicin content by the antitumor drug lonidamine in resistant Ehrlich ascites tumor cells through modulation of energy metabolism. Biochem Pharmacol. 1998;56:841-9.
[54] Rosbe KW, Brann TW, Holden SA, Teicher BA, Frei E, 3rd. Effect of lonidamine on the cytotoxicity of four alkylating agents in vitro. Cancer Chemother Pharmacol. 1989;25:32-6.
[55] Pelicano H, Martin DS, Xu RH, Huang P. Glycolysis inhibition for anticancer treatment. Oncogene. 2006;25:4633-46.
[56] Onnis B, Rapisarda A, Melillo G. Development of HIF-1 inhibitors for cancer therapy. J Cell Mol Med. 2009;13:2780-6.
[57] Rapisarda A, Zalek J, Hollingshead M, Braunschweig T, Uranchimeg B, Bonomi CA, et al. Schedule-dependent inhibition of hypoxia-inducible factor-1alpha protein accumulation, angiogenesis, and tumor growth by topotecan in U251-HRE glioblastoma xenografts. Cancer Res. 2004;64:6845-8.
[58] Spigel DR, Waterhouse DM, Lane S, Legenne P, Bhatt K. Efficacy and safety of oral topotecan and bevacizumab combination as second-line treatment for relapsed small-cell lung cancer: an open-label multicenter single-arm phase II study. Clin Lung Cancer. 2013;14:356-63.

[59] Schulz TJ, Thierbach R, Voigt A, Drewes G, Mietzner B, Steinberg P, et al. Induction of oxidative metabolism by mitochondrial frataxin inhibits cancer growth: Otto Warburg revisited. J Biol Chem. 2006;281:977-81.
[60] Hewer RL. Study of fatal cases of Friedreich's ataxia. British Medical Journal.3:649.
[61] Durr A, Cossee M, Agid Y, Campuzano V, Mignard C, Penet C, et al. Clinical and genetic abnormalities in patients with Friedreich's ataxia. New Engl J Med. 1996;335:1169-75.
[62] Gibson TJ, Koonin EV, Musco G, Pastore A, Bork P. Friedreich's ataxia protein: phylogenetic evidence for mitochondrial dysfunction. Trends Neurosci. 1996;19:465-8.
[63] Santos R, Lefevre S, Sliwa D, Seguin A, Camadro JM, Lesuisse E. Friedreich ataxia: molecular mechanisms, redox considerations, and therapeutic opportunities. Antioxid Redox Signal. 2010;13:651-90.
[64] Musco G, Stier G, Kolmerer B, Adinolfi S, Martin S, Frenkiel T, et al. Towards a structural understanding of Friedreich's ataxia: the solution structure of frataxin. Structure. 2000;8:695-707.
[65] Dhe-Paganon S, Shigeta R, Chi YI, Ristow M, Shoelson SE. Crystal structure of human frataxin. J Biol Chem. 2000;275:30753-6.
[66] Huang J, Dizin E, Cowan JA. Mapping iron binding sites on human frataxin: implications for cluster assembly on the ISU Fe-S cluster scaffold protein. J Biol Inorg Chem. 2008;13:825-36.
[67] Rotig A, de Lonlay P, Chretien D, Foury F, Koenig M, Sidi D, et al. Aconitase and mitochondrial iron-sulphur protein deficiency in Friedreich ataxia. Nat Genet. 1997;17:215-7.
[68] Lill R, Muhlenhoff U. Iron-sulfur-protein biogenesis in eukaryotes. Trends Biochem Sci. 2005;30:133-41.
[69] Puccio H, Simon D, Cossée M, Criqui-Filipe P, Tiziano F, Melki J, et al. Mouse models for Friedreich ataxia exhibit cardiomyopathy, sensory nerve defect and Fe-S enzyme deficiency followed by intramitochondrial iron deposits. Nature genetics. 2001;27:181-7.
[70] Mühlenhoff U, Richhardt N, Ristow M, Kispal G, Lill R. The yeast frataxin homolog Yfh1p plays a specific role in the maturation of cellular Fe/S proteins. Hum Mol Genet. 2002;11:2025-61.
[71] Lu C, Cortopassi G. Frataxin knockdown causes loss of cytoplasmic iron-sulfur cluster functions, redox alterations and induction of heme transcripts. Archives of Biochemistry and Biophysics. 2007;457:111-33.
[72] González-Cabo P, Vázquez-Manrique R, García-Gimeno M, Sanz P, Palau F. Frataxin interacts functionally with mitochondrial electron transport chain proteins. Hum Mol Genet. 2005;14:2091-9.
[73] Lodi R, Cooper JM, Bradley JL, Manners D, Styles P, Taylor DJ, et al. Deficit of in vivo mitochondrial ATP production in patients with Friedreich ataxia. Proc Natl Acad Sci U S A. 1999;96:11492-5.
[74] Ristow M, Pfister MF, Yee AJ, Schubert M, Michael L, Zhang CY, et al. Frataxin activates mitochondrial energy conversion and oxidative phosphorylation. Proc Natl Acad Sci U S A. 2000;97:12239-43.
[75] Thierbach R, Drewes G, Fusser M, Voigt A, Kuhlow D, Blume U, et al. The Friedreich's ataxia protein frataxin modulates DNA base excision repair in prokaryotes and mammals. Biochem J. 2010;432:165-72.

[76] Lewis PD, Corr JB, Arlett CF, Harcourt SA. Increased sensitivity to gamma irradiation of skin fibroblasts in Friedreich's ataxia. Lancet. 1979;2:474-5.
[77] Evans HJ, Vijayalaxmi, Pentland B, Newton MS. Mutagen hypersensitivity in Friedreich's ataxia. Ann Hum Genet. 1983;47:193-204.
[78] Barr H, Page R, Taylor W. Primary small bowel ganglioneuroblastoma and Friedreich's ataxia. J R Soc Med. 1986;79:612-3.
[79] Ackroyd R, Shorthouse AJ, Stephenson TJ. Gastric carcinoma in siblings with Friedreich's ataxia. Eur J Surg Oncol. 1996;22:301-3.
[80] De Pas T, Martinelli G, De Braud F, Peccatori F, Catania C, Aapro MS, et al. Friedreich's ataxia and intrathecal chemotherapy in a patient with lymphoblastic lymphoma. Ann Oncol. 1999;10:1393.
[81] Misiakos EP, Siama E, Schizas D, Petropoulos C, Zavras N, Economopoulos N, et al. Massive Uterine Leiomyoma in a Patient with Friedreich's Ataxia: Is There a Possible Association? Case Rep Med. 2011;2011:648217.
[82] Kidd A, Coleman R, Whiteford M, Barron LH, Simpson SA, Haites NE. Breast cancer in two sisters with Friedreich's ataxia. Eur J Surg Oncol. 2001;27:512-4.
[83] Deutsch EC, Seyer LA, Perlman SL, Yu J, Lynch DR. Clinical monitoring in a patient with Friedreich ataxia and osteogenic sarcoma. J Child Neurol. 2012;27:1159-63.
[84] Thierbach R, Schulz TJ, Isken F, Voigt A, Mietzner B, Drewes G, et al. Targeted disruption of hepatic frataxin expression causes impaired mitochondrial function, decreased life span and tumor growth in mice. Hum Mol Genet. 2005;14:3857-64.
[85] Shoichet SA, Baumer AT, Stamenkovic D, Sauer H, Pfeiffer AF, Kahn CR, et al. Frataxin promotes antioxidant defense in a thiol-dependent manner resulting in diminished malignant transformation in vitro. Hum Mol Genet. 2002;11:815-21.
[86] Guccini I, Serio D, Condo I, Rufini A, Tomassini B, Mangiola A, et al. Frataxin participates to the hypoxia-induced response in tumors. Cell Death Dis. 2011;2:e123.
[87] Weinstein JN. Fishing expeditions. Science. 1998;282:628-9.
[88] Evans GA. Designer science and the "omic" revolution. Nat Biotechnol. 2000;18:127.
[89] Geurts van Kessel A. The 'omics' of cancer. Cancer Genet Cytogenet. 2010;203:37-42.
[90] Merrick BA, London RE, Bushel PR, Grissom SF, Paules RS. Platforms for biomarker analysis using high-throughput approaches in genomics, transcriptomics, proteomics, metabolomics, and bioinformatics. IARC Sci Publ. 2011:121-42.
[91] Garay JP, Gray JW. Omics and therapy - a basis for precision medicine. Mol Oncol. 2012;6:128-39.
[92] Milne SB, Mathews TP, Myers DS, Ivanova PT, Brown HA. Sum of the parts: mass spectrometry-based metabolomics. Biochemistry. 2013;52:3829-40.
[93] Fiehn O. Combining genomics, metabolome analysis, and biochemical modelling to understand metabolic networks. Comp Funct Genomics. 2001;2:155-68.
[94] Ma Y, Zhang P, Yang Y, Wang F, Qin H. Metabolomics in the fields of oncology: a review of recent research. Mol Biol Rep. 2012;39:7505-11.
[95] Florian CL, Preece NE, Bhakoo KK, Williams SR, Noble M. Characteristic metabolic profiles revealed by 1H NMR spectroscopy for three types of human brain and nervous system tumours. NMR Biomed. 1995;8:253-64.
[96] Kim YS, Maruvada P, Milner JA. Metabolomics in biomarker discovery: future uses for cancer prevention. Future Oncol. 2008;4:93-102.

[97] Giskeodegard GF, Grinde MT, Sitter B, Axelson DE, Lundgren S, Fjosne HE, et al. Multivariate modeling and prediction of breast cancer prognostic factors using MR metabolomics. J Proteome Res. 2010;9:972-9.
[98] Anderson NL, Anderson NG. Proteome and proteomics: new technologies, new concepts, and new words. Electrophoresis. 1998;19:1853-61.
[99] Tyers M, Mann M. From genomics to proteomics. Nature. 2003;422:193-7.
[100] Chandramouli K, Qian PY. Proteomics: challenges, techniques and possibilities to overcome biological sample complexity. Hum Genomics Proteomics. 2009;2009.
[101] Shi Y, Xiang R, Horvath C, Wilkins JA. The role of liquid chromatography in proteomics. J Chromatogr A. 2004;1053:27-36.
[102] Schirmer EC, Yates JR, 3rd, Gerace L. MudPIT: A powerful proteomics tool for discovery. Discov Med. 2003;3:38-9.
[103] Wright GL, Jr. High resolution two-dimensional polyacrylamide electrophoresis of human serum proteins. Am J Clin Pathol. 1972;57:173-85.
[104] Hillenkamp F, Karas M. Mass spectrometry of peptides and proteins by matrix-assisted ultraviolet laser desorption/ionization. Methods Enzymol. 1990;193:280-95.
[105] Iribarne JV, Thomson BA. EVAPORATION OF SMALL IONS FROM CHARGED DROPLETS. J Chem Phys. 1976;64:2287-94.
[106] Felitsyn N, Peschke M, Kebarle P. Origin and number of charges observed on multiply-protonated native proteins produced by ESI. Int J Mass Spectrom. 2002;219:39-62.
[107] Aebersold R, Mann M. Mass spectrometry-based proteomics. Nature. 2003;422:198-207.
[108] Makarov A. Electrostatic axially harmonic orbital trapping: a high-performance technique of mass analysis. Anal Chem. 2000;72:1156-62.
[109] Thompson A, Schafer J, Kuhn K, Kienle S, Schwarz J, Schmidt G, et al. Tandem mass tags: a novel quantification strategy for comparative analysis of complex protein mixtures by MS/MS. Anal Chem. 2003;75:1895-904.
[110] Gygi SP, Rist B, Gerber SA, Turecek F, Gelb MH, Aebersold R. Quantitative analysis of complex protein mixtures using isotope-coded affinity tags. Nat Biotechnol. 1999;17:994-9.
[111] Ross PL, Huang YN, Marchese JN, Williamson B, Parker K, Hattan S, et al. Multiplexed protein quantitation in Saccharomyces cerevisiae using amine-reactive isobaric tagging reagents. Mol Cell Proteomics. 2004;3:1154-69.
[112] Choe L, D'Ascenzo M, Relkin NR, Pappin D, Ross P, Williamson B, et al. 8-plex quantitation of changes in cerebrospinal fluid protein expression in subjects undergoing intravenous immunoglobulin treatment for Alzheimer's disease. Proteomics. 2007;7:3651-60.
[113] Ong SE, Blagoev B, Kratchmarova I, Kristensen DB, Steen H, Pandey A, et al. Stable isotope labeling by amino acids in cell culture, SILAC, as a simple and accurate approach to expression proteomics. Mol Cell Proteomics. 2002;1:376-86.
[114] Zhou W, Liotta LA, Petricoin EF. The spectra count label-free quantitation in cancer proteomics. Cancer Genomics Proteomics. 2012;9:135-42.
[115] McIntosh M, Fitzgibbon M. Biomarker validation by targeted mass spectrometry. Nat Biotechnol. 2009;27:622-3.
[116] Gillet LC, Navarro P, Tate S, Rost H, Selevsek N, Reiter L, et al. Targeted data extraction of the MS/MS spectra generated by data-independent acquisition: a

new concept for consistent and accurate proteome analysis. Mol Cell Proteomics. 2012;11:O111 016717.
[117] Domon B, Aebersold R. Challenges and opportunities in proteomics data analysis. Mol Cell Proteomics. 2006;5:1921-6.
[118] Kohlbacher O, Reinert K, Gropl C, Lange E, Pfeifer N, Schulz-Trieglaff O, et al. TOPP--the OpenMS proteomics pipeline. Bioinformatics. 2007;23:e191-7.
[119] Deutsch EW, Mendoza L, Shteynberg D, Farrah T, Lam H, Tasman N, et al. A guided tour of the Trans-Proteomic Pipeline. Proteomics. 2010;10:1150-9.
[120] Reymond MA, Schlegel W. Proteomics in cancer. Adv Clin Chem. 2007;44:103-42.
[121] Pin E, Fredolini C, Petricoin EF, 3rd. The role of proteomics in prostate cancer research: biomarker discovery and validation. Clin Biochem. 2013;46:524-38.
[122] Craven RA, Vasudev NS, Banks RE. Proteomics and the search for biomarkers for renal cancer. Clin Biochem. 2013;46:456-65.
[123] Kolch W, Pitt A. Functional proteomics to dissect tyrosine kinase signalling pathways in cancer. Nat Rev Cancer. 2010;10:618-29.
[124] Quintas-Cardama A, Cortes JE. Chronic myeloid leukemia: diagnosis and treatment. Mayo Clin Proc. 2006;81:973-88.
[125] Brehme M, Hantschel O, Colinge J, Kaupe I, Planyavsky M, Kocher T, et al. Charting the molecular network of the drug target Bcr-Abl. Proc Natl Acad Sci U S A. 2009;106:7414-9.
[126] Mann M, Jensen ON. Proteomic analysis of post-translational modifications. Nat Biotechnol. 2003;21:255-61.
[127] Olsen JV, Blagoev B, Gnad F, Macek B, Kumar C, Mortensen P, et al. Global, in vivo, and site-specific phosphorylation dynamics in signaling networks. Cell. 2006;127:635-48.
[128] Bi X, Lin Q, Foo TW, Joshi S, You T, Shen HM, et al. Proteomic analysis of colorectal cancer reveals alterations in metabolic pathways: mechanism of tumorigenesis. Mol Cell Proteomics. 2006;5:1119-30.
[129] Zhou W, Capello M, Fredolini C, Piemonti L, Liotta LA, Novelli F, et al. Proteomic analysis of pancreatic ductal adenocarcinoma cells reveals metabolic alterations. J Proteome Res. 2011;10:1944-52.
[130] Xue T, Zhang Y, Zhang L, Yao L, Hu X, Xu LX. Proteomic Analysis of Two Metabolic Proteins with Potential to Translocate to Plasma Membrane Associated with Tumor Metastasis Development and Drug Targets. J Proteome Res. 2013.
[131] Sutak R, Xu X, Whitnall M, Kashem MA, Vyoral D, Richardson DR. Proteomic analysis of hearts from frataxin knockout mice: marked rearrangement of energy metabolism, a response to cellular stress and altered expression of proteins involved in cell structure, motility and metabolism. Proteomics. 2008;8:1731-41.
[132] Weaver JC. Electroporation theory. Concepts and mechanisms. Methods Mol Biol. 1995;55:3-28.
[133] Cavadini P, Adamec J, Taroni F, Gakh O, Isaya G. Two-step processing of human frataxin by mitochondrial processing peptidase - Precursor and intermediate forms are cleaved at different rates. J Biol Chem. 2000;275:41469-75.
[134] Dietmair S, Timmins NE, Gray PP, Nielsen LK, Kromer JO. Towards quantitative metabolomics of mammalian cells: development of a metabolite extraction protocol. Anal Biochem. 2010;404:155-64.
[135] Tan HT, Lim TK, Chung MC, Lin Q. iTRAQ labeling coupled with LC-MALDI mass spectrometry for monitoring temporal response of colorectal cancer cells to butyrate treatment. Methods Mol Biol. 2011;716:207-24.

[136] Pichler P, Kocher T, Holzmann J, Mazanek M, Taus T, Ammerer G, et al. Peptide labeling with isobaric tags yields higher identification rates using iTRAQ 4-plex compared to TMT 6-plex and iTRAQ 8-plex on LTQ Orbitrap. Anal Chem. 2010;82:6549-58.
[137] Besson A, Dowdy SF, Roberts JM. CDK inhibitors: cell cycle regulators and beyond. Dev Cell. 2008;14:159-69.
[138] Hunter T, Pines J. Cyclins and cancer. II: Cyclin D and CDK inhibitors come of age. Cell. 1994;79:573-82.
[139] Adams PD. Regulation of the retinoblastoma tumor suppressor protein by cyclin/cdks. Biochim Biophys Acta. 2001;1471:M123-33.
[140] Akli S, Keyomarsi K. Cyclin E and its low molecular weight forms in human cancer and as targets for cancer therapy. Cancer Biol Ther. 2003;2:S38-47.
[141] Wingate H, Puskas A, Duong M, Bui T, Richardson D, Liu Y, et al. Low molecular weight cyclin E is specific in breast cancer and is associated with mechanisms of tumor progression. Cell Cycle. 2009;8:1062-8.
[142] Wingate H, Zhang N, McGarhen MJ, Bedrosian I, Harper JW, Keyomarsi K. The tumor-specific hyperactive forms of cyclin E are resistant to inhibition by p21 and p27. J Biol Chem. 2005;280:15148-57.
[143] Pastore A, Puccio H. Frataxin: a protein in search for a function. J Neurochem. 2013;126 Suppl 1:43-52.
[144] Liberman EA, Topaly VP, Tsofina LM, Jasaitis AA, Skulachev VP. Mechanism of coupling of oxidative phosphorylation and the membrane potential of mitochondria. Nature. 1969;222:1076-8.
[145] Skulachev VP. Membrane electricity as a convertible energy currency for the cell. Can J Biochem. 1980;58:161-75.
[146] Ronn T, Poulsen P, Tuomi T, Isomaa B, Groop L, Vaag A, et al. Genetic variation in ATP5O is associated with skeletal muscle ATP50 mRNA expression and glucose uptake in young twins. PLoS One. 2009;4:e4793.
[147] Gottlieb E, Tomlinson IP. Mitochondrial tumour suppressors: a genetic and biochemical update. Nat Rev Cancer. 2005;5:857-66.
[148] Hofmann B, Hecht HJ, Flohe L. Peroxiredoxins. Biol Chem. 2002;383:347-64.
[149] Toppo S, Vanin S, Bosello V, Tosatto SC. Evolutionary and structural insights into the multifaceted glutathione peroxidase (Gpx) superfamily. Antioxid Redox Signal. 2008;10:1501-14.
[150] Ursini F, Maiorino M, Brigelius-Flohe R, Aumann KD, Roveri A, Schomburg D, et al. Diversity of glutathione peroxidases. Methods Enzymol. 1995;252:38-53.
[151] Holmgren A. Antioxidant function of thioredoxin and glutaredoxin systems. Antioxid Redox Signal. 2000;2:811-20.
[152] Wood ZA, Schroder E, Robin Harris J, Poole LB. Structure, mechanism and regulation of peroxiredoxins. Trends Biochem Sci. 2003;28:32-40.
[153] Finkel T. Signal transduction by reactive oxygen species. J Cell Biol. 2011;194:7-15.
[154] Asensi M, Sastre J, Pallardo FV, Lloret A, Lehner M, Garcia-de-la Asuncion J, et al. Ratio of reduced to oxidized glutathione as indicator of oxidative stress status and DNA damage. Methods Enzymol. 1999;299:267-76.
[155] Oberley TD. Oxidative damage and cancer. Am J Pathol. 2002;160:403-8.
[156] Brigelius-Flohe R, Maiorino M. Glutathione peroxidases. Biochim Biophys Acta. 2013;1830:3289-303.
[157] Arner ES, Holmgren A. Physiological functions of thioredoxin and thioredoxin reductase. Eur J Biochem. 2000;267:6102-9.

[158] Liu Y, Fiskum G, Schubert D. Generation of reactive oxygen species by the mitochondrial electron transport chain. J Neurochem. 2002;80:780-7.
[159] Selak MA, Armour SM, MacKenzie ED, Boulahbel H, Watson DG, Mansfield KD, et al. Succinate links TCA cycle dysfunction to oncogenesis by inhibiting HIF-alpha prolyl hydroxylase. Cancer Cell. 2005;7:77-85.
[160] Bolland M, Benn D, Croxson M, McCall J, Shaw JF, Baillie T, et al. Gastrointestinal stromal tumour in succinate dehydrogenase subunit B mutation-associated familial phaeochromocytoma/paraganglioma. ANZ J Surg. 2006;76:763-4.
[161] Vanharanta S, Buchta M, McWhinney SR, Virta SK, Peczkowska M, Morrison CD, et al. Early-onset renal cell carcinoma as a novel extraparaganglial component of SDHB-associated heritable paraganglioma. Am J Hum Genet. 2004;74:153-9.
[162] Rutter J, Winge DR, Schiffman JD. Succinate dehydrogenase - Assembly, regulation and role in human disease. Mitochondrion. 2010;10:393-401.
[163] Neumann HP, Pawlu C, Peczkowska M, Bausch B, McWhinney SR, Muresan M, et al. Distinct clinical features of paraganglioma syndromes associated with SDHB and SDHD gene mutations. JAMA. 2004;292:943-51.
[164] Habano W, Sugai T, Nakamura S, Uesugi N, Higuchi T, Terashima M, et al. Reduced expression and loss of heterozygosity of the SDHD gene in colorectal and gastric cancer. Oncol Rep. 2003;10:1375-80.
[165] Zhang D, Wang W, Xiang B, Li N, Huang S, Zhou W, et al. Reduced succinate dehydrogenase B expression is associated with growth and de-differentiation of colorectal cancer cells. Tumour Biol. 2013.
[166] Chandel NS, McClintock DS, Feliciano CE, Wood TM, Melendez JA, Rodriguez AM, et al. Reactive oxygen species generated at mitochondrial complex III stabilize hypoxia-inducible factor-1alpha during hypoxia: a mechanism of O2 sensing. J Biol Chem. 2000;275:25130-8.
[167] Chandel NS, Maltepe E, Goldwasser E, Mathieu CE, Simon MC, Schumacker PT. Mitochondrial reactive oxygen species trigger hypoxia-induced transcription. Proc Natl Acad Sci U S A. 1998;95:11715-20.
[168] Guzy RD, Hoyos B, Robin E, Chen H, Liu L, Mansfield KD, et al. Mitochondrial complex III is required for hypoxia-induced ROS production and cellular oxygen sensing. Cell Metab. 2005;1:401-8.
[169] Chua YL, Dufour E, Dassa EP, Rustin P, Jacobs HT, Taylor CT, et al. Stabilization of hypoxia-inducible factor-1alpha protein in hypoxia occurs independently of mitochondrial reactive oxygen species production. J Biol Chem. 2010;285:31277-84.
[170] Jung SN, Yang WK, Kim J, Kim HS, Kim EJ, Yun H, et al. Reactive oxygen species stabilize hypoxia-inducible factor-1 alpha protein and stimulate transcriptional activity via AMP-activated protein kinase in DU145 human prostate cancer cells. Carcinogenesis. 2008;29:713-21.
[171] Brunelle JK, Bell EL, Quesada NM, Vercauteren K, Tiranti V, Zeviani M, et al. Oxygen sensing requires mitochondrial ROS but not oxidative phosphorylation. Cell Metab. 2005;1:409-14.
[172] Hagen T. Oxygen versus Reactive Oxygen in the Regulation of HIF-1alpha: The Balance Tips. Biochem Res Int. 2012;2012:436981.
[173] Yee Koh M, Spivak-Kroizman TR, Powis G. HIF-1 regulation: not so easy come, easy go. Trends Biochem Sci. 2008;33:526-34.

[174] Gao P, Zhang H, Dinavahi R, Li F, Xiang Y, Raman V, et al. HIF-dependent antitumorigenic effect of antioxidants in vivo. Cancer Cell. 2007;12:230-8.
[175] Gatenby RA, Gillies RJ. Why do cancers have high aerobic glycolysis? Nat Rev Cancer. 2004;4:891-9.
[176] Cantor JR, Sabatini DM. Cancer cell metabolism: one hallmark, many faces. Cancer Discov. 2012;2:881-98.
[177] Fischer K, Hoffmann P, Voelkl S, Meidenbauer N, Ammer J, Edinger M, et al. Inhibitory effect of tumor cell-derived lactic acid on human T cells. Blood. 2007;109:3812-9.
[178] Dietl K, Renner K, Dettmer K, Timischl B, Eberhart K, Dorn C, et al. Lactic acid and acidification inhibit TNF secretion and glycolysis of human monocytes. J Immunol. 2010;184:1200-9.
[179] Rofstad EK, Mathiesen B, Kindem K, Galappathi K. Acidic extracellular pH promotes experimental metastasis of human melanoma cells in athymic nude mice. Cancer Res. 2006;66:6699-707.
[180] Rofstad EK. Microenvironment-induced cancer metastasis. Int J Radiat Biol. 2000;76:589-605.
[181] Pinheiro C, Longatto-Filho A, Azevedo-Silva J, Casal M, Schmitt FC, Baltazar F. Role of monocarboxylate transporters in human cancers: state of the art. J Bioenerg Biomembr. 2012;44:127-39.
[182] Ke X, Fei F, Chen Y, Xu L, Zhang Z, Huang Q, et al. Hypoxia upregulates CD147 through a combined effect of HIF-1alpha and Sp1 to promote glycolysis and tumor progression in epithelial solid tumors. Carcinogenesis. 2012;33:1598-607.
[183] Gabison EE, Hoang-Xuan T, Mauviel A, Menashi S. EMMPRIN/CD147, an MMP modulator in cancer, development and tissue repair. Biochimie. 2005;87:361-8.
[184] Tang Y, Nakada MT, Kesavan P, McCabe F, Millar H, Rafferty P, et al. Extracellular matrix metalloproteinase inducer stimulates tumor angiogenesis by elevating vascular endothelial cell growth factor and matrix metalloproteinases. Cancer Res. 2005;65:3193-9.
[185] Nabeshima K, Iwasaki H, Koga K, Hojo H, Suzumiya J, Kikuchi M. Emmprin (basigin/CD147): matrix metalloproteinase modulator and multifunctional cell recognition molecule that plays a critical role in cancer progression. Pathol Int. 2006;56:359-67.
[186] Guo H, Majmudar G, Jensen TC, Biswas C, Toole BP, Gordon MK. Characterization of the gene for human EMMPRIN, a tumor cell surface inducer of matrix metalloproteinases. Gene. 1998;220:99-108.
[187] Kanekura T, Chen X. CD147/basigin promotes progression of malignant melanoma and other cancers. J Dermatol Sci. 2010;57:149-54.
[188] Zhao SH, Wang Y, Wen L, Zhai ZB, Ai ZH, Yao NL, et al. Basigin-2 is the predominant basigin isoform that promotes tumor cell migration and invasion and correlates with poor prognosis in epithelial ovarian cancer. J Transl Med. 2013;11:92.
[189] Kennedy KM, Dewhirst MW. Tumor metabolism of lactate: the influence and therapeutic potential for MCT and CD147 regulation. Future Oncol. 2010;6:127-48.
[190] Stenzinger A, Wittschieber D, von Winterfeld M, Goeppert B, Kamphues C, Weichert W, et al. High extracellular matrix metalloproteinase inducer/CD147 expression is strongly and independently associated with poor prognosis in colorectal cancer. Hum Pathol. 2012;43:1471-81.

[191] Buergy D, Fuchs T, Kambakamba P, Mudduluru G, Maurer G, Post S, et al. Prognostic impact of extracellular matrix metalloprotease inducer: immunohistochemical analyses of colorectal tumors and immunocytochemical screening of disseminated tumor cells in bone marrow from patients with gastrointestinal cancer. Cancer. 2009;115:4667-78.
[192] Boye K, Nesland JM, Sandstad B, Haugland Haugen M, Maelandsmo GM, Flatmark K. EMMPRIN is associated with S100A4 and predicts patient outcome in colorectal cancer. Br J Cancer. 2012;107:667-74.
[193] Su J, Chen X, Kanekura T. A CD147-targeting siRNA inhibits the proliferation, invasiveness, and VEGF production of human malignant melanoma cells by down-regulating glycolysis. Cancer Lett. 2009;273:140-7.
[194] Schneiderhan W, Scheler M, Holzmann KH, Marx M, Gschwend JE, Bucholz M, et al. CD147 silencing inhibits lactate transport and reduces malignant potential of pancreatic cancer cells in in vivo and in vitro models. Gut. 2009;58:1391-8.
[195] Baba M, Inoue M, Itoh K, Nishizawa Y. Blocking CD147 induces cell death in cancer cells through impairment of glycolytic energy metabolism. Biochem Biophys Res Commun. 2008;374:111-6.
[196] Denko NC. Hypoxia, HIF1 and glucose metabolism in the solid tumour. Nat Rev Cancer. 2008;8:705-13.
[197] Culver C, Melvin A, Mudie S, Rocha S. HIF-1alpha depletion results in SP1-mediated cell cycle disruption and alters the cellular response to chemotherapeutic drugs. Cell Cycle. 2011;10:1249-60.
[198] Arredondo M, Núñez M. Iron and copper metabolism. Molecular aspects of medicine.26:313-40.
[199] Yu Y, Kovacevic Z, Richardson DR. Tuning cell cycle regulation with an iron key. Cell Cycle. 2007;6:1982-94.
[200] Le N, Richardson D. The role of iron in cell cycle progression and the proliferation of neoplastic cells. Biochimica et biophysica acta. 2002;1603:31-77.
[201] Toyokuni S. Iron-induced carcinogenesis: the role of redox regulation. Free Radic Biol Med. 1996;20:553-66.
[202] Huang ML, Lane DJ, Richardson DR. Mitochondrial Mayhem: The Mitochondrion as a Modulator of Iron Metabolism and Its Role in Disease. Antioxid Redox Signal. 2011.
[203] Richardson D, Lane D, Becker E, Huang M, Whitnall M, Suryo Rahmanto Y, et al. Mitochondrial iron trafficking and the integration of iron metabolism between the mitochondrion and cytosol. Proceedings of the National Academy of Sciences of the United States of America. 2010;107:10775-857.
[204] Marmolino D. Friedreich's ataxia: past, present and future. Brain research reviews. 2011;67:311-41.
[205] Richardson DR, Lane DJ, Becker EM, Huang ML, Whitnall M, Suryo Rahmanto Y, et al. Mitochondrial iron trafficking and the integration of iron metabolism between the mitochondrion and cytosol. Proc Natl Acad Sci U S A. 2010;107:10775-82.
[206] Adamec J, Rusnak F, Owen W, Naylor S, Benson L, Gacy A, et al. Iron-dependent self-assembly of recombinant yeast frataxin: implications for Friedreich ataxia. American journal of human genetics. 2000;67:549-611.
[207] Torti SV, Torti FM. Iron and cancer: more ore to be mined. Nat Rev Cancer. 2013;13:342-55.

[208] Martin LK, Grecula J, Jia G, Wei L, Yang X, Otterson GA, et al. A dose escalation and pharmacodynamic study of triapine and radiation in patients with locally advanced pancreas cancer. Int J Radiat Oncol Biol Phys. 2012;84:e475-81.
[209] Kakhlon O, Cabantchik ZI. The labile iron pool: characterization, measurement, and participation in cellular processes(1). Free Radic Biol Med. 2002;33:1037-46.
[210] Lipinski P, Drapier JC, Oliveira L, Retmanska H, Sochanowicz B, Kruszewski M. Intracellular iron status as a hallmark of mammalian cell susceptibility to oxidative stress: a study of L5178Y mouse lymphoma cell lines differentially sensitive to H(2)O(2). Blood. 2000;95:2960-6.
[211] Wang J, Pantopoulos K. Regulation of cellular iron metabolism. The Biochemical journal. 2011;434:365-446.
[212] Huang da W, Sherman BT, Lempicki RA. Systematic and integrative analysis of large gene lists using DAVID bioinformatics resources. Nat Protoc. 2009;4:44-57.
[213] Huang da W, Sherman BT, Tan Q, Kir J, Liu D, Bryant D, et al. DAVID Bioinformatics Resources: expanded annotation database and novel algorithms to better extract biology from large gene lists. Nucleic Acids Res. 2007;35:W169-75.